

University of Padova

Department of Physics and Astronomy "Galileo Galilei"

Ph.D. Course in Physics

36° Cycle

Academic Year 2022/2023

Doctoral Thesis

Fluctuations across statistical scales – from
statistical physics theory to biological
applications

Ph.D. Candidate:

Prajwal Padmanabha

Supervisors:

prof. Amos Maritan

prof. Sandro Azaele

Coordinator:

prof. Giulio Monaco

ABSTRACT

Fluctuations at different scales arise naturally as a result of coarse-graining dynamics at smaller spatial levels. In this thesis, we will see how tools from statistical physics can help analyse fluctuations in different systems and the resulting effects, especially in a biological context. We move from theoretical computations in non equilibrium statistical mechanics and numerical simulations of biological examples to brief experimental verifications through microbial communities to understand such stochasticity at different spatiotemporal scales.

We begin initially with techniques to understand fluctuations of non equilibrium currents in a stochastic process. We focus on entropy production which is a significant marker of out-of-equilibrium regime, and propose a simple and graphical method to compute its various moments, not just in a discrete example of interest, but also in general spatially continuous systems. From non-equilibrium produced by heat baths at different temperatures, we pivot to present another kind of out-of-equilibrium processes due to sink-driven boundary dynamics. Such processes, found in systems with absorbing boundaries invalidate standard relations between fluctuations and dissipations. We propose a generalization of powerful fluctuation-dissipation theorems to include the effect of such boundary driven effects, and apply the results to strongly biologically motivated examples of birth-death forest dynamics and DNA target search on proteins. Here, we compute responses of previously infeasible quantities which point to strong ecological considerations.

Boundary effects due to sinks in a local setting is significantly different from a spatially structured system. This necessitates an explicit incorporation of information of the landscape structure into biological models, offered through the lens of metapopulation theory. We present a first principles derivation of classical theoretical models and demonstrate additional benefits that this statistical mechanics route offers, including the ability to incorporate heterogeneous landscape and dispersal network information. In such systems, close to extinction, demographic fluctuations become significant. Contrarily, at the opposite spatial scale, in a laboratory environment, this regime is hardly reached, with minimum population of microbes being in tens to hundreds of thousands of individuals. Nevertheless, a natural setting involves constant environmental variability, captured through stochasticity in parameters in theoretical mod-

els. Specifically, serial dilution, a common experimental technique, gets represented as a periodic fluctuation in the dynamics of species and resources. Incorporating the different aspects of this technique through theoretical methods demonstrates a relation between different associated parameters which enable a sensible comparison across different dilution frequencies, opening the doors to further analysis of effects of environmental variability in microscale biological systems.

Techniques developed for specific processes yield specific results whose scope remain limited. However, generalizations open up new paths of investigation into extended systems offering novel findings. Through investigations of systems at different levels using generalizing methods, we not only understand the specific process, but also observe the potential patterns of non-equilibrium across scales. Such results serve to underscore the importance of fluctuations, either thermal or externally driven, in determining different observed behaviours. This not only aids in the search for general non-equilibrium principles, which is inspired by biological systems, but also motivates further interdisciplinary research.

ACKNOWLEDGEMENTS

Growing up, I had absolutely no idea what research entails or what an academic life means. While I rushed blindly into this unknown abyss, my parents stood by me as pillars of support, with all the strength they could muster and beyond. Where I stand today would be very different if it were not for the unwavering, unflinching and unconditional backing of my brother. The past three years, I've not only had to contend with the pressures of a PhD, but also the struggles of living abroad and the fights against loneliness, among a multitude of other things. If there is a significant contributing factor to me being here right now, it is my parents and my brother. While this thesis serves as a reflection of my academic progress, I can never forget that underneath it all, I stand on the shoulders of giants, who keep me propped up.

I cannot thank Amos and Sandro enough for everything through this journey. Amos has been a source of inspiration even before I began my PhD. I will forever be grateful to him for believing in me, even when I didn't, for guiding me, and for demonstrating levels of excellence I can only aspire to reach. I can never forget the multitude of things I have learnt from Sandro, both within academics and all the important things around it. I only hope that at least a fraction of his commitment to rigour stays with me for my future journey. A special thanks, also to his booming laugh which never failed to light up a room in smiles. I extend my heartfelt gratitude to Deepak, who not only guided me, academically and otherwise, from my very first day in Padova, but also turned into a personal friend; one who I could rely on for advice regardless of the situation. I cannot forget the number of times I have relied on Giorgio in these last three years. In addition to his excellent skills, his patience in helping people is truly commendable. Half the opportunities I had would have been missed without all his help, especially with the bureaucracy. On the topic of bureaucracy, I would really like to thank Giannina, who is the real gem of the Physics department. Without her, I would have most likely left Italy long time ago. She went above and beyond in every problem I brought to her. The LIPh life would not have been complete without the PhiL PhDs. Going from locked down Covid times to late night bowling sessions, your company has made this journey not just bearable, but truly enjoyable. In no particular order, thank you, Emanuele, Davide, Elisa, Clelia, Giacomo, Benedetta, Alice, Jacopo, Francesco, Fabio, Chris-

tian, Marika, and Samuele. Keep the balls rolling, the pizza cooking, the techno partying, the wine flowing, the chess going, and the jokes coming.

Such a journey is impossible without the dear company of friends. Thank you Marah, Marco and Ilaria for constant company, laughs, and sarcasm. Legatoria would be a sadder place without your companionship to lighten it up. Thank you for sharing the joys and the pains in the last three years. Last but not least, a small thanks to Shesha, who has been around always, but still needed the threat of disembowelment to visit Padova. There are countless people who have featured in my life and have had an impact that has led me to this point. What I am today is because of all of you. I thank you from the bottom of my heart.

CONTENTS

1 Introduction	7
1.1 Mathematical tools for stochastic processes	9
1.2 Fluctuations and dissipations	14
1.3 Description of biological systems	18
1.4 Philosophy of complex systems	23
2 Fluctuations of entropy production	27
2.1 Introduction	27
2.2 Cumulants of entropy production	29
2.3 Entropy Production in the run-and-tumble model	39
2.4 Spatially continuous limit	43
2.5 Conclusion	45
3 Fluctuation-dissipation theorem with absorbing states	47
3.1 Introduction	47
3.2 Stationary systems	49
3.2.1 Standard FDT	49
3.2.2 Application in forest dynamics	51
3.3 Absorbing systems	52
3.3.1 Discrete Systems	53
3.3.2 Continuous State Space	60
3.3.3 Examples and Verification	69
3.3.4 Extension to arbitrary times	79
3.3.5 Biological Examples	81
3.4 Conclusion	86
4 Extinction of biological populations in complex landscapes	89
4.1 Introduction	89
4.2 Historic models of metapopulation	91
4.3 Microscopic model and derivations	92
4.3.1 Model	92
4.3.2 Rate equations	94
4.3.3 Quasistationary approximation	95

4.3.4	Explicit dispersal kernel	97
4.4	Results	98
4.4.1	Effects of network topology	98
4.4.2	Effects of modularity and fragmentation	101
4.4.3	Effects of landscape topography	103
4.5	Conclusion	106
5	Forced fluctuations of microbial communities	107
5.1	Introduction	107
5.2	Competitive exclusion principle	108
5.3	Serial transfer induced coexistence	110
5.3.1	Scaling of parameters	113
5.4	Conclusion	118
6	Conclusion and Discussion	121
7	Appendices	125
7.1	Appendix A	125
7.2	Appendix B	127

INTRODUCTION

Comprehending the natural world to its fundamental details has been a long-standing goal of physics. Possessing insights of the smallest of scales gives hope of completely understanding the universe, down to its most intricate details. Paradoxically, such granular detail makes it nearly impossible to predict behaviour at macroscopic levels starting from fundamental processes, due to the sheer volume of information and complexity involved. The shift from a deterministic description using Newtonian dynamics to a more statistical description of certain phenomena was in line with the increasing complexity due to the large number of system constituents [1]. In an era where the underlying philosophy of science was reductionism, statistical mechanics sought to move against the flow by accounting for large systems through the process of ignoring the exact microscopic details but only focussing on the macroscopic effect of small-scale processes. The benefits it brought not only improved our understanding of many classical systems, but also had implications outside of traditional physics. This spark of interdisciplinarity soon extended into chemical and biological systems, albeit in very limited capacity.

The limitations in part arose due to a missing key ingredient. Statistical mechanics started with systems that are in equilibrium. Initial forays by Boltzmann and Einstein gave a way for statistical mechanics to connect microscopic processes to macroscopic properties [2]. Einstein and Smoluchowski's work on connecting the diffusion constant (a measurable quantity) to Avagadro's number gave initial estimates for validation of atomic theory of matter [3]. The core idea necessitated an understanding of thermal fluctuations at the molecular scale. These thermal fluctuations lead to fluctuations in positions of particles, which eventually lead to fluctuations in probability of collision between molecules and hence result in eventual fluctuations in chemical reactions [4]. Typically, these variations are negligible in standard experimental settings, as the vast number of molecules involved diminishes the relative impact of such fluctuations.

In certain scenarios, notably where reacting molecules are few and confined, these fluctuations assume critical importance. Such conditions are often encountered in cellular vesicles [5]. Though one cannot draw an exact and quantified relationship between these different scales of fluctuations, the qualitative connection is unmistakably apparent. In equilibrium systems at non-zero temperatures, these fluctuations are constant with no external driving. Life, contrarily, found a way to maintain constant driving (through the use of energy) that keeps the system out-of-equilibrium, thus harnessing the resulting fluctuations for work [6]. This inherent non-equilibrium nature of biological systems meant that any study through equilibrium lens underestimates the space of possible new behaviours that can arise [7]. Advancement in understanding these phenomena required novel mathematical frameworks, particularly the development of stochastic process tools, which conceptualize environmental fluctuations as effective random forces impacting the variables of interest [8, 9, 10].

Such tools immediately open a vast number of fields that have inherent noise in them. A notion of equilibrium can be extended to non-thermal systems by considering other kinds of fluxes in the system and not just that of energy. This conceptual leap frees us from the constraints of being limited to a specific definition of non-equilibrium arising from thermodynamics and allows us to extend these mathematical tools into broad areas, even outside of traditional physics.

At the smallest scale, one can find proteins on DNA performing diffusion while searching for a target [11]. At intermediate biochemical scales, gene regulation has been found to be inherently stochastic in nature [12, 13]. Reactions in cellular vesicles happen at such low concentration of chemicals that the rate of reaction can no longer be described by mass action principle [5]. Cell growth and division are effectively stochastic processes, partly due to the nature of environment the microbes reside in [14]. Cells in the gut experience a periodic fluctuation of available resources, mirroring phenomena at larger scale due to seasonality of climate [15]. At the macroscale, forests undergo birth death dynamics which once again happen at a fixed rate only on average [16]. Going even beyond, urban mobility links back to diffusive behaviours with stochasticity [17] arising even in economic domain where, the stock market has inherent fluctuations in prices arising due to collective action of millions of people [18].

Central to all these examples is the concept of fluctuations. The ability to incorporate them into mathematical framework is broadly provided by stochastic processes theory. True to its nature and to the philosophy of statistical mechanics, these tools manage to bridge the gap across diverse fields and across diverse scales. In this thesis, I attempt to elucidate a small part of this grand scale of things by analysing these fluctuations at different scales and demonstrate a selection of biological applications. Extending ideas of entropy from thermodynamics into stochastic non-equilibrium system leads to entropy as a fluctuating variable. The characterization of these fluctuations provides estimates for

quantification of how far a process is out of equilibrium. In the same vein, a system at equilibrium can be turned into an out-of-equilibrium system by introducing boundary effects into fluxes. Such effects propagate through in the system which manipulate the equilibrium relation between fluctuations and dissipations. One can then try to study the effect of such boundaries in macroecological examples, where extinctions are a concern. A set of such macroecological interacting systems necessitates a broader perspective to look at populations of such systems to determine when extinction is eminent. Furthermore, when fluctuations are not inherent in the system but are imposed upon it, this leads to forced out-of-equilibrium behaviour. In order to look at these topics, I will start with a brief introduction of tools and uses of stochastic processes which will lay the groundwork for the rest of the thesis. This part will also include brief descriptions of the relations between fluctuations and dissipations in equilibrium system and its history, and certain simple examples of how one can apply stochastic tools for different biological systems. The interdisciplinary essence of this introductory part will then be carried through the remainder of the thesis.

1.1 Mathematical tools for stochastic processes

Diffusive phenomena were described throughout various points in history [4]. One of the most notable early accounts was from Robert Brown's observation of the seemingly random motion of pollen grains in water, which was initially misattributed to a living phenomena coming from pollen. However, similar observations in other areas invalidated this hypothesis. In 1904, Einstein famously describes that this random movement occurs due to a bombardment of the pollen grain by an extremely large number of water molecules. He went on to connect the diffusion constant of this random motion to the viscosity of the fluid, which was one of the earliest forms of what we term today as the fluctuation-dissipation theorem. This pivotal insight also contributed to quantifying Avogadro's number, offering empirical support for the atomic theory of matter [3]. Soon after this, Langevin wrote a seminal paper describing an equation with random forces, solving a stochastic differential equation, marking a significant milestone in the genesis of non-equilibrium statistical mechanics [19].

Though diffusive phenomena occurs in continuous space, a simplified initial point of analysis is to consider a one dimensional space where a certain particle performs a random walk, by jumping to one site on the right with a certain probability and one site on the left with another probability [9]. Over time, the probability distribution of the particle's location tends to follow a Gaussian distribution, an outcome attributed to the Central Limit Theorem. As the spatial separation between sites decreases, the model increasingly resembles continuous diffusion. Integrating the notion of a drag force from the surrounding fluid

into this framework allows for a derivation of Einstein’s relation, linking the diffusion constant to the fluid’s viscosity [4]. This approach quite effectively models a random walker’s behaviour. However, to extend these insights to more complex systems, a comprehensive mathematical framework is necessary, provided by the theory of Markov processes.

Going beyond the one dimensional line, a set of arbitrary states (finite or infinite) can be considered to be accessible by a random walker. The “position” of the walker then changes at random to one of the other states with a given probability. A reasonable assumption we can make is that the walker’s future state depends solely on its current position, not its prior history - this is the principle of memorylessness intrinsic to Markov processes. This facilitates the construction of a Markov chain describing the probability of finding the walker at different states at different times. By reducing the time intervals between transitions, one can derive a continuous-time Markov chain, often represented by the Master equation [8]. Since the nature of the walker is inherently random, the description of the system is given by the probability to move out of that state and the effective probability to move into that state, i.e.,

$$\frac{dP(x, t)}{dt} = \sum_{y \neq x} [W_{y \rightarrow x} P(y, t) - W_{x \rightarrow y} P(x, t)] \quad (1.1)$$

where $P(x, t)$ is the probability of being in state x at time t . $W_{y \rightarrow x}$ and $W_{x \rightarrow y}$ represent the rates of transition between the states x and y . By defining a matrix H such that $H_{xy} = W_{y \rightarrow x} - \delta_{xy} \sum_z W_{x \rightarrow z}$, we can express Eq (1.1) as a matrix multiplication.

$$\frac{d\vec{P}(t)}{dt} = \hat{H} \vec{P}(t) \quad (1.2)$$

where $\vec{P}(t)$ is the vector of probabilities $P(x, t)$. The Master equation’s states are abstractly defined, making the framework versatile across various fields. In a random walker scenario, the states represent the walker’s positions, whereas, in ecological models like forest dynamics, states might correspond to species populations. The time independence of the transition rate matrix H in Eq (1.2) allows for a direct calculation of solutions through spectral decomposition. This method resembles the spectral decomposition of Hermitian operators in Schrödinger’s equation, highlighting a commonality in mathematical techniques across fields. A spectral decomposition of the solution is given by

$$P(x, t) = \sum_n \varphi_n(x) c_n e^{-\lambda_n t} \quad (1.3)$$

where φ_n are the eigenvectors of H corresponding to the eigenvalue $-\lambda_n$ and

c_n are constants set by the initial condition of the system [8]. Several properties become apparent immediately. Due to the nature of the transition rate matrix, i.e., the total sum along the rows of H is always zero, a zero eigenvalue is always guaranteed. Further mathematical theorems demonstrate that other eigenvectors' contribution to the spectral solution eventually decay, thereby leaving the zero-eigenvalue eigenvector as the stationary solution of the dynamics.

While the abstract mathematical framework of Markov processes and Master equations is powerful for generalizing various phenomena, a more tangible connection to physical insights demands a description of diffusive phenomena in continuous space. One approach to achieving this is through the proposal of Langevin, which begins with a stochastic differential equation. However, starting from such stochastic differential equations relies on observed behaviours and empirical relationships to formulate the equations governing the system's dynamics.

An alternate approach is to begin with the Master equation and consider transitions occurring between closely spaced states in real space, i.e, $|x - y| \ll 1$ (or $\|\vec{x} - \vec{y}\| \ll 1$ in the case of higher dimensions). This assumption facilitates the transition from discrete to continuous descriptions and leads to an infinite order partial differential equation, known as the Kramers-Moyal expansion, given by

$$\frac{\partial P(x, t)}{\partial t} = \sum_{k=1}^{\infty} \frac{(-1)^k}{k!} \frac{\partial^k}{\partial x^k} [a_k(x)P(x, t)] \quad (1.4)$$

where a_k are the jump coefficients of the transition rate matrix, i.e.,

$$a_k(x) = \sum_y (x - y)^k W_{y \rightarrow x} \quad (1.5)$$

The Kramers-Moyal expansion contains infinite terms. To describe the time evolution of the probability similar to the one of Master equation, these terms have to be considered to one of the two limits: either all the infinite terms are needed, or only the first two orders are enough. When this expansion truncates after the second term, it is known as the Fokker-Planck equation [10]. This termination essentially simplifies the infinite series into a more manageable form, capturing the essence of the process with two key coefficients: a_1 representing the drift, which captures the systematic change or trend in the process, and a_2 representing the diffusion, which accounts for the random fluctuations.

This second-order truncation isn't just a mathematical convenience; it's often a robust approximation for a wide range of physical systems, especially when there are finite size effects at play. When systems are large, but finite, fluctuations arising from the third order of the Kramers-Moyal expansion are too negligible compared to the diffusive fluctuations that truncation at the second order describes the time evolution of the probabilities very closely to that of the Master equation. Such scenarios are addressed by what's known as the van

Kampen system size expansion, which provides a framework for understanding how fluctuations behave in finite systems. This understanding is crucial in fields like chemical kinetics, population dynamics, and other areas where the discrete nature and finite size of the system significantly influence its behaviour [14]. The Fokker-Planck equation, therefore, serves as a foundational tool in the study of stochastic processes, offering a balance between detailed physical representation and mathematical tractability.

Translating the Fokker-Planck equation into a form that resembles an equation of motion in the presence of random forces necessitates additional mathematical constructs. To achieve this, one has to start from a Langevin equation and write an equivalent second order partial differential equation, which corresponds to the Fokker-Planck equation. This was developed by Ito and Stratonovich separately, giving two different types of mathematical descriptions of how to handle integration and interpretation of stochastic forces over time [20]. Ito calculus, known for its non-anticipative nature, assumes that the future increment of the stochastic process does not depend on the current state [21]. Stratonovich calculus, on the other hand, incorporates a more physical intuition of noise by considering a symmetric interpretation of the stochastic integral, aligning more closely with the classical equations of motion [22]. However, for a functional approach to stochastic dynamics, Ito calculus is preferred, giving a one to one mapping between the drift and diffusive terms in the Langevin equation to those in the Fokker-Planck equation.

By applying either of these calculus rules to integrate the random forces detailed in the Fokker-Planck equation, one can derive a stochastic differential equation that not only resembles Langevin's original formulation but also generalizes it. This generalized form provides a more robust and comprehensive description of systems influenced by stochasticity, allowing for a deeper and more accurate modelling of physical phenomena where random forces play a critical role. A general Langevin equation in a one dimensional space is given by

$$\dot{x}(t) = f(x) + \sqrt{g(x)}\eta(t) \quad (1.6)$$

where now, $\eta(t)$ is a Gaussian random variable with zero mean and delta correlated variance, i.e., $\langle \eta(t)\eta(t') \rangle = \delta(t - t')$. The functions $f(x)$ and $g(x)$ are related to the drift and diffusion coefficients of the Fokker-Planck equation, in a manner that depends on the interpretation of stochastic integrals. Such an equation is termed Langevin equation in honour of the insight he had long before this was formally shown.

Having this stochastic differential equation, let us consider the case of a particle of a mass m diffusing in a fluid. Instead of analysing the position, if we consider the velocity of the particle v , then, it randomly changes with time, but also experiences a drag force due to the viscosity of the fluid given by $-m\gamma v$. Then, the equilibrium distribution of the velocity which can be derived from

the Fokker-Planck equation is given exactly by the Boltzmann distribution of velocity of gaseous molecules!

$$P_{st}(v) = \mathcal{N} e^{-\frac{mv^2}{2k_B T}} \quad (1.7)$$

where \mathcal{N} is the normalization factor of the probability distribution, k_B is the Boltzmann constant and T is the temperature of the system. Since we know that this particle is also diffusing with the diffusion constant D , we obtain the famous Einstein-Smoluchowski relation

$$D\gamma = k_B T \quad (1.8)$$

which connects the diffusion constant to the drag force in the fluid

The Boltzmann distribution is indeed predicated on the assumption of equilibrium. But we need a way to formalize this in our presented mathematical tools. Motivated by the thermodynamic idea that equilibrium implies no net energy flux between a system and any connected heat bath, we can consider the fluxes of the probability distribution at stationarity of the Fokker-Planck equation. which, at equilibrium, is zero. At this point, the system's microstates are redistributed according to the Boltzmann distribution, and there's no net movement or flow of probability, reflecting the system's equilibrium with its surroundings. From the velocity distribution, given a starting velocity v_0 at time t_0 , the probability to have a velocity v at time t is given by the propagator $P(v, t|v_0, t_0)$ which is the Green's function of the Fokker-Planck equation. Then, at stationarity, since there are no fluxes in the system, the probability to move in one direction and the probability to move in reverse has to be the same which is given mathematically as

$$P(v, t|v_0, t_0)P_{st}(v_0) = P(v_0, t|v, t_0)P_{st}(v) \quad (1.9)$$

for any arbitrary pair of velocities v, v_0 . This condition, known as Detailed Balance, states that for every microscopic change that takes place, the reverse change occurs with equal probability in equilibrium. This condition takes on a similar form for the discrete version in the Master equation, with the transition rates replacing the propagator. When this condition is satisfied, then, equilibrium is attained. The beauty of the Detailed Balance condition is that it is agnostic to the specific nature of the drift and diffusion forces acting within the system. Instead, it offers a broad criterion for equilibrium, applicable regardless of the exact forces or potentials at play. This universality allows for the examination of equilibrium distributions under various potential forces.

Considering an additional potential force $F(v) = -m\partial_v U(v)$, then, the equi-

librium distribution maintains a Boltzmann-like form, given by

$$P_{st}(v) = \mathcal{N} e^{-\frac{mv^2 + 2mU(v)}{2k_B T}} \quad (1.10)$$

Even within the equilibrium regime, the system exhibits fluctuations in velocity, underpinning phenomena such as the Einstein-Smoluchowski relation. These fluctuations, along with the accompanying dissipative forces, are explored in a broader class of theorems addressing the relationship between inherent fluctuations and dissipation in systems [4]. These theorems offer profound insights into how systems behave under various conditions and constraints, shaping our understanding of statistical mechanics and thermodynamics in equilibrium and near-equilibrium scenarios.

1.2 Fluctuations and dissipations

The interplay between the diffusion constant and frictional drag force reveals deeper insights into the behaviour of systems, particularly in how they respond to and recover from perturbations. Consider a scenario where a particle experiences a temporary increase in temperature, leading to a transient increase in velocity. Once the temperature returns to its original state, the system's stationary distribution will also revert, necessitating a relaxation of the velocity distribution back to its equilibrium form. This reversion is driven by the inability of diffusion to sustain the elevated velocities in the face of the prevailing drag force. The drag, therefore, acts as a restorative mechanism, guiding the out-of-equilibrium system back to its equilibrium state.

At the core of this dynamic lies a deep insight: one aspect of the system governs equilibrium fluctuations (diffusion), while another manages the response to out-of-equilibrium fluctuations (drag). The connection between these two seemingly disparate facets reflects an elegant principle of how systems dissipate energy and redistribute momentum, ensuring a return to equilibrium conditions, highlighting the inherent balance and self-regulating properties of physical systems.

The principles underlying the balance between fluctuations and dissipative forces extend well beyond the realms of diffusion and drag. In any system with fluctuations described by statistical mechanics, these dissipative forces have to be in balance. This balance manifests in various forms across different domains, including the behaviour of charged particles in electric fields [23], the relationship between the density of holes and electrochemical potential in semiconductors [24], the mobility of ions versus the conductivity of electrolytes, and even the behaviour of noisy electric currents in vacuum tubes [25].

Onsager's work in 1931 provided a pivotal formalization of the relationship between fluctuations and dissipation with his regression hypothesis [26, 27]. The central point of the hypothesis was that a relaxation back to equilibrium

after perturbation mirrors the pre-existing fluctuations of the system while at equilibrium. Essentially, the system's fluctuations are characterized by their correlation functions, and its recovery from perturbations is described by response functions. Hence, the fluctuation-dissipation theorem, which was proved a couple of decades later, was essentially a formulation also of response theory.

In the late 1960s, Kubo's formulation of linear response theory for Hamiltonian systems provided a rigorous framework for the fluctuation-dissipation theorem [28, 29]. The key argument was that given a Hamiltonian dynamics with (\vec{p}, \vec{q}) being the conjugate position and momenta, the perturbation can be expressed as a change in the Liouvillian, \mathcal{L} , resulting in a change in the associated phase space probability distribution $f(\vec{p}, \vec{q})$. If the perturbation is small enough, the subsequent change in f can be approximated to the first order. Then, an ensemble average of an arbitrary function in the phase space can be expressed as the convolution of a time-correlation function and the perturbation. Notably, Kubo's argument, while initially framed for Hamiltonian dynamics, is equally applicable when the Liouvillian is replaced with the Fokker-Planck operator. This relation, where the response of the system (or an observable) is connected to the time correlation of fluctuations at equilibrium, encapsulates the essence of the fluctuation-dissipation theorem.

The fluctuation-dissipation theorem prompts a departure from the conventional equilibrium-centric view of thermodynamic systems. It underscores the fact that any perturbation nudges an equilibrium system into a transient, non-equilibrium state. During this period, the principle of detailed balance is temporarily disrupted as the system evolves back towards equilibrium, reflecting the transient imbalances in probabilistic transitions.

However, the real intrigue arises in scenarios where a system is perpetually prevented from achieving equilibrium. Consider a gas exposed to two thermal baths at differing temperatures. Here, the gas acts as a conduit for energy, continuously transferring it from the hotter to the cooler reservoir without ever settling into an equilibrium state. In such scenarios, detailed balance is perpetually disrupted; the system is in a constant state of flux and disequilibrium [7].

Yet, reaching a stationary state in the Fokker-Planck equation doesn't necessarily require detailed balance. It allows for the existence of a time-invariant, yet non-equilibrium, stationary state. For the dual-temperature gas system, although it never achieves thermal equilibrium, it can reach a steady state where the temperature gradient and energy flux between the two reservoirs stabilize, and the system's overall behaviour becomes time-invariant. These scenarios are described as non-equilibrium stationary states (NESS), characterized by constant but directional flows of properties like energy, matter, or charge. They represent a fascinating class of systems that, while stable in certain macroscopic properties, perpetually operate away from equilibrium.

In thermodynamics, the principle that equilibrium systems maximize entropy is a cornerstone concept, implying that any deviation from equilibrium

necessitates energy expenditure, and subsequently, a non-constant entropy. For use in statistical mechanics, this requires an understanding of entropy beyond the classical thermodynamic sense. An arbitrary system described by a Master equation or Fokker-Planck equation might have a NESS which may not directly align with traditional thermodynamic behaviour. Hence, to connect thermodynamics to non-equilibrium systems, we need to refine the notion of detailed balance, leading to local detailed balance.

Local detailed balance applies the principle of detailed balance to each pair of states individually rather than to the system as a whole, allowing for the description of systems where not all states may simultaneously be at equilibrium [30]. This means,

$$\frac{P(x, t|x_0, t_0)}{P(x_0, t|x, t_0)} = e^{-s(x, x_0)} \quad (1.11)$$

The function $s(x, x_0)$ represents the energy expended during the transition which corresponds to the differences between forward flux and reverse flux. When this function simplifies to a difference of two functions whose arguments are x and x_0 respectively, i.e., $s(x, x_0) = s(x) - s(x_0)$, we recover detailed balance from local detailed balance with the corresponding equilibrium distribution being Boltzmann-like.

The hypothesis/notion of local detailed balance allows us to connect non-equilibrium systems to thermodynamics by explicitly showing that energy is being used to keep the system out-of-equilibrium. In various complex systems, a non-equilibrium steady state can be reached even when it's challenging to explicitly define the function $s(x, x_0)$. These situations might not allow for a straightforward application of classical thermodynamic entropy. Instead, the concept of entropy can be expanded and reinterpreted as informatic entropy, which offers an understanding of the system's reversibility or predictability. By treating entropy as a measure of information rather than solely as a physical quantity related to heat and work, the concept can be generalized to apply to a wider range of systems and scenarios [31].

A key point about equilibrium dynamics is that trajectories reversed in time have the same statistical weight as forward trajectories forward. To extend the concept of entropy for stochastic dynamics, one can consider the ratio of weights of forward path and reverse path, i.e., given a trajectory Γ_t at time t , define Γ_t^\dagger as the set of states reversed in time. Then, the entropy for the trajectory Γ_t is

$$\Sigma(\Gamma_t) \equiv \log \left(\frac{\mathcal{P}(\Gamma_t)}{\mathcal{P}(\Gamma_t^\dagger)} \right) \quad (1.12)$$

where \mathcal{P} signifies the probability of a trajectory. Under conditions of local detailed balance, this trajectory entropy can be shown to be the sum of entropies

caused by a directional energy flux between a pair of states. Note that since we are in a stochastic system, the entropy measure itself is stochastic, which means certain jumps between states could decrease entropy for a short period of time. However, if one considers both the system and the associated thermal bath in their entirety, the second law of thermodynamics remains intact [32]. But in a stochastic system where we do not explicitly consider the entropy of the heat bath, in a non-equilibrium regime, entropy *on average* always increases. This leads to the concept of entropy production rate, which serves as an indicator of how far a system is from equilibrium [33].

Hence, an alternate way to distinguish the non-equilibrium nature of a steady state is to measure the entropy production and to examine if this quantity is zero or increasing. Since entropy is a stochastic path variable, it follows a distribution of possible values at a given time. This leads to a powerful generalization of the Fluctuation-Dissipation Theorem for out-of-equilibrium systems, called fluctuation relations [34, 35]. This was first described by Evans in 1993, who showed that the ratio of positive entropy production to negative entropy production can be shown to be exponentially related to the entropy produced, i.e.,

$$\frac{Pr(-\Sigma)}{Pr(\Sigma)} = e^{-t\Sigma} \quad (1.13)$$

This implies that as time increases, the probability of observing a jump that goes against the second law of thermodynamics decreases exponentially. Furthermore, this also allows a generalization of the second law of thermodynamics for non-equilibrium systems by considering the trajectory-ensemble average of the probabilities of entropy leading to

$$\langle e^{-t\Sigma} \rangle = 1 \quad \forall t \quad (1.14)$$

The ability to quantify entropy production in non-equilibrium systems has broad implications. It enables the establishment of Thermodynamic Uncertainty Relations, which provide bounds on the average and variance of different currents in the system based on entropy production [36]. It also leads to Crook's work fluctuation theorem [37], which analyzes the fluctuations of work performed during forward versus reverse transitions, and the Jarzynski equality, which relates the work done on a system to the free energy change [38], even when the system is driven far from equilibrium. A broad field of study started due to advances in these areas, called stochastic thermodynamics. A big feature of this field is its closeness to biological systems which appear to operate at out-of-equilibrium regimes in order to extract maximum work.

However, not all non-equilibrium states are characterized by non-zero entropy production. A significant class of systems, resembling glasses, demonstrates out-of-equilibrium behaviour due to their unique relaxation times and memory effects [39]. In such systems, typically stemming from disordered in-

interactions like in spin glasses, the assumption of time translation invariance (where correlations depend only on the time difference) is violated. The system retains a memory of its initial state, leading to a breakdown of the traditional fluctuation-dissipation theorem. Instead, the relationship between fluctuations and dissipations is distinct from unity, indicating a departure from equilibrium behaviour. The Fluctuation-Dissipation Ratio (FDR), represented by $\chi_{A,B}(t, s)$, offers a measure of this departure. It is defined as

$$\chi_{A,B}(t, s) = \frac{TR_{A,B}(t, s)}{\frac{\partial}{\partial s}C_{A,B}(t, s)} \quad (1.15)$$

where T is the temperature, $R_{A,B}$ is the response function and $C_{A,B}$ is the correlation function between two observables A and B . It provides an index of the system's effective temperature, which can differ significantly from the ambient or actual temperature, thereby serving as an indicator of the system's non-equilibrium state. This ratio and the concept of effective temperature are particularly useful in understanding and characterizing the complex dynamics of glassy and other disordered systems.

The diverse mechanisms by which systems can be driven out of equilibrium indeed open up a vast landscape of potential behaviours, many of which diverge significantly from our established understanding of equilibrium processes. Such systems exhibit complex phenomena such as memory effects, ageing, and hysteresis, and can adapt and self-organize in ways that are not feasible at equilibrium. These behaviours are crucial for understanding a wide array of phenomena, from the intricate workings of biological organisms and ecosystems to the dynamics of climate and geophysical processes, as well as the functional principles of engineered systems and materials.

1.3 Description of biological systems

The development of various tools in non-equilibrium statistical mechanics over the last century has significantly contributed to an anti-reductionist, holistic approach, finding applications in a myriad of domains beyond traditional physics. Complex systems, characterized by their emergent properties, defy simplification into merely the sum of their parts. For a quantitative understanding, it's essential to start with a foundational description of the underlying processes, incorporating the influence of smaller-scale processes as effective impacts on the system of interest.

Statistical mechanics provides tools for this endeavour, particularly through coarse-graining techniques that integrate over different levels of detail to reveal macro-scale behaviours. This approach is particularly relevant to biochemical and sociological systems, where interactions occur across various scales, necessitating a framework that can accommodate and explain the interplay of

components [40]. For instance, the influence of external media on chemical reactions can be incorporated as stochastic noise [41], or movement of individuals in densely populated areas can be described using diffusive models [42]. Such an approach is particularly well suited for ecological systems, where the stochasticity is manifest in variations in birth and death rates, which can be modelled using the tools described before [43].

The random walker model on a line, traditionally described using the Master equation, is readily extendible to more complex one-dimensional systems with a discrete set of states where the transition rates are dependent on the current state. In such an extended model, transitions between states aren't uniform but vary according to specific rates that depend on the current state. The rate for a "birth" event, or an increase from state n to state $n + 1$, is denoted by $b_{n+1,n}$, while the rate for a "death" event, or a decrease from n to $n - 1$ is given by $d_{n-1,n}$. This state-dependent mechanism allows the model to capture a wide variety of processes and systems.

For example, in a physical context, the states might represent the position of a particle moving in a potential field, with the transition rates corresponding to the probability of the particle moving from one position to another under the influence of the potential. In macroecological studies, the states could represent the population size of a particular species, with birth and death rates modelling the growth and decline of the population due to reproduction, predation, and other ecological interactions. The Master equation for a birth-death process then is simply given by

$$\dot{P}_n = b_{n-1}P_{n-1} + d_{n+1}P_{n+1} - (b_n + d_n)P_n \quad (1.16)$$

where the time dependence of P_n has been suppressed for clarity, and $b_{n+1,n} \equiv b_n$ and $d_{n-1,n} \equiv d_n$. Depending on the support of P , which is based on the processes being described, the transition rates are set appropriately.

Somewhat similar to a random walker, if in a forest, the rate of birth of a species of a tree and the death are independent of the population, then $b_n = b$ with $d_n = d$. In such a case, the support is all non-negative states (arising from the description of state being the population size), with transition into negative states having zero value. This can also be represented as a set of "reactions", borrowing terminology from chemistry, to describe the underlying "microscopic process" (microscopic not in the spatial sense, but rather, where the stochasticity is present). If in a forest, ϕ describes an empty site and X describes a tree of a species, under well-mixed conditions, the reactions are



The first reaction refers to the birth event while the second one refers to a death event. Before proceeding to the solution of the Master equation and the effects of stochasticity, we can first compute the equation for the means given by

$$N(t) \equiv \langle N \rangle = \sum_{N=0}^{\infty} N P_N(t) \quad (1.19)$$

On using the birth-death Master equation, Eq (1.16), we find that the time evolution for mean population is simply

$$\dot{N}(t) = (b - d)N(t) \quad (1.20)$$

whose solution is the classic exponential growth/decay from theoretical ecology, with the parameter $r \equiv b - d$ and initial population N_0 , $N(t) = N_0 e^{rt}$. Many equations in classical theoretical ecology can similarly be expressed as arising from stochastic processes, whose equations of means were earlier given by phenomenological observation-based models [44].

Another great example of such a description is the classical consumer-resource model [45, 46], where N_s species reside in a well-mixed space with M_r number of unique resources. Each individual of species i denoted by X_i can use one or more of these resources given by C_μ to reproduce at a certain rate or die at a constant rate. The depleted resources are replenished by external events whose origins could be from biotic or abiotic processes. The resources can possibly also degrade naturally without the use by species. The microscopic reactions can then be written down as



where ϕ are empty sites for the species and φ are empty sites for the resources, which are much larger in number when compared to the observed number of species or resource units. In such a scenario, two species i and j do not compete directly but introduce second-order competitive effects through the use of common resources. An equation for means in this then gives

$$\dot{n}_i = -d_i n_i + \sum_{\mu=1}^{M_r} \alpha_{i,\mu} n_i r_\mu \quad (1.25)$$

$$\dot{r}_\mu = s_\mu - \delta_\mu r_\mu - \sum_{i=1}^{M_s} \alpha_{i,\mu} n_i r_\mu \quad (1.26)$$

where n_i and r_μ are the averages of species i and resource μ respectively.

In the context of forest dynamics, the concept of resource units can be somewhat abstract, making it challenging to directly connect the consumer-resource model to real-world scenarios. However, these concepts find a more tangible application in microbial ecology. In this field, resource units are clearly defined as molecules of carbon sources or other nutrients, and populations correspond to the number of individual microbes.

One notable application of these models in microbial ecology is in understanding the competitive dynamics between different species. Under certain simplifying assumptions about the rates of growth and decay, it emerges that the number of species that can coexist in a stable community is limited by the number of distinct resources available. This concept is encapsulated in the competitive exclusion principle, sometimes referred to as the Gause exclusion principle [47]. While this principle suggests a limit to species diversity based on resource availability, the actual observed diversity of microbes, especially in resource-limited environments, poses an intriguing paradox that continues to stimulate research.

In addition to providing insights into competition and diversity, the tools of the Master equation allow for an exploration of the effects of stochasticity on population numbers. In microbial systems, where observed population sizes are typically in the tens or hundreds of thousands, stochastic fluctuations in population size are often negligible, and deterministic models provide a good approximation of the dynamics. However, in macroecological contexts where individual populations may be much smaller, stochastic effects can become significant, influencing the dynamics and stability of populations and communities. Here, the Master equation and related stochastic models become crucial for accurately capturing and understanding the dynamics of these systems.

In considering the birth-death process, moving beyond the mean equations to examine the time evolution of the probability distribution offers a complete description of the process. This approach allows one to derive the stationary distribution for a generic birth-death process with rates b_n and d_n , given by

$$P_{st}(n) = \mathcal{N} \prod_{x=1}^n \frac{b_{x-1}}{d_x} \quad (1.27)$$

where \mathcal{N} is again the normalization constant of the distribution. By choosing

appropriate b_n and d_n , one can derive various distributions known from classical statistical mechanics, although their ecological relevance may vary [16].

In ecological contexts, the relevance and applicability of these models often depend on incorporating density dependence into the transition rates. The simplest form of such a dependence is linear scaling with population size, $b_n = bn$ and $d_n = dn$. Expanding on these ideas, one can consider a null model in ecology where similar birth-death dynamics apply across all species in a community, assuming minimal differences between species. This approach is the foundation of the neutral theory of biodiversity, which posits that the differences in species abundances and distributions are largely due to stochastic processes rather than distinct species characteristics [48]. Despite its simplicity, neutral theory has been remarkably successful in predicting various distributions of species observed in different ecosystems.

While the Master equation provides a rigorous framework for modelling birth-death processes and other stochastic phenomena, solving it can be challenging, especially for complex or large systems. An alternative and often more tractable approach is to use the Fokker-Planck equation. In the context of forest dynamics, considering second-order density dependence in population changes allows for the derivation of an effective Langevin equation [49]. This equation describes the continuous-time evolution of a species' population x and includes both deterministic and stochastic components:

$$\dot{x} = b - \frac{x}{\tau} + \sqrt{2Dx}\eta(t) \quad (1.28)$$

where b represents the birth rate, τ is the characteristic timescale of decay, and D is the noise strength. This Langevin equation can be transformed into a corresponding Fokker-Planck equation, which then allows for the solution of the population's probability distribution both at stationarity and at arbitrary times. When applied within the framework of neutral theory, the resulting distributions from these models provide good approximations to empirical data from various forest ecosystems.

Moreover, the utility of Langevin equations extends far beyond ecological studies. They have become foundational in financial modelling, underlying influential models like the Cox-Ingersoll-Ross and Black-Scholes models [50, 51], among others. While the exact parameters and interpretations may differ between ecological and financial contexts, the underlying dynamics characterized by continuous changes with both deterministic trends and stochastic fluctuations are observed universally across many systems [52]. This universality highlights the fundamental nature of these equations and their wide applicability in understanding and predicting the behaviour of complex, dynamic systems in various domains.

1.4 Philosophy of complex systems

Much of scientific history has been driven by reductionism, starting all the way from Galileo's method of analysis and synthesis [53] (*metodo risolutivo* and *metodo compositivo*) where one goes from the whole to the part, dividing aspects of systems into its constituents and then attempting to put it back together. This drive for seeking atomic units across different domains of science partly worked perhaps due to the tangible nature of discoveries. This approach has led to the proliferation of numerous specialized sub-fields, extending beyond physics into chemistry and biology, despite the latter's origins in observation-based methodologies *a la* Francis Bacon [54]. However, the philosophy of reductionism also aligns with the innate human curiosity to understand the 'why' and 'how' behind natural phenomena to the deepest extent. Ultimately, the Standard Model picture would not have been possible without a strong reductionist undercurrent pinning the physics of 20th century.

While reductionism is an essential component of scientific enquiry, the knowledge of parts need not lend itself to the knowledge of the whole [55]. The *metodo compositivo* of Galileo is effective in situations of limited constituents. The principle "More is different", famously stated by physicist Philip Anderson [56], serves as a critical reminder of this limitation, suggesting that as systems grow in complexity, they exhibit behaviours and properties that are not predictable from the understanding of their simpler, constituent parts alone. But this sentiment is echoed by many other prominent scientists in various fields. Notably, in line with this thesis, one of the most famous theoretical biologist, JBS Haldane mentions the paradox, "If my mental processes are determined wholly by the motions of atoms in my brain, I have no reason to suppose that my beliefs are true ... and hence I have no reason for supposing my brain to be composed of atoms" [57].

Though the importance of holistic approach was understood, it remained a fringe philosophy, not blooming into its full potential till the necessary circumstances came together. The advent of substantial computational power and the maturation of mathematical tools, especially in network theory, have catalyzed the exploration of complex systems [58]. Initially led by statistical physicists dealing with the impracticality of managing excessive detail, this endeavour has expanded significantly with the computational revolution, allowing previously intractable problems to be addressed.

While navigating the philosophical implications of these developments in statistical mechanics, a pertinent question arises regarding the classification of today's complex systems studies within the realm of "physics". This debate is not merely academic but influences the organization and focus of research in university departments worldwide. However, questioning the disciplinary boundaries of physics may inadvertently rest on a reductionist foundation, presupposing a rigid categorization of scientific knowledge. By considering the evolutionary nature of scientific disciplines [59], where today's philosophical

and mathematical inquiries might become tomorrow's physics, we recognize the limitation of strict categorization. Today, the distinction of what constitutes "physics" is increasingly blurred, as complex systems studies permeate various scientific domains, challenging traditional disciplinary boundaries [60, 61].

Just as there are debates around the limitations and applicability of reductionism, exemplified by the discussions around the validity and philosophy of string theory, holism too invites scrutiny about its potential limits. The holistic approach, while offering a comprehensive view of complex systems, risks oversimplification or misinterpretation if taken to an extreme without acknowledgement of individual components' roles and interactions. Norbert Wiener's "The Human Use of Human Beings," a foundational text in cybernetics, embodies the potential overreach of holistic thought. The central thesis of the book suggests that "society can only be understood through a study of the messages and the communication facilities which belong to it" [62]. By suggesting that societal understanding is predominantly a function of communication patterns, it adopts a deterministic view that may conflict with notions of individual autonomy, free will, and the intrinsic unpredictability of human behaviour.

This raises a philosophical dilemma about the extent to which holistic models can or should encapsulate complex systems, whether in society, biology, or other domains. While holistic approaches provide invaluable insights into the emergent properties and behaviours of systems, they must be balanced with an understanding of the systems' granular details and the unpredictable nature of their components. As we delve deeper into the interconnectedness of various scientific fields and the complex systems they study, maintaining a critical awareness of the limitations and appropriate applications of both reductionism and holism becomes crucial. This balance ensures that while embracing the broad view of holism, we don't lose sight of the individual elements and uncertainties that contribute to the richness and diversity of the natural world.

This section represents a personal reflection on the philosophical considerations that underpin my exploration in the field. It is not my intention to provide definitive answers to the questions posed here. Periodically revisiting these questions can significantly enrich the philosophical depth of one's research. It prompts one to continually consider how the underlying philosophy of scientific pursuits aligns with or challenges the broader philosophical facets of human nature.

In the subsequent sections of this dissertation, I will delve into a series of studies focused on out-of-equilibrium behaviours observed across different scales, emphasizing the roles of fluctuations and boundary conditions in driving these dynamics. For each scale, I will present a specific problem that we have attempted to understand and resolve. The scope of these investigations spans from theoretical analyses of entropy production fluctuations in general non-equilibrium systems to practical examinations of induced fluctuations and their emergent, higher-order effects in microbial communities. The thesis will end

with a concluding remark based on these findings, drawing connections between the various scales of study and discussing the broader implications of our results.

FLUCTUATIONS OF ENTROPY PRODUCTION

The following chapter is the basis of published work [63] “Fluctuations of entropy production of a run-and-tumble particle” [P. Padmanabha, D. M. Busiello, A. Maritan, and D. Gupta; Phys Rev E 107, 014129 (2023)]. Parts of the contents presented, including displayed figures, are taken with permission from the published work, copyright (2023) by the American Physical Society.

2.1 Introduction

As discussed previously, biological systems are often found out of equilibrium. They maintain a non-equilibrium steady state by constantly consuming energy [64, 65], displaying a variety of new behaviour not found in equilibrium [66, 67, 68]. A net production of entropy is one of the most relevant signatures indicating non-equilibrium conditions where the time reversal symmetry is broken. This serves as a quantification of the distance from thermodynamic equilibrium [69, 33]. Even outside the context of biological systems, entropy production and its features have been extensively studied [32, 70, 71, 72, 73] since it marks as a fundamental feature of non-equilibrium regime.

Fluctuations of different kinds of fluxes in the system can be investigated within the framework of stochastic thermodynamics for different quantities [74, 32, 75]: the work performed on a system [76, 77, 78], the entropy production [79, 80, 81, 82], the heat flow [83, 84, 78, 85], and the efficiency of a stochastic engine [86, 87, 88, 89, 90].

Equilibrium systems can be described according to certain elementary thermodynamic principles which include minimum free energy and maximum entropy. Contrarily, non-equilibrium systems lack such overarching basic principles that are applicable to all systems. However, some universal laws that hold out-of-equilibrium exist. This is shown through several results which are system independent and are valid not just near equilibrium. Some examples are fluctuation theorems [34, 37, 35, 91, 92], the Jarzynski equality [38], the Crooks work-

fluctuation theorem [37, 93], the non-equilibrium linear response [94, 95], and the thermodynamic uncertainty relations [36, 96, 97, 98].

Entropy production plays a prominent role in this context. Its fluctuations are important in linear response theory, fluctuation theorems, and thermodynamic uncertainty relations. In this context, various studies have focused on the estimation of the mean entropy production, both theoretically and experimentally, by using different methods, such as uncertainty relations [99, 100, 101], waiting-time distributions [102], machine learning [103], and stochastic single-trajectory data [104, 105, 106]. While an explosion of research investigate the mean entropy production, there is a lack of general understanding of the properties of its probability density function (pdf). Nevertheless, researchers have obtained the distribution of entropy production for specific settings using analytical [107, 108, 109], numerical [110], and experimental techniques [111, 112, 113].

Having an estimate for the moments of the entropy production distribution might be as important as quantifying its mean. Measuring a very small average entropy production does not necessarily imply that the system is close to equilibrium, due to potentially large fluctuations of its dissipation. In fact, estimating the entire probability density function provides information about this variability [114]. From a broader perspective, our understanding of biological and chemical systems might benefit from the knowledge of fluctuations of any thermodynamic quantity [115, 116, 33, 117, 118, 119]. Following this research direction, in [120] the authors introduce a method to infer mean and variance of entropy production from short-time experiments, while in [112] these quantities are estimated numerically using differential equations for moments of dissipated heat, following [121]. Some studies place bounds on all steady-state currents, including entropy production [122], specifically through techniques of linear response theory [123], and large deviation theory [97]. There exists no theoretical framework to compute the distribution of entropy production which applies to a large class of systems. One of the difficulties encountered is that entropy production is a trajectory-dependent quantity, a property that makes the analytical computation of its statistics beyond the mean a difficult task.

On the biological application side, modelling of active self-propelled particles has been a buzzing field. These particles break detailed balance via a self-driven term that leads to a wide range of non-equilibrium phenomena [124, 125, 126]. Some examples include self assembly [127, 128], spontaneous segregation [129], and motility induced phase separation [130, 131]. Considering the non-equilibrium nature of such systems, a detailed analysis of their thermodynamic features arises as a natural problem to be addressed. . Fluctuation theorems in active Ornstein-Uhlenbeck processes [132, 133, 134], stochastic thermodynamics of active particles [135, 136], their entropy production [137, 138, 139, 140, 141], heat fluctuations of interacting active particles [142], and experimental measurements of uncertainty relations [143] are only a few ex-

amples of works performed in this area.

One of the most studied models for active matter components is the run-and-tumble motion. Particles undergoing this dynamics capture the typical homonymous behavior displayed by microorganisms, such as *E. Coli*, characterized by driven diffusive dynamics (run) interspersed by random changes of the velocity direction (tumble) [144, 145]. In its simplest form, the model consists of a random walker whose velocity direction is influenced by a dichotomous noise [146, 147], often referred to as ‘telegraphic’ noise [148]. Though the use of run-and-tumble models to study non-equilibrium properties is a relatively recent development, the probability of finding a run-and-tumble walker in a particular position obeys the well known telegrapher’s equations, which are coupled linear partial differential equations describing the evolution of voltage and current in an electrical transmission line [149, 150]. This connection to a classic system provides more tools to understand the non-equilibrium properties we wish to investigate. In addition to displaying motion similar to microorganisms, run-and-tumble particles exhibit interesting steady states [151, 147] which also leads to clustering near the boundaries [145]. Recent studies have also investigated the first passage properties of this system with [150] and without stochastic resetting [152].

Run-and-tumble particles have been shown to have non-zero average entropy production in one dimension [153]. Due to their popularity, the dynamics might serve as a paradigmatic model to study active matter systems. In this Chapter, we describe a spatially discrete state run-and-tumble model and present a graphical method to compute cumulants of the entropy production at any order. Although obtaining the full distribution remains a lofty goal, our formalism can be, in principle, extended up to a desired precision. This can also be extended to Langevin systems under a proper coarse-graining procedure, leading to analytical computations of entropy production cumulants in continuous state systems as well.

2.2 Cumulants of entropy production

We consider a run-and-tumble walker on a discrete state-space. The walker hops with a switching rate r between two lanes, representing two different velocity directions in a one-dimensional system. On the upper (lower) lane, the walker hops forward with a rate a (b), and backward with a rate b (a). Without loss of generality, we consider $a > b$. The schematic diagram describing the system is shown in Fig. 2.1. Thus, the system consists of $2N$ states, of which N states are in the $+$ regime (i.e., upper lane), and the remaining N are in the $-$ regime (i.e., lower lane), representing a Markovian and discrete version of the spatially continuous one dimensional run-and-tumble model [153]. Here ‘+’ and ‘-’ correspond to the direction in which the walker hops on average.

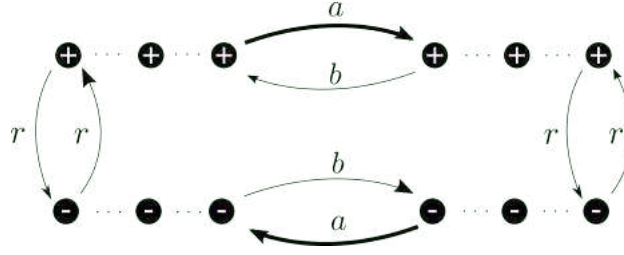


Figure 2.1: Schematic representation of a run-and-tumble particle. Top layer: + regime. Bottom layer: - regime. The particle hops forward and backward, respectively, with a rate a (b) and b (a) in the + (-) regime, where $a > b$. Moreover, the particle switches states in between the two layers with a rate r .

Summarizing, the master equation governing the probability of finding a particle in the i -th state is [9]

$$\dot{P}(i, t) = \sum_j H_{ij} P(j, t) \quad (2.1)$$

Since the probability distribution is normalized at all times, i.e. $\sum_i P(i, t) = 1$, and we consider a system in which if $H_{ij} \neq 0$, so is H_{ji} , since there are no unidirectional transitions (an assumption which we will relax in the following Chapters).

In the case of a discrete state-space, the total entropy production, Σ_{tot} , at the level of a single trajectory is defined as follows. Given a forward trajectory $\Gamma \equiv \{(i_0, t_0), (i_1, t_1), \dots, (i_M, t_M)\}$, where the state i_k is visited at time t_k and changes to state i_{k+1} at time t_{k+1} , the asymmetry between the probability of forward and reverse trajectories quantifies the total entropy production [74, 32, 154, 155]:

$$\Sigma_{\text{tot}}(\Gamma) \equiv \ln \frac{\mathcal{P}(\Gamma)}{\mathcal{P}(\Gamma^\dagger)}, \quad (2.2)$$

where $\mathcal{P}(\Gamma)$ and $\mathcal{P}(\Gamma^\dagger)$, respectively, are the probabilities of observing a forward and a time-reversed trajectory. Following [156], the total entropy production along the trajectory Γ reads:

$$\Sigma_{\text{tot}}(\Gamma) = \ln \left[\frac{P(i_0, t_0)}{P(i_M, t_M)} \prod_{i,j \in \Gamma} \left(\frac{W_{ij}}{W_{ji}} \right)^{n_{ij}} \right], \quad (2.3)$$

where $P(i_0, t_0)$ and $P(i_M, t_M)$, respectively, are the probabilities of initial and final states of the trajectory, and $n_{ij} \equiv n_{i \leftarrow j}$ counts the number of jumps from the state j to i in the trajectory Γ . Σ_{tot} can be split into two contributions: system entropy production Σ_{sys} , and environment entropy production Σ_{env} . In particular, Σ_{env} is associated with the heat dissipated by the particle into the surrounding bath along the trajectory Γ , taking into account the transitions occurring along

the trajectory:

$$\Sigma_{\text{env}}(\Gamma) \equiv \sum_{i,j \in \Gamma} n_{ij} \ln \frac{W_{ij}}{W_{ji}}, \quad (2.4)$$

where j precedes i in the trajectory Γ . Σ_{env} is the only term that survives in the stationary state, when averaged over many trajectories [156]. Additionally, for any finite discrete-state systems, $\Sigma_{\text{sys}} = \Sigma_{\text{tot}} - \Sigma_{\text{env}}$ is a boundary term involving the initial and final states for each trajectory, and is the sub-leading contribution to the total entropy production in the long-time limit.

Since the number of jumps, n_{ij} , performed by the run-and-tumble walker is a trajectory-dependent quantity, i.e., it varies from one realization to another, the knowledge of its statistics is required to obtain the fluctuations of the entropy production in Eq. (2.4).

To compute the various correlations of the number of jumps, we start from a simpler dynamical model: a Markov chain [8, 157]. Unlike the master equation in which the time changes continuously, now the time increases in discrete steps, Δt . In one time increment, the transition probability of the system to jump from the state j to i is $\mathcal{P}(i, t + \Delta t | j, t) \equiv A_{ij} = W_{ij} \Delta t$ for $i \neq j$, and the probability of staying in the state i is $A_{ii} = 1 - \sum_{j \neq i} W_{ji} \Delta t = 1 + W_{ii} \Delta t$. It follows that the sum of the elements of each column is unity, i.e., $\sum_i A_{ij} = 1$. Therefore, the Markov chain equation is

$$P(i, t + \Delta t) = \sum_{j=1}^{2N} A_{ij} P(j, t). \quad (2.5)$$

In the limit $\Delta t \rightarrow 0$, the above equation (2.5) reduces to the master equation (2.1). Note that herein we are considering time-independent transition rates.

Since the time evolution runs only over times multiple of Δt , fixing the observation time T is equivalent to fixing the total number of jumps to $T/\Delta t$. In a Markov chain, time is a bookkeeping measure, and therefore, we are able to consider equally spaced time intervals for the trajectory. Hence, the probability of a Markov chain (MC) trajectory $\Gamma_{\text{MC}} \equiv \{(i_0, t_0), (i_1, t_1), \dots, (i_M, t_M)\}$, where $t_k = t_0 + k\Delta t$ is:

$$\mathcal{P}(\Gamma_{\text{MC}}) \equiv A_{i_M i_{M-1}} A_{i_{M-1} i_{M-2}} \cdots A_{i_2 i_1} A_{i_1 i_0} P(i_0, 0), \quad (2.6)$$

where $P(i_0, 0)$ is the initial probability distribution of the run-and-tumble walker at time $t_0 = 0$. Note that in Eq. (2.6), it is possible that $i_{k+1} = i_k$ for some k 's, i.e., there is a possibility of staying in the same state after the time interval Δt which is a consequence of imposing M equally spaced time intervals. When we move back to the master equation, these probabilities of staying in the same state lead to exponential waiting time distributions of times between jumps from one state to another, thereby Γ_{MC} converges to Γ .

The path probability, $\mathcal{P}(\Gamma_{\text{MC}})$, is normalized over all trajectories, i.e.,

$$\begin{aligned} \sum_{\Gamma_{\text{MC}}} \mathcal{P}(\Gamma_{\text{MC}}) &= \sum_{i_M, i_{M-1}, \dots, i_1, i_0} A_{i_M i_{M-1}} A_{i_{M-1} i_{M-2}} \cdots \\ &\quad \times A_{i_2 i_1} A_{i_1 i_0} P(i_0, 0) = 1, \end{aligned}$$

where we used $\sum_i A_{ij} = 1$ for each summation.

The number of jumps performed up to the time T across a link from ℓ to m in a trajectory Γ is then:

$$n_{m\ell}(\Gamma_{\text{MC}}) \equiv \sum_{k=0}^{M-1} \delta_{i_{k+1}, m} \delta_{i_k, \ell}, \quad (2.7)$$

where the Kronecker deltas give 1 whenever the system performs jumps from state ℓ to m .

Let us first compute the average number of jumps over all possible trajectories:

$$\langle n_{m\ell} \rangle_{\Gamma_{\text{MC}}} = \sum_{\Gamma_{\text{MC}}} \mathcal{P}(\Gamma_{\text{MC}}) \sum_{k=0}^{M-1} \delta_{i_{k+1}, m} \delta_{i_k, \ell} \quad (2.8a)$$

$$= \sum_{k=0}^{M-1} \sum_{i_M, i_{M-1}, \dots, i_1, i_0} A_{i_M i_{M-1}} A_{i_{M-1} i_{M-2}} \cdots A_{i_2 i_1} A_{i_1 i_0} P(i_0, 0) \delta_{i_{k+1}, m} \delta_{i_k, \ell} \quad (2.8b)$$

$$= \sum_{k=0}^{M-1} \sum_{i_M, \dots, i_{k+1}, i_k, i_{k-1}} A_{i_M i_{M-1}} \cdots A_{i_{k+1} i_k} \delta_{i_{k+1}, m} \delta_{i_k, \ell} A_{i_k i_{k-1}} \\ \times \sum_{i_{k-2}, \dots, i_0} A_{i_{k-1} i_{k-2}} \cdots A_{i_1 i_0} P(i_0, 0) \quad (2.8c)$$

$$= \sum_{k=0}^{M-1} \sum_{i_{k-1}, \dots, i_0} A_{m\ell} A_{\ell i_{k-1}} A_{i_{k-1} i_{k-2}} \cdots A_{i_1 i_0} P(i_0, 0) \quad (2.8d)$$

$$= \sum_{k=0}^{M-1} A_{m\ell} P(\ell, k\Delta t). \quad (2.8e)$$

To go from Eq. (2.8b) to (2.8c), we move the Kronecker deltas next to the \hat{A} 's matrix elements with the corresponding indices, and identify two groups of indices. Then, the summation over i_M, \dots, i_{k+2} gives 1 using the property $\sum_i A_{ij} = 1$, while the one over the indices $k+1$ and k can be carried out using the Kronecker delta. The resulting expression is in Eq. (2.8d). Finally, we use the Markov chain evolution in Eq. (2.5) to perform the summation on indices i_{k-1} to i_0 to obtain the last equality, Eq. (2.8e).

Similarly, we compute the correlations between two sets of jumps:

$$\begin{aligned}
\langle n_{m\ell} n_{m'\ell'} \rangle_{\Gamma_{\text{MC}}} &= \sum_{\Gamma_{\text{MC}}} \mathcal{P}(\Gamma_{\text{MC}}) \sum_{k=0}^{M-1} \delta_{i_{k+1},m} \delta_{i_k,\ell} \\
&\times \sum_{k'=0}^{M-1} \delta_{i_{k'+1},m'} \delta_{i_{k'},\ell'} \\
&= \sum_{k=0}^{M-1} \sum_{k'=0}^{M-1} \sum_{i_M, \dots, i_0} \delta_{i_{k+1},m} \delta_{i_k,\ell} \delta_{i_{k'+1},m'} \\
&\times \delta_{i_{k'},\ell'} A_{i_M i_{M-1}} \dots A_{i_1 i_0} P(i_0, 0).
\end{aligned}$$

We split the second summation over k' depending on three different scenarios: 1) $k' < k$, 2) $k' = k$, and 3) $k' > k$. Performing similar calculations as in the case of the first moment, we obtain, for $k' < k$,

$$\begin{aligned}
\langle n_{m\ell} n_{m'\ell'} \rangle_{\Gamma_{\text{MC}}} &= \sum_{k=0}^{M-1} \sum_{k'=0}^{k-1} A_{m\ell} \mathcal{P}(\ell, k\Delta t | m', (k'+1)\Delta t) \\
&\times A_{m'\ell'} P(\ell', k'\Delta t),
\end{aligned} \tag{2.10}$$

for $k < k'$,

$$\begin{aligned}
\langle n_{m\ell} n_{m'\ell'} \rangle_{\Gamma_{\text{MC}}} &= \sum_{k=0}^{M-1} \sum_{k'=k+1}^{M-1} A_{m'\ell'} \mathcal{P}(\ell', k'\Delta t | m, (k+1)\Delta t) \\
&\times A_{m\ell} P(\ell, k\Delta t),
\end{aligned} \tag{2.11}$$

and for $k' = k$,

$$\langle n_{m\ell} n_{m'\ell'} \rangle_{\Gamma_{\text{MC}}} = \sum_{k=0}^{M-1} A_{m\ell} P(\ell, k\Delta t) \delta_{m,m'} \delta_{\ell,\ell'}. \tag{2.12}$$

Combining the above three contributions, Eqs. (2.10), (2.11), and (2.12), finally we obtain:

$$\begin{aligned}
\langle n_{m\ell} n_{m'\ell'} \rangle_{\Gamma_{\text{MC}}} &= \\
&\sum_{k=0}^{M-1} \left[\sum_{k'=0}^{k-1} A_{m\ell} \mathcal{P}(\ell, k\Delta t | m', (k'+1)\Delta t) A_{m'\ell'} P(\ell', k'\Delta t) \right. \\
&+ \sum_{k'=k+1}^{M-1} A_{m'\ell'} \mathcal{P}(\ell', k'\Delta t | m, (k+1)\Delta t) A_{m\ell} P(\ell, k\Delta t) \\
&\left. + A_{m\ell} P(\ell, k\Delta t) \delta_{m,m'} \delta_{\ell,\ell'} \right].
\end{aligned} \tag{2.13}$$

Such calculations become tedious on proceeding to higher order correlations. However, we present a graphical method to scale up the calculations to any

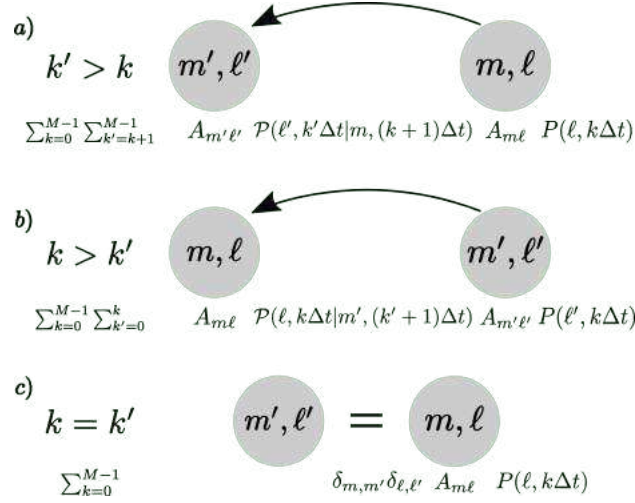


Figure 2.2: Graphical representation for the computation of second order correlation for number of jumps. a) $k' > k$, b) $k > k'$, and c) $k' = k$. Circle indicates the set of states corresponding to the summation label, either k or k' . The arrow and equality, respectively, correspond to the transition probability from left set of states to the right ones, and the Kronecker deltas equating the set of states.

order of correlations of the number of jumps. For a given correlation, we first determine the set of all possible time-orderings of k -s, i.e., the times at which a specific jump takes place. For the first moment, there is only one jump considered, hence no ordering is required. For the correlations between two sets of jumps, say $\{m, \ell\}$ and $\{m', \ell'\}$, happening at times $k\Delta t$ and $k'\Delta t$ respectively, as mentioned earlier, the possible permutations are $k < k'$, $k > k'$, and $k = k'$. Once all the orderings are listed, the set of states are graphically located according to the orderings. For example, corresponding to $k < k'$, the set of states $\{m, \ell\}$ appears before in time than the set of states $\{m', \ell'\}$. Notice that in what follows, we consider the time-axis from right to left to be consistent with the ordering at which propagators appear.

Fig. 2.2 shows possible orderings for the second order correlation.

For $k' > k$ (see Fig. 2.2a), the rightmost circle carries a contribution from its starting state, $\{m, \ell\}$, at time $k\Delta t$. The contribution is equal to its probability $A_{m\ell}P(\ell, k\Delta t)$. Then the system moves towards the left circle, which is associated to the final set of states in this scenario. This transition comes with its propagator: $A_{m'\ell'}\mathcal{P}(\ell', k'\Delta t | m, (k+1)\Delta t)$. Finally the summation runs over all possible indices k and k' with the prescribed ordering ($k' > k$ in this case). Hence, we can immediately write the contribution to the second order correlation as given by Eq. (2.11). Similarly, we can write the contributions for $k' = k$, and $k' < k$.

For the third order correlation, repeating the graphical procedure leads to 13 possible orderings with three k -s indices (i.e., k, k', k''). We show all the orderings in Fig. 2.3. Writing down the summation terms according to the graphical rules, we find them to be equal to those obtained from the full calculation. In order to avoid clutter, we relegate the detailed form of the third order jump

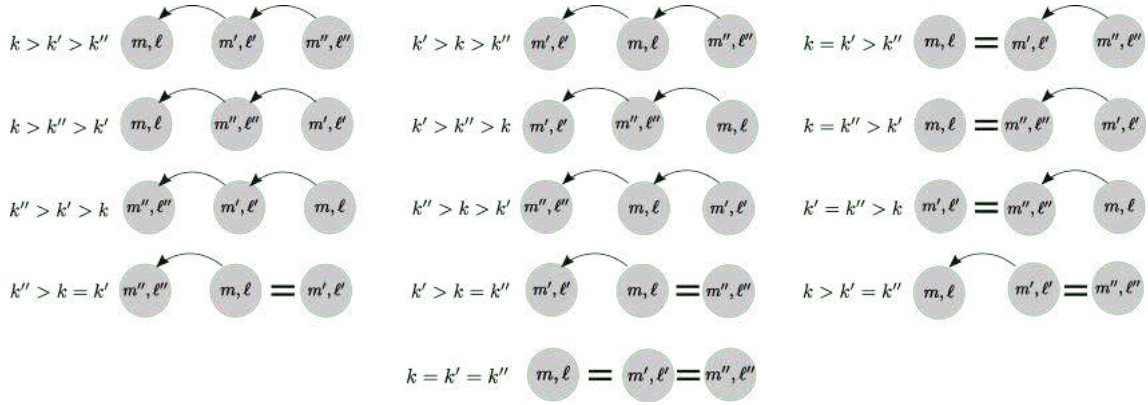


Figure 2.3: Possible orderings in the graphical method for the third order correlation of number of jumps.

correlation to Appendix A in 7.1.

To move back from a Markov chain to a master equation description, we rewrite the transition probability as $A_{m\ell} = W_{m\ell}\Delta t$, $m \neq \ell$, and take the limit $\Delta t \rightarrow 0$. Thus, each summation over k -s appearing in the jump correlations is converted into an integral over time, t . Although the calculations shown above are valid for an arbitrary initial condition, in what follows, we focus on the case in which the system starts from an initial steady state distribution, $P(i_0, t_0) = P^{\text{st}}(i_0)$ and $P(i_M, T) = P^{\text{st}}(i_M)$. Thus, the jump correlations in Eqs. (2.8e) and (2.13) in the continuous-time limit read:

$$\begin{aligned} \langle n_{m\ell} \rangle_{\Gamma} &= \int_0^T dt W_{m\ell} P^{\text{st}}(\ell), \quad (2.14) \\ \langle n_{m\ell} n_{m'\ell'} \rangle_{\Gamma} &= \int_0^T dt \left(\int_0^t dt' W_{m\ell} \mathcal{P}(\ell, t | m', t') W_{m'\ell'} \right. \\ &\quad \times P^{\text{st}}(\ell') + \int_t^T dt' W_{m'\ell'} \mathcal{P}(\ell', t' | m, t) \\ &\quad \left. \times W_{m\ell} P^{\text{st}}(\ell) \right) \\ &\quad + \int_0^T dt W_{m\ell} P^{\text{st}}(\ell) \delta_{\ell, \ell'} \delta_{m, m'}, \quad (2.15) \end{aligned}$$

where $\mathcal{P}(\ell', t' | m, t)$ is the probability to be in the state ℓ' at time t' , starting from the state m at time t , computed from the master equation. The same limit can be computed for the third order correlation.

The integration on the right-hand side of first jump moment, Eq. (2.14), yields:

$$\langle n_{m\ell} \rangle_{\Gamma} = T W_{m\ell} P^{\text{st}}(\ell), \quad (2.16)$$

whereas the computation of higher order jump moments requires the knowl-

edge of the transition probability: $\mathcal{P}(i', t' | i, t)$. To this end, we use the eigenvector expansion of the transition rate matrix \hat{W} to compute such quantity. The master equation can be written in a compact matrix form:

$$|\dot{P}(t)\rangle = \hat{W} |P(t)\rangle, \quad (2.17)$$

where $|P(t)\rangle = [P(1, t), P(2, t), \dots]^\top$ is the probability vector, and \top is the matrix transpose operator. The solution of the above linear differential equation (2.17), given an initial state vector $|P(t_0)\rangle$, is

$$|P(t)\rangle = e^{\hat{W}(t-t_0)} |P(t_0)\rangle. \quad (2.18)$$

Let $\langle\psi_j|$ and $|\phi_j\rangle$, respectively, be the j -th left and right eigenvectors of the transition rate matrix, \hat{W} , corresponding to eigenvalue λ_j . The left and right eigenvectors satisfy the normalization condition [9]:

$$\langle\psi_j|\phi_{j'}\rangle = \delta_{j,j'}. \quad (2.19)$$

Expanding the right-hand side of Eq. (2.18) in the eigenbasis of \hat{W} gives:

$$|P(t)\rangle = \sum_j \langle\psi_j|P(t_0)\rangle e^{-\lambda_j(t-t_0)} |\phi_j\rangle, \quad (2.20)$$

where $0 = \lambda_1 < \text{Re}(\lambda_2) \leq \text{Re}(\lambda_3) \leq \dots \leq \text{Re}(\lambda_{2N})$, where $\text{Re}(\lambda_j)$ represents the real part of λ_j . This hierarchy is guaranteed in finite and discrete system due to the Perron-Frobenius theorem.

The system considered here reaches a steady-state in the long-time limit, $|P(t \rightarrow \infty)\rangle \rightarrow |P^{\text{st}}\rangle$ which is the right eigenvector corresponding to $\lambda_{j=1} = 0$ eigenvalue, i.e., $|\phi_{j=1}\rangle$. Since $\langle\psi_{j=1}|$ is a row vector with all entries equal to 1, it gives the condition $\langle\psi_{j=1}|P(t_0)\rangle = \sum_i P(i, t_0) = 1$.

In particular, if the initial state vector $|P(t_0)\rangle$ is a column vector of all zeros except 1 at i_0 -th location, then the system is in the state i_0 at time t_0 . Let us call this vector $|i_0\rangle$. Then, the probability of the system to be in state i at time t given the initial state i_0 at time t_0 , $\mathcal{P}(i, t | i_0, t_0) \equiv \langle i | P(t) \rangle$, can be written as:

$$\mathcal{P}(i, t | i_0, t_0) = \sum_j c_j(i_0) e^{-\lambda_j(t-t_0)} \phi_j(i), \quad (2.21)$$

where we defined the projection of the left eigenvector onto the initial state as the coefficients of the expansion, i.e., $c_j(i_0) \equiv \langle\psi_j|i_0\rangle$. Similarly, we define $\phi_j(i) \equiv \langle i|\phi_j\rangle$.

Using the eigenvector expansion, Eq. (2.21), in the integrals appearing in Eq. (2.15), we obtain

$$\begin{aligned} \langle n_{m\ell} n_{m'\ell'} \rangle_{\Gamma} &= W_{m\ell} W_{m'\ell'} \left[P^{\text{st}}(\ell) P^{\text{st}}(\ell') T^2 + \sum_{j>1} [c_j(m) \phi_j(\ell') P^{\text{st}}(\ell) + c_j(m') \phi_j(\ell) P^{\text{st}}(\ell')] \right. \\ &\quad \left. \times \frac{1}{\lambda_j} \left(T - \frac{1}{\lambda_j} (1 - e^{-\lambda_j T}) \right) \right] + \delta_{\ell,\ell'} \delta_{m,m'} W_{m\ell} P^{\text{st}}(\ell) T. \end{aligned} \quad (2.22)$$

For the third order jump correlation, let us consider an example of one of the orderings, $k < k' < k''$, with $\{m, \ell\}$, $\{m', \ell'\}$, and $\{m'', \ell''\}$ being the set of states corresponding to k , k' , and k'' respectively. The contribution of this ordering is:

$$\begin{aligned} \langle n_{m,\ell} n_{m',\ell'} n_{m'',\ell''} \rangle_{\Gamma} &= W_{m''\ell''} W_{m'\ell'} W_{m\ell} P^{\text{st}}(\ell) \\ &\quad \times \sum_{j_1, j_2} [\phi_{j_1}(\ell'') c_{j_1}(m')] \\ &\quad \times \phi_{j_2}(\ell') c_{j_2}(m) \mathcal{T}_{j_1, j_2}], \end{aligned} \quad (2.23)$$

where \mathcal{T}_{j_1, j_2} represents the solution to the integral over time appearing in the third order jump correlation (see Appendix A). It is given by:

$$\mathcal{T}_{j_1, j_2} \equiv \frac{\lambda_{j_2}^2 (1 - T\lambda_{j_1} - e^{-T\lambda_{j_1}}) - \lambda_{j_1}^2 (1 - T\lambda_{j_2} - e^{-T\lambda_{j_2}})}{\lambda_{j_2}^2 (\lambda_{j_1} - \lambda_{j_2}) \lambda_{j_1}^2}. \quad (2.24)$$

When $\lambda_{j_1} = \lambda_{j_2}$, Eq. (2.24) is indeterminate. Taking L'Hôpital's rule, we find

$$\lim_{\lambda_{j_1} \rightarrow \lambda_{j_2}} \mathcal{T}_{j_1, j_2} = \frac{T\lambda_{j_1} + e^{-T\lambda_{j_1}} (T\lambda_{j_1} + 2) - 2}{\lambda_{j_1}^3}. \quad (2.25)$$

Eq (2.24) is also indeterminate when either of the eigenvalues is zero. In such circumstances, applying L'Hôpital's rule twice, we obtain its limiting value. As an example, the limit $\lambda_{j_2} \rightarrow 0$ with $\lambda_{j_1} \neq 0$ results in the integral having the form

$$\lim_{\lambda_{j_2} \rightarrow 0} \mathcal{T}_{j_1, j_2} = \frac{2(1 - e^{-T\lambda_{j_1}}) + T\lambda_{j_1} (T\lambda_{j_1} - 2)}{2\lambda_{j_1}^3}. \quad (2.26)$$

The solution (2.26) is similar for λ_{j_2} if $\lambda_{j_1} \rightarrow 0$ with $\lambda_{j_2} \neq 0$. If both eigenvalues are zero, i.e., $\lambda_{j_1} = \lambda_{j_2} = 0$, Eq. (2.24) results in

$$\lim_{\lambda_{j_1}, \lambda_{j_2} \rightarrow 0} \mathcal{T}_{j_1, j_2} = \frac{T^3}{6}. \quad (2.27)$$

Notice that for all the terms in which two events happen at the same time, for example, $k_1 = k_2 < k_3$, the contribution to the n -th order jump correlation can be written in terms of the $n - 1$ -th order one (see Appendix ??). Iterating through all possible orderings and using the solution of the time integral in Eq. (2.24), we can obtain the complete third order correlation for the number of jumps.

The moments and the cumulants of the environmental entropy production

can be calculated from the corresponding moments and correlations for number of jumps. Indeed, for instance,

$$\kappa_1(T) \equiv \langle \Sigma_{\text{env}}(T) \rangle = \sum_{i,j} \langle n_{ij} \rangle_{\Gamma} \ln \frac{W_{ij}}{W_{ji}}, \quad (2.28)$$

where the i, j indices run over all $2N$ states. Scaled cumulants can then be defined as

$$\hat{\kappa}_1(T) \equiv \frac{\kappa_1(T)}{T}, \quad (2.29a)$$

$$\hat{\kappa}_2(T) \equiv \frac{\kappa_2(T)}{T} \equiv \frac{1}{T} (\langle \Sigma_{\text{env}}^2 \rangle - \langle \Sigma_{\text{env}} \rangle^2), \quad (2.29b)$$

$$\hat{\kappa}_3(T) \equiv \frac{\kappa_3(T)}{T} \equiv \frac{1}{T} (\langle \Sigma_{\text{env}}^3 \rangle - 3\langle \Sigma_{\text{env}}^2 \rangle \langle \Sigma_{\text{env}} \rangle + 2\langle \Sigma_{\text{env}} \rangle^3), \quad (2.29c)$$

where the time dependence of Σ_{env} has been omitted for convenience.

We can immediately see that the first jump moment scales linearly with time as seen from Eq. (2.16), so does the average entropy production, $\langle \Sigma_{\text{env}}(T) \rangle$. Concerning the second cumulant, the first term on the right-hand side of Eq. (2.22) scales with T^2 . However, this term cancels out when evaluating the cumulant, since it is equal to $\langle n_{m\ell} \rangle \langle n_{m'\ell'} \rangle$ [see Eq. (2.16)]. Hence, in the long-time limit, i.e., $T \gg \max(1/\lambda_j, 1 < j \leq 2N)$ ($\lambda_1 = 0$ corresponding to the stationary state), the second and third terms on the right-hand side of Eq. (2.22) grow linearly with the observation time T . Therefore, in this limit, the second cumulant defined in Eq. (2.29b) becomes

$$\langle \Sigma_{\text{env}}^2 \rangle - \langle \Sigma_{\text{env}} \rangle^2 \approx T \times \sum_{i,j,k,l} f(i, j, k, l) \quad (2.30)$$

where $f(i, j, k, l)$ is a function that depends only on the states of the system but not on time, and can be readily determined from Eq. (2.22). Hence, Eqs. (2.29a) and (2.29b) give that, in the long-time limit,

$$\hat{\kappa}_1 = \text{constant}, \quad (2.31)$$

$$\hat{\kappa}_2 = \text{constant}. \quad (2.32)$$

Therefore, in any finite discrete system with bidirectional time-independent transition rates, at large times, the mean and the variance of the environmental entropy production scale linearly with time. This agrees with previous results by Lebowitz and Spohn [35] and hence, we expect all cumulants to scale linearly with time at large times, for both discrete and continuous state systems.

2.3 Entropy Production in the run-and-tumble model

In the proposed framework, we return to the run-and-tumble model shown in Fig. 2.1. The transition rate matrix \hat{W} has the following elements: $W_{i_+, i_+ + 1} = b$, $W_{i_+, i_+ - 1} = a$, $W_{i_-, i_- + 1} = a$, $W_{i_-, i_- - 1} = b$, $W_{i_+, i_-} = W_{i_-, i_+} = r$ with zero cross transition rates between two layers, and $W_{1_{\pm}, 0_{\pm}} = 0$ and $W_{N_{\pm}, N_{\pm} + 1} = 0$, where the subscript \pm again denotes the respective regime of the states.

We analytically calculate the cumulants of the environmental entropy production for this system in the stationary state (up to the third one, for the sake of simplicity). Furthermore, we simulate the dynamics, generating trajectories that start from the steady state, and numerically compute the entropy production. Figure 2.4 shows a comparison of the scaled cumulants of Σ_{env} for various values of switching rate r , obtained from analytical results with their numerical simulation counterpart. We find that each scaled cumulant reaches a stationary value in the long-time limit. The non-vanishing value of the third cumulant reflects the fact that the probability density function of the entropy production is asymmetric about its mean value.

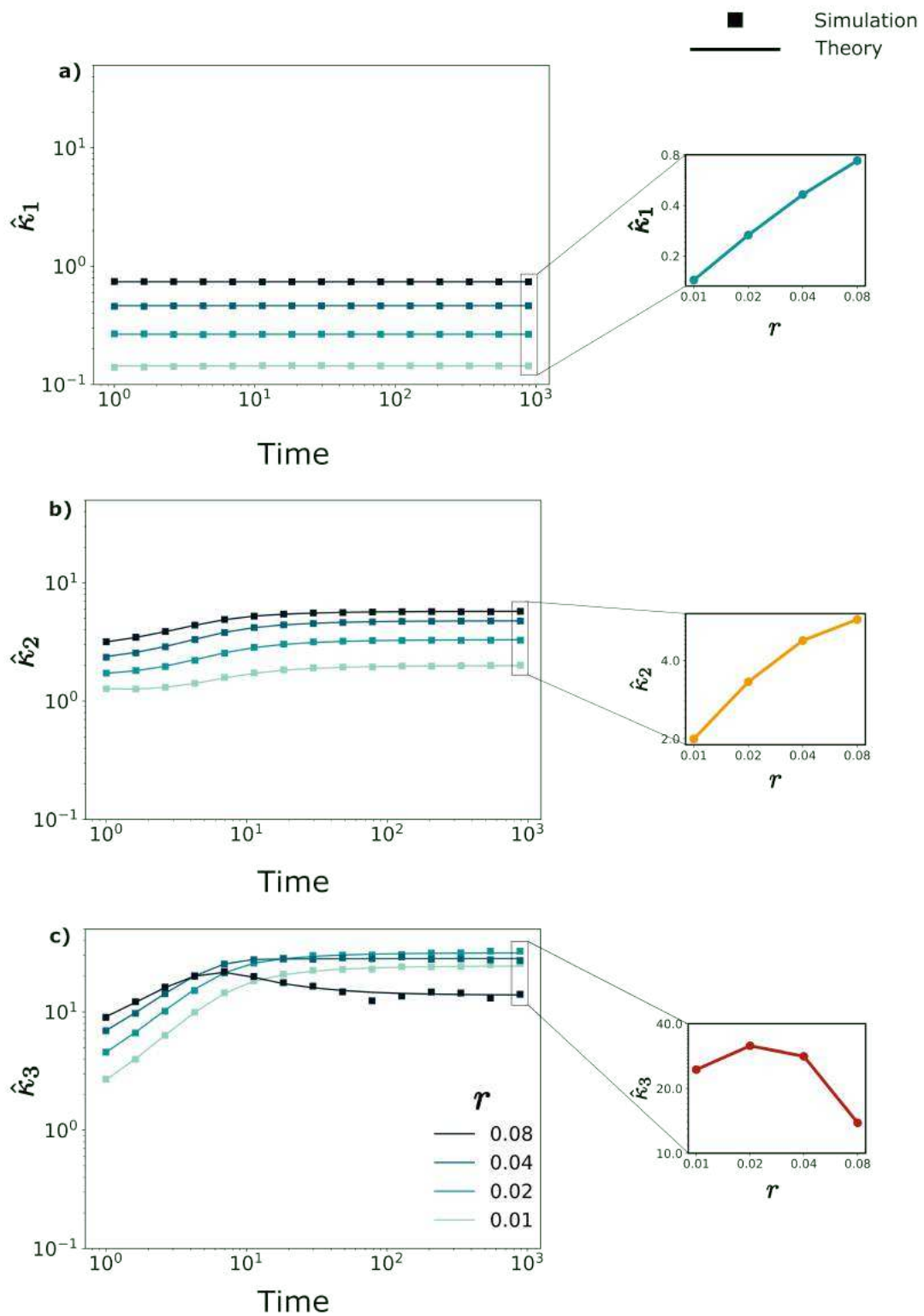


Figure 2.4: Scaled cumulants of entropy production. Dots: Numerical simulation. Lines: theoretical predictions. Number of states in each regime $N = 8$, with transition rates $a = 1.0$, and $b = 0.1$. Inset shows the variation of $\hat{\kappa}_{1,2,3}$ with different switching rates r . Here the averaging is performed over 10^5 trajectories (generated using the Gillespie algorithm). In each panel, the color intensity increases with r .

Figure 2.4 also shows how $\hat{\kappa}_{1,2,3}$ change with increasing r as a function of time. We notice that the scaled average entropy production increases when the switching rate increases. This effect can be understood by realizing that, when $r \rightarrow 0$, each layer will relax to an equilibrium distribution, hence generating no entropy into the environment on average. Hence, when r increases, the system starts to feel the non-equilibrium condition that is generated by the presence of two regimes, $+$ and $-$, and the entropy production increases. Due to the same reason, the variance of the entropy production also increases with increasing r . As a second observation, the third cumulant is consistently far from zero, stressing the non-Gaussianity of the pdf of entropy production.

It is also important to analyze the scaling of the cumulants with the number of nodes, in order to investigate how the distribution of entropy production changes as a function of the system size. We analytically compute the scaled cumulants $\hat{\kappa}_{1,2,3}$ for various system sizes, starting from the steady state, and show them in Fig. 2.5a. We observe that the first two cumulants increase with N . Then, we consider simulations of the system for different N , starting from the steady state, to compute the distribution of entropy production. We numerically find the leading order scaling with N for the complementary cumulative density function (c-cdf) of Σ_{env} to be $(\ln(N))^{5/3}$. In Fig. 2.5b, we show the collapse of different c-cdf for an increasing number of nodes, N . Clearly, there are also sub-leading contributions to the scaling of the moments that play a role in determining the behavior of the third cumulant shown in Fig. 2.5a.

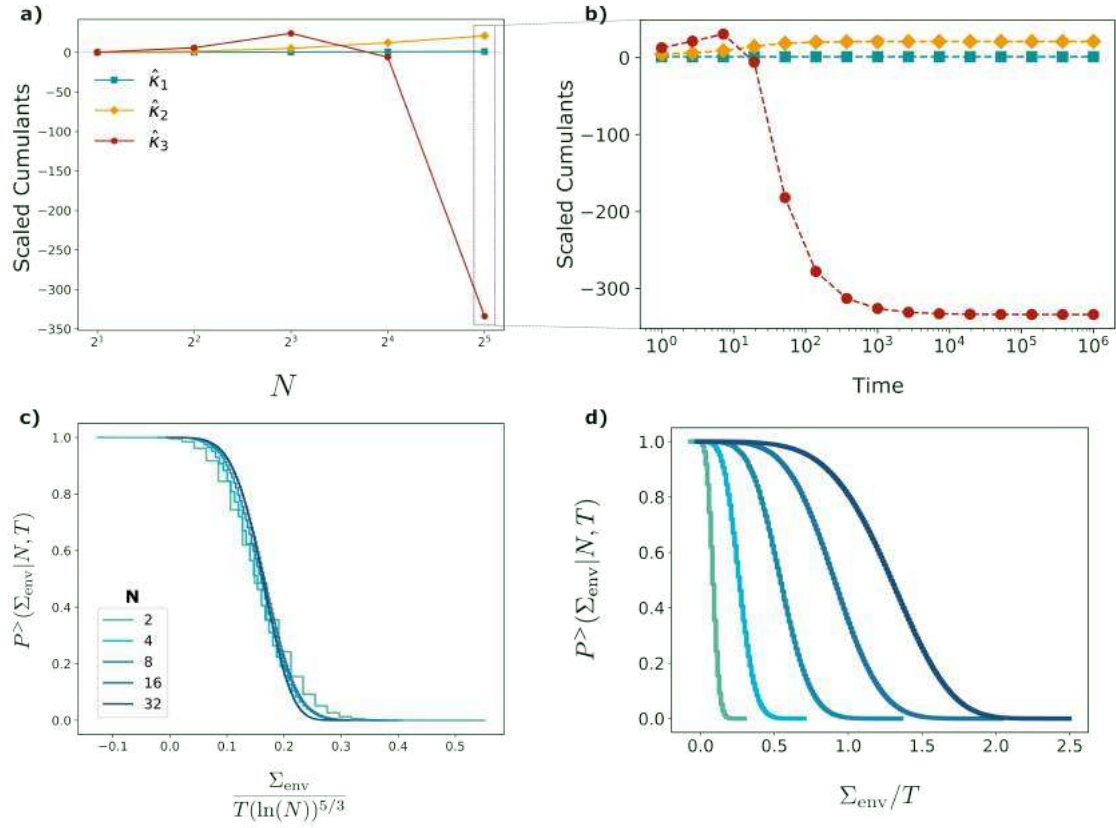


Figure 2.5: a) Scaling of cumulants ($\hat{\kappa}_{1,2,3}$) of entropy production for different number of states of the discrete run-and-tumble model. Points are obtained using analytical expressions (lines serve as a visual aid to connect the dots). b) Cumulants against time for largest time predicted from theory (dashed lines) and compared to simulations (points) c) Collapse of the complementary cumulative density function (c-cdf) of entropy production, $P^{>}(\Sigma_{\text{env}}|N, T)$, for different number of nodes in the discrete run-and-tumble model. Entropy production at time $T = 200$ is obtained from numerical simulation using 10^6 trajectories initialized from stationary state. Inset shows the uncollapsed c-cdf, without appropriate rescaling with number of nodes. d) Uncollapsed complementary cumulative density function for probability in panel c. Parameters for all panels are $a = 1.0$, $b = 0.1$ and $r = 0.05$.

Notice that increasing the number of states without scaling the rates by N does not correspond to the correct continuum limit [72]. In the next section, we present how to generalize our findings to the case of a run-and-tumble particle in a continuous domain by considering appropriate rescaling of the transition rates.

2.4 Spatially continuous limit

Let us start from the description of a particle experiencing run-and-tumble dynamics in a $1D$ continuous space $[-L, L]$, with reflecting boundary conditions and noise. The Langevin equation describing this dynamics is [147]:

$$\dot{x} = v \sigma(t) + \sqrt{2D}\eta(t), \quad (2.33)$$

where $\sigma(t) = \pm 1$ is a dichotomous noise that switches between $+1$ and -1 with a constant rate r , v the bare velocity of the particle in either direction in the absence of thermal noise, D the diffusion constant, and $\eta(t)$ is the Gaussian white noise with zero mean and unit variance. The corresponding Fokker-Planck equation reads:

$$\partial_t \rho_+ = -v \partial_x \rho_+ + D \partial_x^2 \rho_+ - r(\rho_+ - \rho_-), \quad (2.34a)$$

$$\partial_t \rho_- = +v \partial_x \rho_- + D \partial_x^2 \rho_- - r(\rho_- - \rho_+), \quad (2.34b)$$

where ρ_+ and ρ_- , respectively, are the probability density functions for the system to be in the state $\sigma = +1$ and $\sigma = -1$, respectively, at the position x and time t [147]. For convenience, we have omitted the position and time dependence from $\rho_{\pm}(x, t)$.

Let us now go back to our original discrete-state description. The particle can move either in the upper or in the lower $1D$ lattices, i.e., lanes, with a rate of switching between the lanes equal to r . The master equation associated solely with the motion along the upper lane (+), ignoring the switching between lanes, is:

$$\dot{P}(i_+, t) = aP(i_+ - 1, t) + bP(i_+ + 1, t) - (a + b)P(i_+, t). \quad (2.35)$$

A similar equation holds also for the lower lane, interchanging a with b , following the model sketched in Fig. 2.1). In order to map this dynamics to a continuous space, we introduce the information that the system exists in a $1D$ box, $[-L, L]$. Hence, as we increase the number of states N in each lane, the spacing between the states has to decrease. In particular, let the spacing between the states $\delta \equiv 2L/N$. Considering again the upper lane, employing this mapping, the spatial position of the particle, $x = i_+ \delta$, and the probability density function transforms as follows: $\rho_+(x) = P(i_+)/\delta = P(x/\delta)/\delta$.

A standard Kramers-Moyal expansion [8] on Eq. (2.35), taking δ as small parameter in the limit $N \rightarrow +\infty$, up to the second order, gives:

$$\partial_t \rho_+ = -(a - b)\delta \frac{\partial \rho_+}{\partial x} + \frac{(a + b)}{2} \delta^2 \frac{\partial^2 \rho_+}{\partial x^2}. \quad (2.36)$$

Performing the same expansion on the lower lane dynamics as well, and adding the switching process between these two regimes, we can compare the resulting set of coupled differential equation with Eq. (2.34). The matching between

these two dynamical evolution becomes exact in the $N \rightarrow +\infty$ limit, when the following scaling holds:

$$a = \frac{N}{4L} \left(\frac{DN}{L} + v \right), \quad (2.37a)$$

$$b = \frac{N}{4L} \left(\frac{DN}{L} - v \right). \quad (2.37b)$$

It is indeed always true that when performing the continuum limit starting from a discrete-state process, the rates have to properly scaled with the number of states.

Let us now compute the thermodynamics of the continuous process. Given the Langevin equation (2.33), the amount of the heat absorbed by the run-and-tumble particle from the heat bath during an observation time, T , is [75]:

$$Q \equiv \int_0^T d\tau [\sqrt{2D\gamma^2}\eta(\tau) - \gamma\dot{x}(\tau)] \circ \dot{x}(\tau), \quad (2.38)$$

where γ is the dissipation constant, and \circ denotes the Stratonovich product. Substituting Eq. (2.33), we obtain

$$Q = -\gamma \int_0^T d\tau v\sigma(\tau)\dot{x}(\tau). \quad (2.39)$$

Thus, the environmental entropy production is [74]:

$$S_{\text{env}}(T) = \frac{v}{D} \int_0^T d\tau \sigma(\tau) \dot{x}(\tau). \quad (2.40)$$

where we use the Einstein relation, $D\gamma = k_B\mathbb{T}$ where \mathbb{T} is the temperature of the bath and we set $k_B = 1$. This system is known to have non zero mean entropy production rate [153].

Fig. 2.6 shows the first two scaled cumulants of the entropy production for various system sizes, using the scaling in Eq. (2.37), against their value for the continuous system. In particular, the mean entropy production rate has been computed analytically in [153] while we compute the variance of S_{env} in Eq. (2.40) from Langevin simulations. The convergence to the continuous case as N increases can be clearly appreciated.

Unlike the mean entropy production rate, to the best of our knowledge, there have been no theoretical considerations into calculating the variance of entropy production of the run-and-tumble model in continuous space. We have shown that we can compute it using our method under appropriate scaling, and its value converges to what is observed in the continuous system. Similar procedure can also be performed for any moment of the entropy production, but the computation of the third moment in discrete-state system already scales as $\mathcal{O}(N^3)$, making its computation intensive for a large number of states.

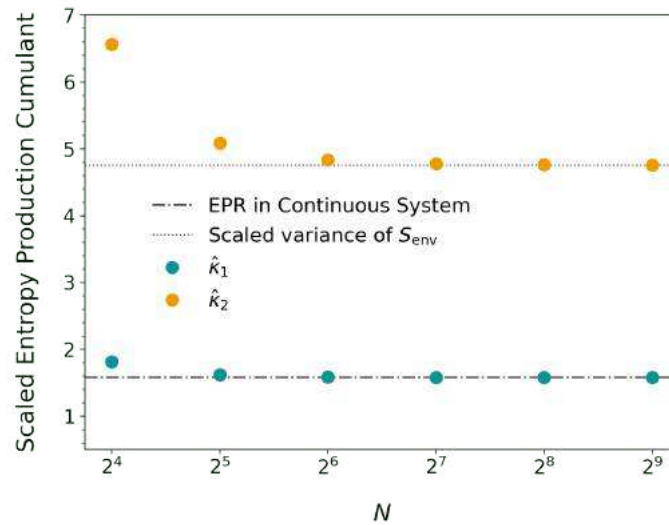


Figure 2.6: Comparison between scaled cumulants of entropy production in the discrete and the continuous run-and-tumble model. The dashed line is the mean entropy production rate (EPR) given analytically in Ref. [153]. The dotted line is the variance of environmental entropy production calculated from Langevin simulations of the continuous run-and-tumble model on 1D box within $[-5, 5]$ with velocity of the particle $v = 1.0$, diffusion coefficient $D = 0.5$, and switching rate $r = 1.0$. The points are analytically calculated scaled cumulants of environmental entropy production in the discrete run-and-tumble model with scaling of transition rates given by (2.37).

2.5 Conclusion

In summary, this chapter presents a graphical method to compute the exact moments of entropy production for any finite and discrete-state Markovian system. Employing this method, we have shown that the first and second cumulants scale linearly with time in the long-time limit.

Then, we have applied the developed framework to predict the cumulants of the environmental entropy production in the discrete run-and-tumble model at stationarity, finding non-zero mean, variance and skewness. Additionally, increasing the system size, the environmental entropy production exhibits a remarkable non-Gaussian behavior, highlighting the potential relevance of higher moments when studying the fluctuations of discrete-state systems. Finally, we have performed the continuum limit on the proposed model, finding the correct scaling of the rates with the number of nodes. Within this description, we computed the cumulants of the environmental entropy production for a Langevin run-and-tumble model. We found striking agreement between our predictions, numerical simulations, and a theoretical result previously obtained only for the mean [153].

The graphical method here presented can be straightforwardly extended to analyze the moments of currents of any discrete-state systems (and also their

continuous counterparts). These findings suggest that cumulants other than the first two might be relevant in quantifying out-of-equilibrium fluctuations. In principle, one could try to estimate the full probability density function (pdf) of the entropy production including more than the first two moments, using a Maximum Entropy Principle. This task is usually computationally expensive even with only the first three cumulants. Hence, a smarter approach to move from cumulants to an estimation of the PDF would be an interesting topic for future investigations.

The critical role of entropy production is featured in its application to fluctuation relations, which are fundamental to understanding systems even in non-equilibrium steady states and more generally, far from equilibrium conditions. Entropy production in such non-equilibrium steady states (NESS) is largely influenced by external or environmental factors. For instance, in the run-and-tumble particle model, environmental driving forces can cause the particle to switch its directional bias from right to left, significantly affecting the system's dynamics.

However, even systems that have reached a NESS can be disrupted and driven out of this state by introducing boundary effects. When a system experiences a boundary leakage, it induces a perpetual flux that continuously influences the system. This introduced flux does not dissipate but rather interacts with the system's inherent fluctuations, leading to alterations in fluctuation relations and potentially modifying the classical fluctuation-dissipation theorems observed in equilibrium states. Such interactions highlight the delicate balance and dynamic interplay between system boundaries, environmental forces, and internal fluctuations in determining the behaviour and properties of both equilibrium and non-equilibrium systems. Understanding these effects is crucial for a comprehensive understanding of complex systems and their responses to external perturbations.

FLUCTUATION-DISSIPATION THEOREM WITH ABSORBING STATES

Part of the following chapter is the basis of published work [158] “Generalisation of fluctuation-dissipation theorem to systems with absorbing states” [P. Padmanabha, S. Azaele, A. Maritan; New J. Phys. 25 113001 (2023)]. Parts of the contents presented, including displayed figures, are taken with permission from the published work, copyright with the authors.

3.1 Introduction

Studying the fluctuations of entropy production provides a valuable perspective on non-equilibrium systems, often focusing on their behavior at steady states. However, an equally important and revealing approach involves examining transient dynamics, those periods during which a system is adjusting to changes and is inherently out-of-equilibrium. Such transient states offer insights into the mechanisms and behaviours of systems as they respond to and recover from perturbations.

The fluctuation-dissipation theorem is particularly pertinent in the study of transient dynamics. It bridges the gap between the system’s response to a transient perturbation and its inherent equilibrium fluctuations. Even in a system that has reached a state of maximum entropy, any perturbation will momentarily disrupt this equilibrium, leading to non-zero entropy production as the system goes through a non-equilibrium regime before eventually settling back into equilibrium. Understanding these transient dynamics improves our comprehension of the principles underlying non-equilibrium statistical mechanics.

The bridge between microscopic dynamics and macroscopic observables is provided in multiple forms, such as the Einstein-Smoluchowski equation, the regression hypothesis by Onsager [4, 26, 27], linear response theory by Kubo [28, 29], and fluctuation-dissipation relations in stochastic systems [10,

159]. Though equilibrium dynamics is a useful description, studies into non-equilibrium systems have gained much traction due to the numerous reasons outlined previously. In this context, attempt to understand the regimes of failure of these relations promises to improve our search in underlying fundamental principles in non-equilibrium statistical mechanics.

A large body of literature exists on the violation of the fluctuation-dissipation theorem in glassy systems [39]. Additionally, there have been attempts at extending the validity of FDT to non-equilibrium systems [160, 161] using the concepts of asymmetry [162, 163], frenesy [95], local currents [164, 165, 166]. In particular, successes have been obtained at predicting response to perturbation in an arbitrary non-stationary state [167]. However, the focus has been mainly on systems that have some form of non-trivial long-time steady state. Instead, the focus of this chapter is on an entirely different class of non-equilibrium systems with absorbing states/boundaries.

Systems with absorbing states are widespread in many fields. Some of the examples include chemical reactions, epidemics, and population dynamics [168, 16, 8, 9]. In such systems, the net flux out of the system is positive, and hence the total probability distribution decays with time, rendering the steady-state trivial. However, such systems are also frequently found in a quasi-stationary state for a long time before reaching extinction. There exists extensive mathematical literature analysing the properties of quasi-stationary systems [169, 170, 9]. The properties of extinction time distributions, the existence of quasi-stationary distribution [171, 172], simulation methods [173] have been studied with applications to cellular automata [174], birth-death processes [175], Brownian motion [176], contact process [177], and many others.

Despite the presence of literature on quasi-stationary systems, there have been no attempts into looking at the change in FDT in such systems. Previous studies to develop a linear response theory in “quasi-stationary” states considered systems that remain in metastable states before reaching thermal equilibrium [178, 179]. In general, there appears to be a gap between fields of quasi-stationary systems and non-equilibrium FDT. This gap in literature will be attempted to be bridged in the following chapter by considering modifications needed by linear response theory to accommodate the presence of absorbing states. This is performed through the method of conditioning observable averages over trajectories that have not yet hit the absorbing state, calling this operation conditioning to survival. Within this framework, a new FDT arises with new observables that account for the survival of trajectories. This new FDT is benchmarked against several paradigmatic examples, thereby generalizing the equilibrium (and near-equilibrium) fluctuation-dissipation theorems to a different class of non-equilibrium processes.

3.2 Stationary systems

3.2.1 Standard FDT

Consider a stochastic system comprised of a finite set of discrete states, represented by Ω . Let $P_x(t)$ be the probability of finding the system in state $x \in \Omega$ at time t . The evolution of the probability $P_x(t)$ is governed by the familiar Master equation

$$\dot{P}_x(t) = \sum_{y \neq x} [W_{xy} P_y(t) - W_{yx} P_x(t)] \quad (3.1)$$

where W_{xy} is the rate of transition from state y to state x . By defining a matrix with elements $H_{xy} \equiv W_{xy} - \delta_{xy} \sum_z W_{zy}$, the Master equation can be written as

$$\dot{\vec{P}}(t) = H \vec{P} \quad (3.2)$$

and hence has the solution $P(t) = P(0) e^{H t}$ [9]. Without any absorbing boundaries, at large times a stationary state is reached [180], where the probability of finding the system in state x is P_x^{st} . Any external perturbation will shift the system away from this steady state. Assuming that the perturbation is small, the response of the system can be analyzed within the linear approximation. The perturbations to the transition matrix can then be written as [10]

$$H(t) = H_0 + \delta H(t) \quad (3.3)$$

Here, $H_0(x)$ is the unperturbed transition matrix. We consider small perturbations and hence, retain terms upto the first order. Similarly, we also write the solution to the perturbed distribution in terms of the stationary distribution of the master equation and the perturbation:

$$P_x(t) = P_x^{st} + \delta P_x(t) \quad (3.4)$$

Since we are looking at small perturbations, we also assume that the deviation $\delta P_x(t)$ is small. With $H P^{st} = 0$, we can write:

$$\dot{P}(t) = \dot{\delta P}(t) = H \delta P(t) + \delta H(t) P^{st} + \delta H(t) \delta P(t) \quad (3.5)$$

of which the last term is negligible. Solving this, we obtain

$$\delta P(t) = \int_{-\infty}^t dt' e^{H(t-t')} \delta H(t') P^{st} \quad (3.6)$$

Having obtained this, we also assume that $\delta H(t)$ can be split into state components and temporal components.

$$\delta H_{xy}(t) = \delta H_{xy} F(t) \quad (3.7)$$

Let A be any observable. Then, the deviation of A from its mean value $\langle A \rangle$, where the mean is computed over an ensemble average, caused due to the perturbation can be written as

$$\langle \Delta A(t) \rangle = \int_{-\infty}^{\infty} dt' R_{A,\delta H}(t-t') F(t') \quad \text{where} \quad (3.8)$$

$$R_{A,\delta H}(t) = \Theta(t) \sum_{x,y,z} A_x [e^{H t}]_{xy} \delta H_{yz} P_z^{st} \quad (3.9)$$

Assuming that the perturbation occurs in one of the parameters of the system, $f \equiv (f_1, f_2, \dots, f_N)$, i.e, $f \rightarrow f + \Delta f(t)$. If $H = H(f)$ then,

$$H(f) P^{st}(f) = 0 \quad (3.10a)$$

$$P^{st} = e^{\phi(f)} \quad (3.10b)$$

$$H(f + \Delta f(t)) = H(f) + \Delta f(t) \delta H + \mathcal{O}(\Delta f^2) \quad (3.11)$$

$$\delta H = \frac{\partial H(f)}{\partial f} \quad (3.12)$$

From (3.10) and (3.12), we can obtain the following

$$\delta H P^{st}(f) = -H(f) \frac{\partial P^{st}(f)}{\partial f} \quad (3.13)$$

Subsequently, the response function in (3.9) can now be written as

$$\begin{aligned} R_{A,f}(t-t') &= -\Theta(t-t') \frac{\partial}{\partial t} \left\langle A(t) \frac{\partial \phi}{\partial f}(t') \right\rangle \\ &= -\Theta(t) \frac{d}{dt} \left\langle A(t) \frac{\partial \phi(t'=0)}{\partial f} \right\rangle \end{aligned} \quad (3.14)$$

Suppose we denote $X_f = \frac{\partial \phi(t=0)}{\partial f}$, then, (3.14) can be written as

$$R_{A,X_f}(t) = -\Theta(t) \frac{d}{dt} K_{A,X_f}(t) \quad (3.15)$$

where $K_{A,B}(t)$ is the two time correlation function between observables A and B . Equation (3.15) forms the main Fluctuation Dissipation Theorem we wish to pursue in a generalized form. Though we have presented the discrete case here, the same calculations hold for continuous state space with the Fokker-Planck operator being analogous to the transition matrix H [10].

3.2.2 Application in forest dynamics

An application of the linear response theory can be seen from the second-order forest density dependant forest dynamics equation presented in Eq (1.28). The Langevin equation describing the evolution of population of a species is given by

$$\dot{x} = b - \frac{x}{\tau} + \sqrt{2Dx} \eta(t) \quad (3.16)$$

where $\eta(t)$ is a Gaussian white noise with zero mean and delta-correlated variance. The corresponding Fokker-Planck equation, under Ito prescription, takes the form

$$\dot{P}(x, t) = -\frac{\partial}{\partial x} \left(b - \frac{x}{\tau} \right) P(x, t) + \frac{\partial^2}{\partial x^2} DxP(x, t) \quad (3.17)$$

whose stationary solution is a Gamma distribution given by

$$P_{st}(x) = \frac{1}{\mathcal{N}} x^{\frac{b}{D}-1} e^{-\frac{x}{D\tau}} \quad (3.18)$$

with \mathcal{N} as the normalization factor. Hence, this obeys the Boltzmann-like form ($P_{st}(x) = e^{-\phi(x)}$) that a stationary distribution takes in equilibrium, with the effective potential being given by

$$\phi(x) \equiv \frac{x}{D\tau} - \left(\frac{b}{D} - 1 \right) \log(x) \quad (3.19)$$

With this effective potential, the response for a change in an observable due to a perturbation in b , τ or D can be computed using Eq (3.15). For instance, the change in average population $\langle x \rangle$ due to various parameters is given by the response functions

$$R_{x,\tau} = \frac{-1}{D\tau^2} \frac{dK_{x,x}}{dt} \quad (3.20)$$

$$R_{x,b} = \frac{-1}{D} \frac{dK_{x,\log(x)}}{dt} \quad (3.21)$$

$$R_{x,D} = \frac{1}{D} (\tau R_{x,\tau} - b R_{x,b}) \quad (3.22)$$

where $K_{A,B}(t) = \langle A(t)B(0) \rangle$ is the correlation function evaluated at stationarity.

A point of note is that the response is only determined by two independent parameters. Any perturbation in D can be represented as weighted perturbations in b and τ . Using the definition of correlation function and the Fokker-Planck equation, we can compute the differential equation obeyed by the correlation function. On solving the requisite ODEs, we find the correlation functions, and subsequently, the response functions

$$K_{x,x}(t) = \langle x(t)x(0) \rangle - \langle x \rangle^2 = bD\tau^2 e^{-t/\tau} \quad (3.23)$$

$$K_{x,\log(x)} = \langle x(t)\log(x(0)) \rangle - \langle x \rangle \langle \log(x) \rangle = D\tau e^{-t/\tau} \quad (3.24)$$

$$R_{x,\tau} = \frac{b}{\tau} e^{-t/\tau} \quad (3.25)$$

$$R_{x,b} = e^{-t/\tau} \quad (3.26)$$

$$R_{x,D} = 0 \quad (3.27)$$

It is interesting to note that demographic stochasticity has zero linear response to average population levels. However, higher cumulants of the population will potentially have non zero response functions for all three parameters. Notably, the model remarkably reproduces observed distribution of species population even though it makes a neutral theory assumption. The application of this model to contemporary data from perturbation experiments, such as those conducted at the Paracou station where forest surveys are performed and compared between plots which are both perturbed and unperturbed, represents a promising avenue for research. These field studies provide valuable data on how populations and communities respond to various environmental changes and disturbances. In both this example and in the standard theory, the inherent assumption rests on there being a stationary distribution, which is invalidated on introducing absorbing boundary into the system, (for instance, setting b to zero), necessitating a generalization of the presented FDT.

3.3 Absorbing systems

Before proceeding to the derivation of fluctuation-dissipation theorem in absorbing systems, we make clear the distinction between different kinds of non-equilibrium. There are states which break detailed balance, but due to local detailed balance, reach a non-equilibrium stationary states. Run-and-tumble particle considered in the previous chapter is one example of this, where there are stationary but non zero fluxes with a non-trivial stationary state. Another kind of out-of-equilibrium occurs due to slow relaxation, for instance, in glassy systems where there are memory effects in correlation functions, thereby also violating fluctuation-dissipation theorems. We consider systems that belong to neither classes of non-equilibrium processes. Our examples centre around states being sinks for probability fluxes, i.e., trajectories routinely “disappear” by getting stuck in the absorbing state. A long-time steady state does exist in such systems, however, that steady state is trivial and is delta peaked at the absorbing state, having no fluctuations around it. However, we will proceed to show that there exists a regime of time when the statistics of survived trajectories offer a kind of stationarity (which is what we call quasi-stationarity since it is only stationarity of the unabsorbed trajectories and not a complete non-trivial

stationarity) and the statistics of this stationarity leads us to a new fluctuation-dissipation theorem.

3.3.1 Discrete Systems

If the system has an absorbing boundary, this boundary is represented by a set of states where all trajectories eventually end up in. We can denote the boundary of this space by $\partial\Omega$ and the interior by $\Omega^\circ = \Omega - \partial\Omega$. The transition rates between different states shall be represented by $W_{y \rightarrow x} = W_{xy}$. The absorbing boundary condition can be represented by setting the rate of transition out of the boundary states to be zero.

$$\begin{aligned} W_{xy} &= 0 \quad \forall x \in \Omega, y \in \partial\Omega \\ W_{xy} &\geq 0 \end{aligned}$$

With these, we can now split the ME between absorbing boundary and the interior.

$$\begin{aligned} \dot{P}_x(t) &= \sum_{y \in \Omega} [W_{xy} P_y(t) - W_{yx} P_x(t)] \\ &= \sum_{y \in \Omega^\circ} W_{xy} P_y(t) && \text{if } x \in \partial\Omega \\ \text{or} &= \sum_{y \in \Omega^\circ} W_{xy} P_y(t) - \sum_{y \in \Omega} W_{yx} P_x(t) && \text{if } x \in \Omega^\circ \end{aligned} \quad (3.28)$$

To make expressions simpler, we can introduce a single state 0 to represent the entire boundary. The corresponding entries for this state that would go into the Master equation would be

$$P_0(t) \equiv \sum_{x \in \partial\Omega} P_x(t) \quad (3.29)$$

$$W_{0x} \equiv \sum_{y \in \partial\Omega} W_{yx} \quad \text{and} \quad W_{x0} \equiv \sum_{y \in \partial\Omega} W_{xy} = 0 \quad (3.30)$$

These represent the total probability of being on the boundary and the total rates of transition into and out of the boundary respectively. Note that these also imply $W_{0x} = 0$ if $x \in \partial\Omega$.

Let us now redefine our state space to include this special 0 state. The corresponding rates are defined in Eq. (3.29) and (3.30) and

$$\Omega' = \Omega^\circ \cup \{0\} \quad (3.31)$$

In this new space, we can rewrite our ME as follows

$$\dot{P}_x(t) = \sum_{y \in \Omega'} [W_{xy} P_y(t) - W_{yx} P_x(t)] \quad (3.32)$$

which can similarly be broken down depending on whether $x = 0$ or otherwise. Note that since P_0 never enters on the r.h.s. of the previous equation due to our rates, we only need to solve the redefined ME for non zero states, i.e, only the interior. It is always possible to get back the individual boundary states on $\partial\Omega$ by integrating

$$\dot{P}_y(t) = \sum_{x \in \Omega^\circ} W_{yx} P_x(t)$$

We continue representing the entire boundary by state 0. This also helps avoid degenerate ground states for each boundary state in the initial Ω .

Eigenvalues and Eigenvectors

Note that $\sum_x \dot{P}_x(t) = 0$ (since the sum over states includes the absorbing state), i.e, the total probability is conserved (and equivalently we can normalize it). We can define the operator H with which we have $\dot{P}(t) = H P(t)$

$$H_{xy} = W_{xy} - \delta_{xy} \sum_z W_{zy} \quad (3.33)$$

Normalizing the left and right eigenvectors of H such that $\langle \psi^n | \varphi_m \rangle = \delta_{m,n}$, the first left eigenvector is $\psi_x^0 = 1 \quad \forall x \in \Omega$ for the corresponding eigenvalue $\lambda_0 = 0$. The corresponding right eigenvector is $\varphi_{0x} = \delta_{x,0}$ as it can be easily verified.

In general, for the n^{th} right eigenvector and eigenvalue, with $\text{Re}(z)$ representing the real part of a complex number z ,

$$H\varphi_n = -\lambda_n\varphi_n$$

and hence $0 = \lambda_0 < \text{Re}(\lambda_1) < \text{Re}(\lambda_2) \leq \text{Re}(\lambda_3) \dots$ (3.34)

We will always work with an irreducible W , i.e. for any pair of interior nodes, there is always a path of non zero W 's from one to the other. This implies that the boundary state is not visited, since such a visit would correspond to the reverse transition rate being equal to zero. In such a system, (3.34) can be proved using Perron-Frobenius Theorem (See Appendix B)

With the preliminaries we have listed above, we can start looking at how this affects observable quantities like correlation functions. We find results that differ from the more standard case where there is no absorbing boundary while looking at survived trajectories only.

Average and Correlation Functions

Let us consider an initial condition to be $P^{lt}(0) = \varphi_0 + \varphi_1$. This is a valid initial condition since it satisfies all requirements for a physical initial condition.

$$P_x^{lt}(0) = \varphi_{1x} \geq 0 \quad x \neq 0 \quad (3.35)$$

$$P_x^{lt}(0) = 0 \quad x = 0 \quad (3.36)$$

$$\sum_x P_x^{lt}(0) = \langle \psi^0 | P^{lt}(0) \rangle = 1 \quad (3.37)$$

Then, $P_x^{lt}(t) = \varphi_{0x} + e^{-\lambda_1 t} \varphi_{1x}$. We also define an observable $\chi_x = 1 - \delta_{x,0}$, whose average value at time t gives the survival probability, i.e. the probability that the system has not yet been absorbed by the boundary. For any other observable A , we require that $A_x = 0$ on the boundary state, i.e. $x = 0$. If the observable does not have this criteria, we can always multiply it by χ and have $\chi_x A_x$ satisfying this criterion.

$$\langle A \rangle_t^{lt} = \sum_x A_x P_x^{lt}(t) = e^{-\lambda_1 t} \sum_{x \neq 0} A_x \varphi_{1x}$$

$$\langle \chi \rangle_t^{lt} = e^{-\lambda_1 t} \sum_{x \neq 0} \varphi_{1x} = e^{-\lambda_1 t} \quad \text{this represents the survival probability}$$

Conditional Average

$$\frac{\langle A \rangle_t^{lt}}{\langle \chi \rangle_t^{lt}} = \sum_{x \neq 0} A_x \varphi_{1x} \equiv \langle A | | \chi \rangle^{lt} \quad (3.38)$$

We use double delimiter in $\langle \bullet | | \bullet \rangle$ to avoid confusion with the inner product of left and right eigenvectors. For an arbitrary initial condition (IC), at large times, it is equivalent to averaging over the defined P^{lt} as seen from below. For arbitrary $P(0)$,

$$P(t) = \varphi_0 + c_1 e^{-\lambda_1 t} [\varphi_1 + \mathcal{O}(e^{-t(\text{Re}(\lambda_2) - \lambda_1})}]$$

$$\langle A \rangle_t = \sum_x A_x P_x(t) = c_1 e^{-\lambda_1 t} \sum_{x \neq 0} A_x \varphi_{1x} [1 + \mathcal{O}(e^{-t(\text{Re}(\lambda_2) - \lambda_1})}]$$

$$\langle \chi \rangle_t = c_1 e^{-\lambda_1 t} \sum_{x \neq 0} \varphi_{1x} [1 + \mathcal{O}(e^{-t(\text{Re}(\lambda_2) - \lambda_1})}] = c_1 e^{-\lambda_1 t} [1 + \mathcal{O}(e^{-t(\text{Re}(\lambda_2) - \lambda_1})}]$$

$$\frac{\langle A \rangle_t}{\langle \chi \rangle_t} \underset{t \rightarrow \infty}{=} \sum_{x \neq 0} A_x \varphi_{1x} = \langle A | | \chi \rangle^{lt}$$

This gives us the conditional average. For the time correlation function, we need to consider the propagator.

Time Evolution

The ME can be written as matrix operation with the H defined earlier.

$$\dot{P}(t) = H P(t) \quad \implies \quad P(t) = e^{Ht} P(0)$$

If $P_x(0) = \delta_{x,x_0}$, we obtain the propagator $P(x, t|x_0, 0) = [e^{Ht}]_{x,x_0}$. Hence, for a general IC,

$$P_x(t) = \sum_{x_0} P(x, t|x_0, 0) P_{x_0}(0)$$

Since $H_{x,0} = 0$ we have

$$P(x, t|x_0 = 0, 0) = [e^{Ht}]_{x,0} = \delta_{x,0} \quad \forall t \quad (3.39)$$

Correlation functions are defined as $\langle A(t)B(t') \rangle = \sum_{x,y} A_x P(x, t|y, t') B_y P_y(t')$ and similarly for correlations involving more than two observables evaluated at different times. Since we have defined observables to be zero at node 0 (boundary) it follows from (3.39) and the Chapman Kolmogorov equation that

$$\langle A(t)B(t') \cdots C(t'')\chi(t''') \rangle = \langle A(t)B(t') \cdots C(t'') \rangle \quad \text{if } t''' \leq \max\{t, t' \dots t''\} \quad (3.40)$$

This has to be true logically too. Since we are calculating the correlation till $\max\{t, t' \dots t''\}$, the only contributing trajectories have to last at least till time $\max\{t, t' \dots t''\}$. Hence, at time $\leq t'''$ the trajectories have not yet hit the boundary, i.e. $\chi(t''') = 1$. But for the contrary case, this is not true

$$\langle A(t)B(t') \cdots C(t'')\chi(t''') \rangle \neq \langle A(t)B(t') \cdots C(t'') \rangle \quad \text{if } t''' > \max\{t, t' \dots t''\} \quad (3.41)$$

since on the l.h.s. we are requiring that trajectories have not hit the boundary at least till time t''' whereas in the r.h.s. we require that they only survive till a time $\geq t''$. This is a consequence of having absorbing boundary. In the standard no absorbing boundary case, $\chi = 1$ trivially and $\sum_x P(x, t|y, t') = 1$. With the absorbing boundary, we are forced to neglect the 0 state and hence the sum over $x \neq 0$ is no longer unity. If the IC is P^{lt} ,

$$\begin{aligned} \langle A(t)B(t') \rangle^{lt} &= \sum_{x,y} A_x B_y P(x, t|y, t') P_y^{lt}(t') \\ &= \sum_{x,y} A_x B_y P(x, t|y, t') \varphi_{1y} e^{-\lambda_1 t'} \quad t' < t \end{aligned} \quad (3.42)$$

In this case, a conditional correlation function, which represents the correlation with only surviving trajectories is written as

$$\begin{aligned} \frac{\langle A(t)B(t') \rangle^{lt}}{\langle \chi \rangle_t^{lt}} &= \sum_{x,y} A_x B_y P(x, t|y, t') \varphi_{1y} e^{\lambda_1(t-t')} \\ &= Tr[A e^{(H+\lambda_1 \mathbb{I})(t-t')} B \Phi_1] \equiv \langle A(t) B(t') || \chi \rangle^{lt} \quad t' < t \end{aligned} \quad (3.43)$$

where \mathbb{I} is the identity matrix. In this, we define $A_{xy} = A_x \delta_{xy}$ and $B_{xy} = B_y \delta_{xy}$. $(\Phi_1)_{xy} = \varphi_{1x} \delta_{xy}$. Similar to the conditional average, we can start from arbitrary IC and at large times, it becomes equivalent to averaging over the long time state. Hence, in further calculations, we can just use $P^{lt}(t)$ to determine correlations at large times.¹

At large time limit, $t' \rightarrow \infty$ and denoting $\Delta t = t - t'$, the propagator can be approximated as

$$[e^{H\Delta t}]_{xy} = \psi_y^0 \varphi_{0,x} + \psi_y^1 \varphi_{1x} e^{-\lambda_1 \Delta t} + \mathcal{O}(e^{-\text{Re}(\lambda_2) \Delta t})$$

Using this in (3.43),

$$\langle A(t) B(t') | \chi \rangle^{lt} = \sum_x A_x \varphi_{1x} \sum_y B_y \varphi_{1y} \psi_y^1 (1 + \mathcal{O}(e^{-(\text{Re}(\lambda_2) - \lambda_1) \Delta t})) \quad (3.45)$$

By defining $\langle B | \chi \rangle_{cond}^{lt} \equiv \sum_y B_y \varphi_{1y} \psi_y^1 = \langle B \psi^1 | \chi \rangle^{lt}$. Therefore, at large time limit, $t - t' \rightarrow \infty$,

$$\langle A(t) B(t') | \chi \rangle^{lt} = \langle A | \chi \rangle^{lt} \langle B | \chi \rangle_{cond}^{lt} (1 + \mathcal{O}(e^{-(\text{Re}(\lambda_2) - \lambda_1) \Delta t})) \quad (3.46)$$

Since $\psi_x^1 > 0$, we also have $\langle B | \chi \rangle_{cond}^{lt} > 0$ if $B_x \geq 0$. If $B = \chi$, $\langle \chi | \chi \rangle_{cond}^{lt} = \sum_{y \neq 0} \varphi_{1y} \psi_y^1 = \sum_y \varphi_{1y} \psi_y^1 = 1$ (since $\psi_0^1 = 0$ thanks to the normalization of left and right eigenvectors). It is important to note that this is a significant difference from the standard treatment where $\langle A(t) B(t') \rangle^{st} = \langle A \rangle^{st} \langle B \rangle^{st}$ at large time separation. This is because in the standard case with a non trivial stationary state, φ_0 , one has $\psi_x^0 = 1$ for all x . This can also be generalized to multiple correlations

$$\begin{aligned} \langle A(t) B(t') \cdots C(t'') | \chi \rangle^{lt} &= \langle A | \chi \rangle^{lt} \langle B | \chi \rangle_{cond}^{lt} \cdots \langle C | \chi \rangle_{cond}^{lt} \times \\ &\times (1 + \mathcal{O}(e^{-(\text{Re}(\lambda_2) - \lambda_1) \min(\Delta t, \Delta t' \cdots)})) \end{aligned} \quad (3.47)$$

when $t'' < t' < t$ in the $t - t' = \Delta t$ and $t' - t'' = \Delta t'$ large limit.

Using some examples illustrates this point and provides further insight. If we have $A = \chi$, then, $\langle \chi(t) B(t') | \chi \rangle^{lt} \rightarrow \langle B | \chi \rangle_{cond}^{lt}$. This is in contrast to the standard treatment. Correlation in standard treatment would be defined using the stationary state, i.e, the non trivial $P_{st} = \varphi_0$. Standard correlation, $K_{A,B}^{st} = \sum_{x,y} A_x P(x, t | y, t') B_y P_{st}(y)$. Therefore, if $A_x = 1$, $K_{1,B}^{st} = \sum_{x,y} P(x, t | y, t') B_y P_{st}(y) = \sum_y B_y P_{st}(y) = \langle B \rangle_{st}$

Remark. Looking at the previous two examples, we can see that using $A = \chi$ the average is over trajectories that survive in the interior and don't get ab-

¹In practice in order to calculate conditional averages at large times, as defined above (see for example (3.43)), we can use the following formula

$$\langle A(t) B(t') | \chi \rangle^{lt} = \lim_{t_0 \rightarrow -\infty} \frac{\sum_{x,y,z} A_x P(x, t | y, t') B_y P(y, t' | z, t_0) P_{initial}(z)}{\sum_{x,z} \chi_x P(x, t | z, t_0) P_{initial}(z)} \quad (3.44)$$

and similarly for multiple time correlation functions. The initial condition $P_{initial}$ at time t_0 is arbitrary as far as $P_{initial}(0) < 1$. But for our purposes, it is easier to choose $P_{initial}(0) = 0$.

sorbed by the boundary at least till time t where $A = \chi$ is evaluated. So, we are essentially averaging over only the remaining/surviving particles/trajectories.

With these preliminaries in place, we can now look at how a perturbation in the system affects the observables. We now proceed to look at linear response to perturbation in such systems.

Linear Response

To capture the effect of perturbation, let us consider the perturbation to be represented by a change in the rates, i.e, consequently a change in H . The effect of this perturbation will be a change in the long time state. The general case at all times will be treated in Section 3.3.4

$$\begin{aligned} H &\rightarrow H + \delta H(t) \\ P^{lt}(t) &\rightarrow P^{lt}(t) + \delta P(t) \end{aligned}$$

where $P^{lt}(t) = \varphi_0 + c_1 e^{-\lambda_1 t} \varphi_1$ which is a more general version of the long time state starting from $P^{lt}(0)$ defined in the earlier subsection. Therefore, we can write an equation for the time evolution of $\delta P(t)$ and solve it as a first order ODE.

$$\dot{P}^{lt}(t) + \delta \dot{P}(t) = (H + \delta H(t))(P^{lt}(t) + \delta P(t)) \quad (3.48)$$

$$\delta \dot{P}(t) = H \delta P(t) + \delta H(t) P^{lt}(t) + \text{higher order terms} \quad (3.49)$$

The solution of this with initial condition, $\delta P(0) = 0$ is

$$\delta P(t) = \int_0^t ds e^{H(t-s)} \delta H(s) P^{lt}(s) \quad (3.50)$$

Then, the change in our conditional average of observable is going to be

$$\delta \frac{\langle A \rangle_t}{\langle \chi \rangle_t} = \frac{\delta \langle A \rangle_t}{\langle \chi \rangle_t^{lt}} - \langle A | | \chi \rangle^{lt} \frac{\delta \langle \chi \rangle_t}{\langle \chi \rangle_t^{lt}} + \text{higher order terms} \quad (3.51)$$

$$\begin{aligned} \frac{\delta \langle A \rangle_t}{\langle \chi \rangle_t^{lt}} &= \sum_x A_x \delta P_x(t) / \langle \chi \rangle_t^{lt} \\ &= \frac{1}{\langle \chi \rangle_t^{lt}} \int_0^t ds \sum_{x,x',y} A_x P(x, t | x', s) \delta H_{x',y} P_y^{lt}(s) \end{aligned}$$

Let us assume that the perturbation can be split into time and state components, i.e, $\delta H(s) = V \delta F(s)$, with $V_{x,0} = 0$. Then, we can write the perturbation of the operator average as a response function times the time component of

the perturbation. That is,

$$\frac{\delta\langle A \rangle_t}{\langle \chi \rangle_t^{lt}} = \int_0^\infty ds R_{A,V}(t,s) \delta F(s) \quad (3.52)$$

with $R_{A,V}(t,s) = \frac{\Theta(t-s)}{\langle \chi \rangle_t^{lt}} \sum_{x,x',y} A_x P(x,t|x',s) V_{x',y} P_y^{lt}(s) \equiv \Theta(t-s) \langle A(t) B(s) | \chi \rangle^{lt}$

and

$$B_{x'} = \frac{1}{\varphi_{1x'}} \sum_y V_{x',y} \varphi_{1y} \quad (3.53)$$

Similarly we also write $\frac{\delta\langle \chi \rangle_t}{\langle \chi \rangle_t^{lt}} = \int_0^\infty ds R_{\chi,V}(t,s) \delta F(s)$. Ultimately, with the defined B , we have

$$\delta \frac{\langle A \rangle_t}{\langle \chi \rangle_t} = \int_0^\infty ds \hat{R}_{A,V}(t-s) \delta F(s) \quad (3.54)$$

$$\hat{R}_{A,V}(t-s) = \Theta(t-s) [\langle A(t) B(s) | \chi \rangle^{lt} - \langle A | \chi \rangle^{lt} \langle \chi(t) B(s) | \chi \rangle^{lt}] \quad (3.55)$$

Notice that, thanks to Eq.(3.46) and $\langle \chi | \chi \rangle^{lt} = 1$, we have $\lim_{t \rightarrow \infty} \hat{R}_{A,V}(t) = 0$. Now that we have the form of the response function with conditional correlations, we can try and understand the fluctuation dissipation theorems associated with it.

Fluctuation Dissipation Theorem

Similar to the standard case, let us assume that the transition rate matrix H depends on some parameter f (can also be a set of parameters. For simplicity, we consider one, but the calculations remain the same for multiple parameters). We can now Taylor expand H around no perturbation in f

$$H(f + \Delta f) = H(f) + \left. \frac{\partial H(f)}{\partial f} \right|_{\Delta f=0} \Delta f + \mathcal{O}(\Delta f^2)$$

We drop the subscript $\Delta f = 0$ for visual simplicity. We see that $V = \partial_f H(f)$. Since $(H + \lambda_1 \mathbb{I})\varphi_1 = 0$, differentiating the left hand side with respect to the parameter f ,

$$\left(V + \frac{\partial \lambda_1}{\partial f} \mathbb{I} \right) \varphi_1(f) + (H(f) + \lambda_1 \mathbb{I}) \frac{\partial \varphi_1}{\partial f}(f) = 0 \quad (3.56)$$

Using the above and Eq (3.43) and (3.53), we can write the correlation function

$$\begin{aligned}
\langle A(t) B(s) | \chi \rangle^{lt} &= \sum_{xy} A_x \left(e^{(H(f) + \lambda_1 \mathbb{I})(t-s)} \right)_{xy} (V \varphi_1)_y \\
&= \left[-\frac{\partial}{\partial t} \langle A(t) \frac{\partial \phi(s)}{\partial f} | \chi \rangle^{lt} - \langle A | \chi \rangle^{lt} \frac{\partial \lambda_1(f)}{\partial f} \right] \quad (3.57)
\end{aligned}$$

In (3.57), if we use $A = \chi$, we get a similar form for the second term in (3.55) and we finally obtain (we have dropped the f dependence in ϕ only for simplicity of expression)

$$\hat{R}_{A,V}(t-s) = -\Theta(t-s) \frac{\partial}{\partial t} \left\langle \left(A(t) - \chi(t) \langle A | \chi \rangle^{lt} \right) \frac{\partial \phi(s)}{\partial f} | \chi \right\rangle^{lt} \quad (3.58)$$

Equation (3.58) is the **Fluctuation Dissipation Theorem** for our case of absorbing state in finite and discrete systems! Notice that

$$\left\langle \left(A(t) - \chi(t) \langle A | \chi \rangle^{lt} \right) | \chi \right\rangle^{lt} = 0. \quad (3.59)$$

In the standard treatment without absorbing boundaries, the second term involving $\chi(t) \langle A | \chi \rangle$ in eq.(3.58), is absent. Its presence is important since, from, the remark at the end of the previous section, we expect that, in general

$$\frac{\partial}{\partial t} \left\langle \chi(t) \frac{\partial \phi(s)}{\partial f} | \chi \right\rangle^{lt} \neq 0 \quad (3.60)$$

3.3.2 Continuous State Space

The Fokker-Planck Equation (FPE) describes the time evolution of probability density function under drift and diffusive forces [10]. Though the FPE can be derived from the Master equation assuming small jumps, the derivations we have for discrete state systems may no longer hold in the case of continuous space. One of the primary reason is the change in the eigenvalue spectrum. The formulation developed earlier assumes finite set of states and hence has a finite number of eigenvalues. The spectrum of eigenvalues is infinite or even continuous in certain cases as we shall see.

For simplicity, we consider a one dimensional case. Let us consider the system to be defined on a space $S \subseteq \mathbb{R}$. S contains absorbing boundaries at $S_a \subset S$. Then, using the Fokker-Planck Equation, we can write the probability of finding a particle at x at time t

$$\frac{\partial P(x,t)}{\partial t} = \mathcal{L}(x) P(x,t) \quad (3.61)$$

where $\mathcal{L}(x)$ is the Fokker Planck Operator given by

$$\mathcal{L}(x) = -\frac{\partial}{\partial x} D_1(x) + \frac{\partial^2}{\partial x^2} D_2(x) \quad (3.62)$$

In the absence of a sufficient source term, if an absorbing boundary is present, then, the probability $P(x, t|x_0, t_0) \rightarrow 0$ for $t \rightarrow \infty$. In such cases, the probability is not normalized at all times, i.e, the total probability is not conserved. But, like with discrete case, certain considerations on the asymptotic nature of the probability distribution allows us to make progress.

Let us consider a perturbation occurring at time $t = 0$ and consider $t_0 < 0$. The solution to (3.61) can be written with $P(x, t_0)$ being the initial condition,

$$P(x, t) = e^{\mathcal{L}(x)(t-t_0)} P(x, t_0) \quad (3.63)$$

Similar to the standard case, we represent the perturbation by a change in the Fokker Planck Operator and equivalently the resulting change in the solution to the FPE, i.e, the probability

$$\begin{aligned} \mathcal{L}_{\text{perturb}}(x, t) &= \mathcal{L}(x) + \delta\mathcal{L}(x, t) \\ P_{\text{perturb}}(x, t) &= P(x, t) + \delta P(x, t) \end{aligned} \quad (3.64)$$

$P(x, t)$ and $\mathcal{L}(x)$ are used to represent the unperturbed quantities. We assume that the F-P operator has the same form as without the perturbation, i.e.

$$\delta\mathcal{L}(x, t) = -\frac{\partial}{\partial x} \delta D_1(x, t) + \frac{\partial^2}{\partial x^2} \delta D_2(x, t) \quad (3.65)$$

At the leading order, we get,

$$\delta\dot{P}(x, t) = \delta\mathcal{L}(x, t) P(x, t) + \mathcal{L}(x) \delta P(x, t) \quad (3.66)$$

Because of causality, the solution to (3.66) can be written down as follows

$$\delta P(x, t) = \int_{-\infty}^t d\tau e^{\mathcal{L}(x)(t-\tau)} (\delta\mathcal{L}(x, \tau) P(x, \tau)), \quad (3.67)$$

since $\delta\mathcal{L} = 0$ for all negative times. Until this stage, it has a common form as that of the standard case. The survival probability of finding a non-absorbed trajectory at time t starting from the initial condition at t_0 is

$$\Pi(t) = \int_S dx P(x, t) \quad (3.68)$$

We can also see the total probability conservation failing from (3.68) given absorbing boundary conditions. For an observable $A(x)$, the average at time t

is given by

$$\langle A(t) \rangle = \int dx A(x) P(x, t) \quad (3.69)$$

This average decays to zero due to the decay of the probability. But, if we condition the observable average to be calculated on only the surviving trajectories, we can expect a non-trivial result. Then, we define

$$\langle A(t) \rangle_s = \frac{\langle A(t) \rangle}{\text{prob of survival}} = \frac{\langle A(t) \rangle}{\Pi(t)} \quad (3.70)$$

It is now useful to define a conditional distribution $Q(x, t)$. Eventually, at long times, this will give us the quasi stationary distribution [169].

$$Q(x, t) = \frac{P(x, t)}{\int dx' P(x', t)} \rightarrow_{t \rightarrow \infty} Q_{st}(x) \quad (3.71)$$

At this point, we are assuming that a quasi stationary distribution (QSD) exists, for the unperturbed state. This is equivalent to saying $\Pi(t)$ and $P(x, t)$ have the same rate of decay. The implications of this can be seen in terms of averages and correlation of observables. In terms of (3.71), the average can be written as

$$\langle A(t) \rangle_s = \int dx A(x) Q(x, t)$$

Since we assume QSD exists, as $t \rightarrow \infty$, $\langle A(t) \rangle_s \rightarrow \langle A \rangle_s \equiv \int dx A(x) Q_{st}(x)$

For correlation between two observables, we can also perform similar operation conditioned on survival. If $A(x)$ and $B(x')$ are two observables, assuming $t' < t$ without loss of generality, the correlation is written as

$$\langle A(t) B(t') \rangle = \int \int dx dx' A(x) P(x, t | x', t') B(x') P(x', t') \quad (3.72)$$

Since $P(x, t | x', t') = \exp\{\mathcal{L}(x)(t - t')\} \delta(x - x')$ we get

$$\langle A(t) B(t') \rangle = \int dx A(x) e^{\mathcal{L}(x)(t-t')} (B(x) P(x, t')) \quad (3.73)$$

Correlation conditioned on survived trajectories have to be divided by the survival probability at time t . The caveat is that the survival probability should be considering when the system started, i.e, at t_0 and not just from t' . Then, we have

$$\begin{aligned} \langle A(t) B(t') \rangle_s &= \frac{\langle A(t) B(t') \rangle}{\int dx' P(x', t)} = \frac{1}{\Pi(t)} \int dx A(x) e^{\mathcal{L}(x)(t-t')} (B(x) P(x, t')) \\ &= \int dx A(x) e^{\mathcal{L}(x)(t-t')} (B(x) Q(x, t')) \frac{\Pi(t')}{\Pi(t)} \end{aligned} \quad (3.74)$$

Since (3.63) depends on $t - t_0$, what we need is the difference to go to infinity to reach QSD. Hence, we can also take the limit $t_0 \rightarrow -\infty$. This is consistent with our formulation of the perturbation happening at $t = 0$. With $t_0 \rightarrow -\infty$, we can assume that $\frac{\Pi(t')}{\Pi(t)}$ should approach the form $\exp\{\lambda(t - t')\}$ for some λ (which will turn out to be the leading eigenvalue of $\mathcal{L}(x)$). Further in the calculations, we consider different cases where we make some deeper assumptions based on the eigenvalue spectrum from which the exponential behaviour immediately follows. Although the long time ratio does not depend on t_0 , this does not mean that the individual $\Pi(t)$ do not depend on t_0 . This is a heuristic assumption based on the nature of eigenvalues and a broad class of examples which show this behaviour.

Then,

$$\langle A(t) B(t') \rangle_s =_{t_0 \rightarrow -\infty} e^{\lambda(t-t')} \int dx A(x) e^{\mathcal{L}(x)(t-t')} (B(x) Q_{st}(x)). \quad (3.75)$$

Having seen how conditioning on survival changes the original definitions, we can use them to modify our response function. Change in the observable caused by perturbation in the operator can then be written as

$$\begin{aligned} \delta \langle A(t) \rangle_s &= \delta \left[\frac{1}{\int dx' P(x', t)} \int dx A(x) P(x, t) \right] \\ &= \frac{1}{\int dx' P(x', t)} \int dx A(x) \delta P(x, t) - \frac{\int dx \delta P(x, t)}{(\int dx P(x, t))^2} \int dx A(x) P(x, t) \end{aligned} \quad (3.76)$$

Using (3.67),

$$\begin{aligned} \delta \langle A(t) \rangle_s &= \int dx \int_{-\infty}^t d\tau A(x) e^{\mathcal{L}(x)(t-\tau)} (\delta \mathcal{L}(x, \tau) Q(x, \tau)) \frac{\Pi(\tau)}{\Pi(t)} - \int dx A(x) Q(x, t) \\ &\quad \times \left(\int dx \int_{-\infty}^t d\tau e^{\mathcal{L}(x)(t-\tau)} (\delta \mathcal{L}(x, \tau) Q(x, \tau)) \frac{\Pi(\tau)}{\Pi(t)} \right) \end{aligned} \quad (3.77)$$

We assume that the perturbation is separable, i.e, the spatial and temporal components are described separately. Assuming $\delta \mathcal{L}(x, t) = \delta \mathcal{L}(x) F(t)$, we can then write (3.77) in terms of a response function. We also assume $t_0 \rightarrow -\infty$. This is equivalent to allowing the system to evolve for a long period of time before introducing the perturbation. In the standard case, i.e. when a non-trivial stationary state exists, it is equivalent to starting at stationarity.

$$\begin{aligned} \delta \langle A(t) \rangle_s &= \int_{-\infty}^{\infty} d\tau R_{A,L}(t, \tau) F(\tau) \\ R_{A,L}(t, \tau) &=_{t_0 \rightarrow -\infty} \Theta(t - \tau) \left[\int dx A(x) e^{\mathcal{L}_0(x)(t-\tau)} (\delta \mathcal{L}(x) Q_{st}(x)) e^{\lambda(t-\tau)} \right. \\ &\quad \left. - \langle A \rangle_s \int dx e^{\mathcal{L}_0(x)(t-\tau)} (\delta \mathcal{L}(x) Q_{st}(x)) e^{\lambda(t-\tau)} \right] \end{aligned} \quad (3.78)$$

In the standard case the last term of (3.78) would be

$$I(t) \equiv \int dx e^{\mathcal{L}(x)t} \delta \mathcal{L}(x) P_{st}(x) \quad (3.79)$$

and it is zero due to the normalization of $P_{st}(x)$.

If we define the observable $B(x) = Q_{st}^{-1}(x) \delta \mathcal{L}(x) Q_{st}(x)$, then, we can write the response function in terms of correlation like in the standard case. In doing so, we assume that $Q_{st}(x) > 0 \forall x$. We define an additional variable that accounts for survival of the trajectories. Let $\chi(x) = 1 \quad \forall x \in S-$ (absorbing boundary). Then,

$$R_{A,B}(t, t') = \langle A(t) B(t') \rangle_s - \langle A \rangle_s \langle \chi(t) B(t') \rangle_s \quad (3.80)$$

Here it becomes clear that χ accounts for survival of the trajectories till the time t , according to the definition given in eq.(3.75).

Fluctuation Dissipation Theorem

While (3.80) connects the response of an observable to a correlation, it is quite uninformative since we do not know anything about the perturbation. Like in the standard case, we can analyze the effect of change in parameters and how this affects the response function.

Before we proceed further, it is necessary to take into account the decaying nature of the distribution. Systems that reach a stationary state do not need such considerations. In the standard case, the leading eigenvalue of the Fokker-Planck operator, $\lambda_0 = 0$. The associated eigenfunction is the stationary state. But in decaying systems, while the solution to the FPE is still determined by the eigenvalues and the eigenfunctions, we no longer know anything about the leading eigenvalue except that it is non zero. Since that is the case, we also need the information about the spectrum of eigenvalues. Unlike in discrete space, the eigenvalue spectrum can be discrete or continuous in the continuous space case. This changes the problem significantly but also helps us in arriving at a FDT!

Discrete Eigenvalue Spectrum

Let us assume that the eigenvalue spectrum of $\mathcal{L}(x)$ is discrete. If λ is an eigenvalue and ψ is the associated right eigenfunction,

$$\mathcal{L}\psi = -\lambda\psi \quad (3.81)$$

Then, we assume that the spectrum is of the form

$$0 < \lambda_1 < \text{Re}(\lambda_2) \leq \text{Re}(\lambda_3) \dots \quad (3.82)$$

Note: In discrete and finite systems, we proved the analogous of (3.82) starting from irreducible matrices. In continuous systems, in cases where without absorbing boundaries, there is a stationary solution and x -variables are even under time reversal, then, all the eigenvalues of the system are real. This is because we can write a measure such that the operator \mathcal{L} is Hermitian (see V.7 in [9]). Consequently, if our system remains the same except for the boundary conditions changed to ensure decaying distribution, we can still use the same measure (Section 5.4 of [10]) to make the operator Hermitian and hence, all eigenvalues and eigenfunctions are real. But if we are more general, then, the eigenvalues can be complex. Asymptotically, the leading eigenvalue is what we expect to have dominant contribution to the probability. Since probability is real and non negative, we can expect the leading eigenvalue to be real and corresponding eigenfunction to be real and non-negative. Hence, (3.82) is a general assumption encompassing different examples.

With (3.82), the solution to the FPE (3.63), with initial condition $\delta(x - x_0)$ can be written in term of the eigenfunctions and eigenvalues [10].

$$P(x, t) = \sum_{k=1}^{\infty} c_k(x_0) \psi_k(x) e^{-\lambda_k(t-t_0)} \quad (3.83)$$

where $c_k(x_0)$ are determined by the initial conditions. They are also the left eigenfunctions of the FP operator, i.e, eigenfunctions of adjoint of $\mathcal{L}(x)$. Hence, at long times, $t - t_0 \rightarrow \infty$, (3.83) and the corresponding survival probability are

$$\begin{aligned} P(x, t) &= c_1(x_0) \psi_1(x) e^{-\lambda_1(t-t_0)} [1 + \mathcal{O}(e^{-(\text{Re}(\lambda_2)-\lambda_1)(t-t_0)})] \\ \Pi(t) &= c_1(x_0) e^{-\lambda_1(t-t_0)} \int dx' \psi_1(x') [1 + \mathcal{O}(e^{-(\text{Re}(\lambda_2)-\lambda_1)(t-t_0)})] \end{aligned} \quad (3.84)$$

From this, it can be seen that $\Pi(t)$ is equivalent to $\langle \chi \rangle_t$ in the finite system case. Hence, from Eq (3.71) and (3.68),

$$Q_{st}(x) = \lim_{t_0 \rightarrow -\infty} \frac{P(x, t)}{\Pi(t)} = \frac{\psi_1(x)}{\int dx' \psi_1(x')} \quad (3.85)$$

and

$$\lim_{t_0 \rightarrow -\infty} \frac{\Pi(\tau)}{\Pi(t)} = e^{-\lambda_1(t-\tau)} \quad (3.86)$$

and hence, (3.86) is no longer a primary assumption, but follows from a more basic assumption about the eigenvalue spectrum!

More General Eigenvalue Spectrum

Unlike discrete space with finite states, there is no reason for the eigenvalue spectrum to be discrete. The spectrum can be continuous and discrete together. To be general, we consider a spectral density $\rho(\lambda)$. Solely discrete spectrum is a particular case of the spectral density being a sum of Dirac δ functions. Then, in general, for $\lambda \in D \subset \mathbb{C}$ with $Re(\lambda) > 0$ due to the absorbing boundary, Eq. (3.83) changes to

$$P(x, t) = \int_D \rho(\lambda) \psi_x(\lambda) c_{x_0}(\lambda) e^{-\lambda(t-t_0)} dRe(\lambda) dIm(\lambda) \quad (3.87)$$

While naively, we might try to use asymptotic methods to calculate the dominant value, that would be based on the assumptions that $\rho(\lambda)$, $\psi(\lambda)$ and $c(\lambda)$ are well behaved and non trivial at $\lambda = \lambda_1 \equiv \inf\{Re(\lambda)\}$. As we shall see in some physical examples, like the biased random walk on semi infinite line, the spectrum is real and near the edge of the spectrum, the density of states has power law behaviour $(\lambda - \lambda_1)^{-\beta}$ where $\beta > 0$ and the right and left eigenfunctions depend on the eigenvalues through $\sin(\sqrt{\lambda - \lambda_1}x)$ and $\sin(\sqrt{\lambda - \lambda_1}x_0)$.

For simplicity, we assume that λ is real near the left edge of the spectrum and $\rho(\lambda)$ has the form

$$\rho(\lambda) \sim (\lambda - \lambda_1)^{-\beta} g(\lambda) \quad (3.88)$$

where $g(\lambda)$ is a well behaved function, finite at λ_1 . The right edge of the spectrum is irrelevant since at asymptotically large times, the contribution is exponentially smaller. Assumption (3.88) has the advantage that in case there is no divergence, the exponent can be set to zero.

Similarly, for the right and left eigenfunctions (which are ψ and c), we can make similar assumptions near the edge of the spectrum. But in this case, the functions don't diverge and instead can go to zero. For the case of eigenfunctions going to zero near the edge, let us assume

$$\begin{aligned} \psi_x(\lambda) &= (\lambda - \lambda_1)^\alpha \hat{\psi}_x(\lambda) \\ c_{x_0}(\lambda) &= (\lambda - \lambda_1)^\gamma \hat{c}_{x_0}(\lambda) \end{aligned} \quad (3.89)$$

In principle, we expect $\alpha = \gamma$, but to be more general, we can allow them to

be different. Similar to (3.88), $\hat{\psi}_x(\lambda)$ and $\hat{c}_{x_0}(\lambda)$ are well behaved near the edge of the spectrum. Assumptions (3.88) and (3.89) can actually be presented in a more elegant manner.

Let $\Lambda = \lambda - \lambda_1$ and $\alpha \geq 0, \beta \geq 0$ and $\gamma \geq 0$ be the smallest numbers such that

$$\begin{aligned} \lim_{\Lambda \rightarrow 0} \Lambda^{-\alpha} \psi_x(\Lambda + \lambda_1) &\neq 0 \\ \lim_{\Lambda \rightarrow 0} \Lambda^{-\gamma} c_{x_0}(\Lambda + \lambda_1) &\neq 0 \\ \lim_{\Lambda \rightarrow 0} \Lambda^\beta \rho(\Lambda + \lambda_1) &\in \mathbb{R} \end{aligned} \quad (3.90)$$

The assumptions (3.88) and (3.89) are equivalent to saying α, β and γ are finite. With these assumptions, we are in a position to tackle the beast that is (3.87).

First, we note that at asymptotically large times, the dominant contribution comes from the largest value of the exponential, i.e, the smallest value of $\lambda(t-t_0)$, which would be $\lambda_1(t-t_0)$. But since our functions diverge/decay at that point, we first need to consider the integral in a small range λ_1 to $\lambda_1 + \epsilon$. Then, we are able to use our assumptions.

$$\begin{aligned} P(x, t) &\sim \int_{\lambda_1}^{\lambda_1 + \epsilon} \rho(\lambda) \psi_x(\lambda) c_{x_0}(\lambda) e^{-\lambda(t-t_0)} d\lambda \\ &\sim \int_{\lambda_1}^{\lambda_1 + \epsilon} g(\lambda) \hat{\psi}_x(\lambda) \hat{c}_{x_0}(\lambda) e^{-\lambda(t-t_0)} \Lambda^{\alpha+\gamma-\beta} d\lambda \\ (u = \Lambda(t-t_0)) &\sim \frac{e^{-\lambda_1(t-t_0)}}{(t-t_0)^{1+\alpha+\gamma-\beta}} \int_0^{\epsilon(t-t_0)} du g\left(\frac{u}{(t-t_0)} + \lambda_1\right) \\ &\quad \times \hat{\psi}_x\left(\frac{u}{(t-t_0)} + \lambda_1\right) \hat{c}_{x_0}\left(\frac{u}{(t-t_0)} + \lambda_1\right) e^{-u} u^{\alpha+\gamma-\beta} \end{aligned} \quad (3.91)$$

We now consider the limit $t_0 \rightarrow -\infty$. Let $h(y) = g(y) \hat{\psi}_x(y) \hat{c}_{x_0}(y)$. Then, Taylor expanding h around λ_1 ,

$$\begin{aligned} P(x, t) &\sim \frac{e^{-\lambda_1(t-t_0)}}{(t-t_0)^{1+\alpha+\gamma-\beta}} \int_0^\infty du \left[h(\lambda_1) + \frac{u}{(t-t_0)} h'(\lambda_1) + \mathcal{O}\left(\frac{u^2}{(t-t_0)^2}\right) \right] e^{-u} u^{\alpha+\gamma-\beta} \\ &\sim \frac{e^{-\lambda_1(t-t_0)}}{(t-t_0)^{1+\alpha+\gamma-\beta}} \left[h(\lambda_1) \Gamma(1 + \alpha + \gamma - \beta) + h'(\lambda_1) \frac{\Gamma(2 + \alpha + \gamma - \beta)}{(t-t_0)} + \mathcal{O}\left(\frac{1}{(t-t_0)^2}\right) \right] \\ &\sim \frac{e^{-\lambda_1(t-t_0)}}{(t-t_0)^{1+\alpha+\gamma-\beta}} \Gamma(1 + \alpha + \gamma - \beta) g(\lambda_1) \hat{\psi}_x(\lambda_1) \hat{c}_{x_0}(\lambda_1) + \text{h.o.t} \end{aligned} \quad (3.92)$$

Similarly, we can also perform the asymptotic limit for the survival probability $\Pi(t) = \int dx P(x, t)$ obtaining

$$\Pi(t) \sim \frac{e^{-\lambda_1(t-t_0)}}{(t-t_0)^{1+\alpha+\gamma-\beta}} \Gamma(1+\alpha+\gamma-\beta) g(\lambda_1) \hat{c}_{x_0}(\lambda_1) \int dx \hat{\psi}_x(\lambda_1) + \text{h.o.t} \quad (3.93)$$

Hence, the conditional probability density leads us to the quasi stationary distribution. We denote $\hat{\psi}_x(\lambda_1)$ by $\hat{\psi}_1(x)$.

$$Q(x, t) = \frac{P(x, t)}{\Pi(t)} \xrightarrow{t_0 \rightarrow -\infty} \frac{\hat{\psi}_1(x)}{\int dx' \hat{\psi}_1(x')} = Q_{st}(x)$$

$$\frac{\Pi(t')}{\Pi(t)} \xrightarrow{t_0 \rightarrow -\infty} e^{\lambda_1(t-t')} \quad (3.94)$$

$$\mathcal{L}(x)Q_{st}(x) = -\lambda_1 Q_{st}(x) \quad (3.95)$$

It should be noted that the above relation also holds when the eigenvalue spectrum is discrete since it directly follows from (3.85)

Perturbation of Parameters

We now have all the necessary tools to arrive at a FDT. Like in the standard case, let us consider that $\mathcal{L}(x)$ depends on a set of parameters $f \equiv \{f_1, f_2, \dots, f_n\}$. We show the calculations for a perturbation in one of these parameters because perturbation in multiple parameters follows in a similar manner. Assuming a perturbation in a parameter $f \rightarrow f + \Delta f$, the Fokker-Planck operator can then be written as

$$\mathcal{L}(x, t) = \mathcal{L}(x) + \frac{\partial \mathcal{L}(x)}{\partial f} \Delta f(t) + \mathcal{O}(\Delta f^2) \quad (3.96)$$

Assuming perturbation till linear order, this is of the form

$$\mathcal{L}(x, t) = \mathcal{L}(x) + \delta \mathcal{L}(x) F(t),$$

$$\text{with } \delta \mathcal{L}(x) = \frac{\partial \mathcal{L}(x)}{\partial f}, \quad F(t) = \Delta f(t) \quad (3.97)$$

From (3.95), differentiating with respect to the parameter, we have

$$\delta \mathcal{L}(x)Q_{st}(x) = -(\mathcal{L}(x) + \lambda_1) \frac{\partial Q_{st}}{\partial f} - \frac{\partial \lambda_1}{\partial b} Q_{st} \quad (3.98)$$

Because of (3.95) and $\Pi(\tau)/\Pi(t) \xrightarrow{t_0 \rightarrow -\infty} e^{\lambda_1(t-\tau)}$ in (3.78) with $\lambda = \lambda_1$, the last term in (3.98) does not contribute to the response function. Substituting the rest into (3.78), we get

$$\begin{aligned}
R_{A,f}(t-\tau) &= -\Theta(t-\tau) \left[\int dx A(x) e^{(\mathcal{L}(x)+\lambda_1)(t-\tau)} (\mathcal{L}(x) + \lambda_1) \frac{\partial Q_{st}}{\partial f} + \right. \\
&\quad \left. + \langle A \rangle_s \int dx e^{(\mathcal{L}(x)+\lambda_1)(t-\tau)} (\mathcal{L}(x) + \lambda_1) \frac{\partial Q_{st}}{\partial f} \right] = \\
&= -\Theta(t-\tau) \frac{\partial}{\partial t} \left[\int dx A(x) e^{(\mathcal{L}(x)+\lambda_1)(t-\tau)} \frac{\partial Q_{st}}{\partial f} + \right. \\
&\quad \left. - \langle A \rangle_s \int dx e^{(\mathcal{L}(x)+\lambda_1)(t-\tau)} \frac{\partial Q_{st}}{\partial f} \right] \tag{3.99}
\end{aligned}$$

Since x dependence of (3.92) is given by $\hat{\psi}_1(x)$, we assume that it has to be positive for the probability to be positive. This is equivalent to our earlier statement about $Q_{st}(x) > 0$. Therefore, we are able to write $Q_{st}(x) = e^{\phi(x)}$ where ϕ is some potential. Setting the perturbation to happen at $\tau = 0$ and assuming $t > 0$ in (3.99), we can write it as

$$\begin{aligned}
R_{A,f}(t) &= -\frac{\partial}{\partial t} \left[\int dx A(x) e^{(\mathcal{L}(x)+\lambda_1)(t-\tau)} \frac{\partial \phi(x)}{\partial f} Q_{st}(x) \right. \\
&\quad \left. - \langle A \rangle_s \int dx e^{(\mathcal{L}(x)+\lambda_1)(t-\tau)} \frac{\partial \phi(x)}{\partial f} Q_{st}(x) \right] \\
R_{A,f}(t) &= -\frac{\partial}{\partial t} \left[\left\langle \left[A(t) - \langle A \rangle_s \chi(t) \right] \frac{\partial \phi(\tau=0)}{\partial f} \right\rangle_s \right] \tag{3.100}
\end{aligned}$$

where we have used (3.75).

Equation (3.100) is the Fluctuation Dissipation theorem we desire and we see that this is of the same form as Eq. (3.58). This connects the response of the perturbation of a parameter to a given observable that we can compute if we know the potential, i.e, the QSD. We have made a significant number of assumptions that we believe is based on physical systems. It might very well be possible to arrive at a very particular set of D_1 and D_2 in the Fokker-Planck operator that renders our assumptions invalid. But for the systems we believe the assumptions to hold, it now remains that we take those examples and verify whether the fluctuation dissipation theorem holds.

3.3.3 Examples and Verification

In the derivation of the FDT, we have made several assumptions, especially in the continuous state-space case. Here, we present several examples in increasing order of feasibility of solution/in same order of the assumptions that validate our derivation. Specifically, we start from a simple discrete system where

all quantities can be calculated exactly, proceeding finally towards geometric Brownian motion where we compute the response using directly the long time limit of the propagator.

In each system, we analytically/numerically compute the response functions from the appropriate formula given the system. Then we consider a delta perturbation in the parameters, i.e,

$$\Delta f(t) = \Delta f \times \delta(t) \quad \delta(t) \text{ is a Dirac Delta function}$$

This would reduce our response in the observable to perturbation in a parameter to just the response function, i.e,

$$\delta \langle A(t) \rangle_{survived} = R_{A,f}(t) \Delta f$$

We perform simulation of the system to verify the results obtained analytically. For discrete systems, we perform the simulations using Gillespie algorithm. For continuous systems, we consider the Langevin equation and evolve it in a small time interval dt using the Euler-Maruyama algorithm. The system is allowed to run for a long time before the perturbation is applied, following which the responses are calculated. The response is calculated by measuring the conditional observable, i.e, mean value of the observable computed using only the particles that have survived till that time instant. We then compare it to the unperturbed observable and plot how the perturbation response changes with time.

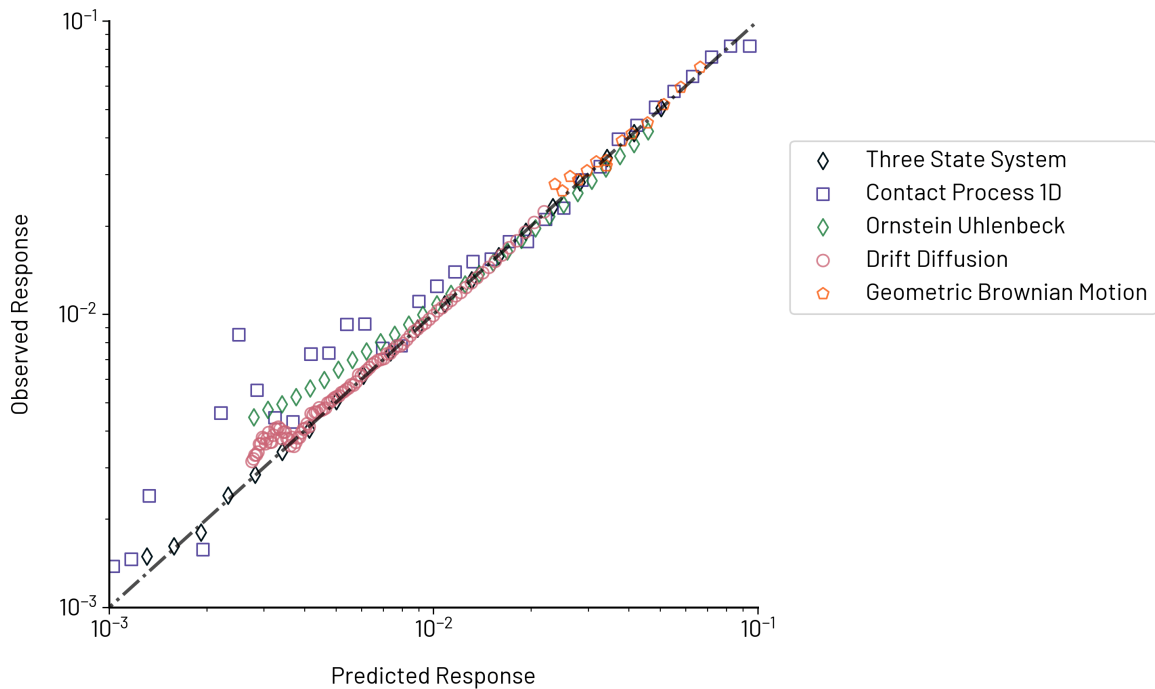


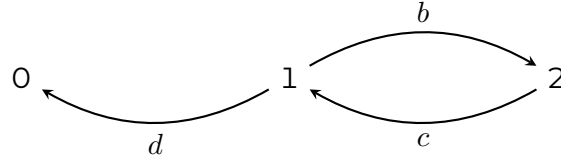
Figure 3.1: Predicted response against observed response for different discrete and continuous processes. Predictions were made using the generalized theory and observations using numerical simulations of the system with averaging over 10^6 trajectories

Figure 3.1 shows the validity of our generalized FDT through comparison between predictions and simulations of various examples. The prediction agrees with the observation at all significant values, with deviations only seen at lower response values where larger number of trajectories are needed to obtain the correct average result (a large number requirement arising from the presence of absorbing boundary and the necessity of good temporal resolution). Subsequently, it is also noted that our assumptions about the continuous eigenvalue spectrum and the ability to make predictions using the generalized FDT with the long-time limit of the probability distribution are correct. While this validates our theory where the prediction occurs at quasi-stationary times, the FDT can be generalized to perturbations at all times.

The details of each example is given below. However, in some examples, though it is possible to analytically compute the quasi-stationary distribution, a computation of the response function is not feasible. In such cases, we have computed the response by numerically integrating Eq (3.100). In simple cases where response function computation is analytically possible, they have been mentioned.

I. Three State System

We consider a simple three state system with an absorbing boundary at zero, from which all the eigenvectors and eigenvalues can be computed.



Corresponding to this, we can also write Master Equation as

$$\dot{P}(t) = HP(t)$$

where H is

$$\begin{bmatrix} 0 & d & 0 \\ 0 & -(b+d) & c \\ 0 & b & -c \end{bmatrix}$$

Writing $t \equiv t' = ct$, $b \equiv b' = b/c$, $d \equiv d' = d/c$, we can set $c = 1$ in our system. The first eigenvalue is 0 as expected, which corresponds to a delta-centered eigenvector on the zero state. The other two eigenvalues are both real and

$$\lambda_{\pm} = \frac{b+d+1 \pm \sqrt{(b+d+1)^2 - 4d}}{2} \quad (3.101)$$

λ_1 is the smaller of the two eigenvalues. It is also seen that the condition on the eigenvalue spectrum is satisfied, as expected. Starting from this, we obtain the eigenvectors as

$$\varphi_1 = \begin{bmatrix} -1 \\ \frac{\lambda_1}{d} \\ \frac{b\lambda_1}{d(1-\lambda_1)} \end{bmatrix} \quad (3.102)$$

To compute the propagator, i.e, the exponential of H , we do diagonal decomposition of $(H + \lambda_1 \mathbb{I})(t - s)$ and exponentiate the diagonal matrix.

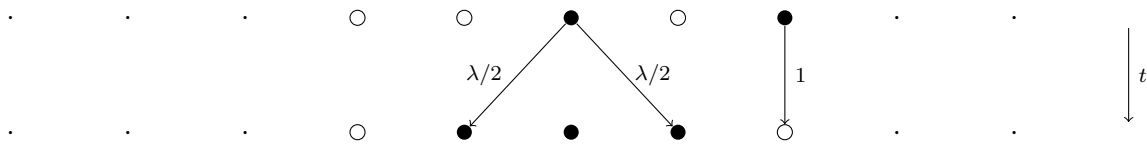
We consider the observable $A_n = n$ and $A_n = n^2$. These satisfy our requirement of $A_0 = 0$. We have two parameters to perturb, the birth rate b and the death rate d . We observe a timescale in the system which we denote by $1/\tau = \sqrt{(b+d+1)^2 - 4d}$. The response functions for perturbations in the parameters then are (for $t > 0$)

$$R_{n,b}(t) = \frac{\lambda_1 e^{-t/\tau}}{d} \quad (3.103)$$

$$R_{n^2,d}(t) = \frac{3(d-1-b^2-b(2+d)) + (b+1)/\tau}{2d^2} e^{-t/\tau} \quad (3.104)$$

II. Contact Process

The Contact Process is one of the important models in continuous time stochastic processes. A simplified model of the Directed Percolation class, the contact process shows many interesting non equilibrium properties and is a useful tool in fields like epidemics. The model consists of N sites, which can be infected $\{1\}$ or not $\{0\}$. Infected sites have chance at infecting their healthy neighbours with rate $\lambda/2d$ (λ is the standard notation used in the Contact Process model. It has no connection to the eigenvalues we have discussed) where d is the dimension of the system. The infected sites heal into healthy sites at rate 1 (any other rate R can be considered to be equal to 1 by appropriate rescaling of time). A representation of the model with the transition rates in 1D is given below. The filled circles represent infected sites and the empty sites are healthy sites.



In the mean field limit this model shows phase transition. For $\lambda < \lambda_c$, all sites eventually heal. Once all sites are healthy, there is no infected site to arise and hence, this is an absorbing state. For $\lambda > \lambda_c$, there exists a non trivial value of the stationary value of average number of infected sites. We consider the absorbing regime to test the validity of our response theory. Notice, however, that as far as the system is finite we always end up in the absorbing state. The master equation for the contact process is

$$\frac{\partial P_i}{\partial t} = \sum_j \left(W_{i,j} P_j - W_{j,i} P_i \right) \tag{3.105}$$

where $i = (i_1, i_2, \dots, i_N), j = (j_1, j_2, \dots, j_N)$ with $i_k, j_k \in \{0, 1\}$ being the possible states of node k , whereas i and j representing the state of the entire system. $i = 0$ is the absorbing state corresponding to $i_k = 0, \forall k$. We consider 1D model of the contact process with $N = 10$ lattice sites and $\lambda = 0.5$ and periodic boundary conditions. There are a total of 2^{10} possible states with absorbing state denoted by 0. The transition matrix is constructed based on the rules presented above. We consider only 1 event per transition. This means if there are two healthy neighbours of an infected site, only one of them can be infected per transition. From the transition matrix, we numerically calculate the second eigenvalue, the second right eigenvector and also the derivative of the eigenvector. Then, we can use this formula to calculate the response function for average number of infected sites, i.e $A_i = x_i = \sum_{k=1}^N i_k$ being the number of infected sites in the

state i :

$$\begin{aligned}
 R_{x,\lambda}(t) &= \frac{\partial}{\partial t} \left(- \sum_{i,j} x_i (e^{(H+\lambda_1 \mathcal{I})t})_{ij} \frac{\partial \varphi_{1j}}{\partial \lambda} + \sum_j x_j \varphi_{1j} \sum_{i,j} \chi_i (e^{(H+\lambda_1 \mathcal{I})t})_{ij} \frac{\partial \varphi_{1j}}{\partial \lambda} \right) \\
 &= - \sum_{i,j} x_i ((H + \lambda_1 \mathcal{I}) e^{(H+\lambda_1 \mathcal{I})t})_{ij} \frac{\partial \varphi_{1j}}{\partial \lambda} \\
 &\quad + \sum_j x_j \varphi_{1j} \sum_{i,j} \chi_i ((H + \lambda_1 \mathcal{I}) e^{(H+\lambda_1 \mathcal{I})t})_{ij} \frac{\partial \varphi_{1j}}{\partial \lambda}
 \end{aligned}$$

$\chi_i = 1$ for all non zero states and zero for $i = 0$. φ_1 is the second right eigenvector and λ_1 is the corresponding eigenvalue of H (see Eq. (3.58)).

III. Ornstein-Uhlenbeck Process with absorbing boundary

The Ornstein-Uhlenbeck process is one of the most standard examples in stochastic processes, describing the evolution of velocity in the overdamped limit. While the process can be considered over the entire real line in 1D, for our purposes, we limit the domain of velocity to be $[0, \infty)$ with an absorbing boundary at zero. The Langevin equation is given by

$$\dot{v}(t) = -\gamma v(t) + \sqrt{D} \eta(t) \quad (3.106)$$

with $\eta(t)$ being a Gaussian white noise with zero mean and delta correlation, $\langle \eta(t) \rangle = 0$ and $\langle \eta(t) \eta(t') \rangle = 2\delta(t - t')$.

The Fokker Planck operator can be transformed into a Hermitian operator. This is achieved by the use of an appropriate function ϕ .

$$\mathcal{L} = e^{\phi_s/2} \mathcal{L} e^{-\phi_s/2} \quad (3.107)$$

The potential ϕ_s is the same one that controls the stationary solution, i.e, $P_{st} = \mathcal{N} e^{-\phi_s}$, where \mathcal{N} is the normalization constant. In the presence of an absorbing boundary, the stationary solution does not exist, but the function ϕ_s can still be written in certain cases. Usually, this can occur from the stationary solution which exists if the boundary condition is changed from absorbing to reflecting. With the Hermitian form of the operator, it is possible to transform the Fokker-Planck equation to a Schrodinger like equation (see 5.4 in [10]). Therefore, problems in stochastic processes can be solved by identifying the appropriate potential that enters into the Schrodinger equation.

For the Ornstein-Uhlenbeck process on the real line with natural boundary conditions, the solution is given by the eigenfunctions which are Hermite poly-

nomials, H_n .

$$\mathcal{L}_0 \psi_n = -\lambda_n \psi_n$$

$$\lambda_n = \gamma n$$

$$\psi_0(v) = \sqrt[4]{\frac{\gamma}{2\pi D}} e^{-\frac{\gamma}{4D}v^2} = \sqrt{P_{st}(v)} = \sqrt{N} e^{-\phi_s(v)/2}$$

$$\psi_n(v) = \sqrt[4]{\frac{\gamma}{2\pi D}} \frac{1}{\sqrt{2^n n!}} H_n \left(\sqrt{\frac{\gamma}{2D}} v \right) e^{-\frac{\gamma}{4D}v^2}$$

$$P(v, t|v_0, 0) = e^{\phi_s(v_0)/2 - \phi_s(v)/2} \sum_n \psi_n(v) \psi_n(v_0) e^{-\lambda_n t} \quad (3.108)$$

For absorbing boundary at zero, only the eigenfunctions which are zero are zero should be retained. Furthermore, the flux at zero should be non zero. The odd Hermite polynomials satisfy these conditions. Hence, only the odd eigenfunctions are eigenfunctions for the problem with absorbing boundary, i.e, only $m = 2n - 1$ for $n \geq 1$ eigenvalues are eigenfunctions of (3.108) are solutions. For our problem, we only need the first non zero eigenvalue and the eigenfunction, which corresponds to $n = m = 1$.

While there is no summation formula for the odd Hermite polynomials, we are able to use the method of images to construct the solution to the problem. To find the probability distribution of finding the velocity to be v at a time t , consider two initial conditions, v_0 and $-v_0$. We know the solution to the OU process on the real line. Using the two initial conditions and consequently the two solutions, imposing the absorbing boundary condition implies that we need the combination of the two solutions to be zero at zero. This is achieved simply by taking the difference of the two. It can be verified that the solution satisfies the corresponding FPE to (3.106) with absorbing BC.

$$P(v, t|v_0, 0) = \sqrt{\frac{\gamma}{2\pi D(1 - e^{-2\gamma t})}} \left\{ \exp \left[-\frac{\gamma(v - v_0 e^{-\gamma t})^2}{2D(1 - e^{-2\gamma t})} \right] - \exp \left[-\frac{\gamma(v + v_0 e^{-\gamma t})^2}{2D(1 - e^{-2\gamma t})} \right] \right\} \quad (3.109)$$

The quasi stationary distribution can be evaluated, both from long time limit of (3.109) and the first eigenfunction. They both match and give the result

$$Q_{st}(v) = \frac{\gamma v}{D} e^{-\frac{\gamma v^2}{2D}} \quad (3.110)$$

IV. Biased Diffusion on positive real line

Diffusion problems are central in the study of stochastic processes with applications to many fields. One of the common extension to diffusion is the presence

of a constant drift term, thereby biasing the diffusion in a certain direction. The presence of a drift term modifies the Langevin equation to

$$\dot{x}(t) = -v + \sqrt{D} \eta(t) \quad (3.111)$$

where $v > 0$ and $\eta(t)$ is a Gaussian white noise as described in the earlier example. There is no stationary solution for the diffusion problem on the entire real line since the distribution decays to zero with larger time. For a biased diffusion, we restrict the domain to the positive part of the real line with absorbing boundary to be at zero. The solution to this problem can be found through the method of images [181, 182].

$$P(x, t|x_0, 0) = \frac{1}{\sqrt{4\pi Dt}} \left(e^{-\frac{(x-x_0+vt)^2}{4Dt}} - e^{\frac{vx_0}{D}} e^{-\frac{(x+x_0+vt)^2}{4Dt}} \right) \quad (3.112)$$

But the solution does not give us the eigenfunctions or the eigenvalues. We can start to find the solution by initially considering the domain to be closed between $[0, L]$. Then, for reflecting BC, the stationary solution gives us the potential with which we can transform the FP operator to a Hermitian operator.

For a closed interval solution, let the system be on the domain $[0, L]$. Then, the corresponding FPE of (3.111) is given by

$$\dot{P} = v\partial_x P + D\partial_x^2 P \quad (3.113)$$

In the case of domain being $[0, \infty)$ with reflecting boundary condition at $x = 0$, the stationary solution of (3.113) is $P_{st} = v/D e^{-vx/D}$. Since the Fokker-Planck operator has the same form for different boundary conditions and domains, we are able to get the potential $\phi_s(x)$ from the stationary solution in semi-infinite problem. Because of the existence of the potential, we are also able to transform the Fokker-Planck operator into a Hermitian operator in the case of closed domain $[0, L]$ with absorbing boundary conditions. Hence, the eigenvalues and the eigenfunctions of the operator are real. We stress that this might not be possible in all examples, but only in examples where the potential can be computed (See [183] for an example of non Hermitian form).

With a closed domain, we split the spatial and the temporal components of the solution to the FPE.

$$P(x, t) = P_\lambda(x) e^{-\lambda t} \quad (3.114)$$

$P_\lambda(x)$ are the eigenfunctions of the FPE. Then, if $e^{-\mu x}$ is a guess solution for the equation obeyed by $P_\lambda(x)$,

$$\mu = \frac{v}{2D} \pm \sqrt{\frac{v^2}{4D^2} - \frac{\lambda}{D}} \quad (3.115)$$

Then, applying the boundary conditions, i.e, $P(x, t) = 0$ at $x = 0$ and $x = L$, with the knowledge that the eigenfunctions and eigenvalues are real, we obtain

$$P_\lambda(x) = \sqrt{\frac{2}{L}} e^{-\frac{vx}{2D}} \sin\left(\frac{\pi k}{L} x\right)$$

$$\lambda_k = \frac{v^2}{4D} + \frac{D\pi^2 k^2}{L^2} \quad (3.116)$$

The eigenvalues in this case are discrete. But note that in the limit $L \rightarrow \infty$, the gap between successive eigenvalues continues to shrink. They then lead to a continuous spectrum. Such mixed spectrum problems can also be solved [184, 185]. Solving for the continuous spectrum, we obtain

$$P(x, t|x_0, 0) = \int_{v^2/4D}^{\infty} d\lambda \left(\frac{\lambda}{D} - \frac{v^2}{4D^2}\right)^{-1/2} e^{-v\frac{x-x_0}{2D}} e^{-\lambda t}$$

$$\sin\left(\sqrt{\frac{\lambda}{D} - \frac{v^2}{4D^2}} x\right) \sin\left(\sqrt{\frac{\lambda}{D} - \frac{v^2}{4D^2}} x_0\right) \quad (3.117)$$

Note that the integral when evaluated also gives the same solution as the one obtained from method of images. The problem can also be solved by making the change into QM perspective [10]. Considering a V shaped potential in the FPE, we get the biased diffusion problem. Imposing absorbing BC is equivalent to restricting the domain and considering eigenfunctions satisfying the BC. This method gives us the same eigenfunctions and the eigenvalues as earlier.

The eigenfunctions approach zero near the edge of the spectrum, i.e, near $\lambda = v^2/4D$. Then, expanding the eigenfunctions and taking the limit as mentioned in the theory, we obtain the quasi stationary distribution. This agrees with the simulations of the systems when we take the conditional distribution at large times from simulation.

$$Q_{st}(x) = \frac{v^2 x}{4D^2} e^{-\frac{vx}{2D}} \quad (3.118)$$

V. Geometric Brownian Motion

In the standard Brownian Motion, the noise strength is constant. But the diffusion coefficient can also depend on the variable under evolution. Geometric Brownian Motion is a model in which the logarithm of the position follows biased diffusion [186] and consequently, the position has a demographic noise component to it. The model has been widely used in finance to model stock prices [51]. The model is usually considered with positive drift and hence, solutions can be found to be a lognormal distribution.

$$\dot{x}(t) = \mu x(t) + \sqrt{2\sigma} x(t) \eta(t) \quad (3.119)$$

For $\mu > 0$ and natural boundary conditions for $\log(x)$, the time dependant distribution is

$$P(x, t|x_0, 0) = \frac{1}{x\sqrt{4\pi\sigma^2 t}} e^{-\frac{[\log(x/x_0) - (\mu - \sigma^2)t]^2}{4\sigma^2 t}} \quad (3.120)$$

This is obtained by considering a change of variables $y = \log(x/x_0)$ under Ito prescription. This leads to the SDE

$$\dot{y}(t) = (\mu - \sigma^2) + \sqrt{2\sigma}\eta(t) \quad (3.121)$$

Note that this is just a biased diffusion Langevin equation, for which we know the solution. By using the solution and changing the variables back to x , we obtain (3.120). But it is important to note that at $x = 0$, $y = -\infty$. This means, applying natural boundary conditions on y , i.e, the flux and the probability are zero at infinities, we also impose that on changing the variables back to x , the flux and probability are zero at $x = 0$. This leads to complications, such as, if $\mu < 0$, then, the particle never reaches zero. The closer it gets to zero, the slower it moves. Hence, although it asymptotically reaches zero, there is no hitting the boundary.

Under this model, it is not possible to impose absorbing boundary condition at $x = 0$ since the particle is effectively never absorbed. We introduce a small $\epsilon > 0$ where the boundary is present. This changes the boundary conditions of the model, but allows us to impose an absorbing boundary at $x = \epsilon$. We replace μ with $-\mu$ so that $\mu > 0$ and then follow similar procedure with the change of variables. Then, under the new boundary conditions, the time dependant distribution is

$$\dot{x}(t) = -\mu x(t) + \sqrt{2\sigma} x(t) \eta(t) \quad (3.122)$$

$$P(x, t|x_0, 0) = \frac{1}{x\sqrt{4\pi\sigma^2 t}} \left[e^{-\frac{(\log(x/x_0) - vt)^2}{4\sigma^2 t}} - e^{\frac{v}{\sigma^2} \log(\epsilon/x_0)} e^{-\frac{(\log(x/x_0/\epsilon) - vt)^2}{4\sigma^2 t}} \right] \quad (3.123)$$

where $v = -(\mu + \sigma^2)$ is the effective drift velocity. The flux at $x = \epsilon$ is negative. Hence, the boundary is absorbing. Furthermore, the original model is recovered in the limit $\epsilon \rightarrow 0$ as expected.

Since we have the time dependant distribution, we can also compute the long time distribution and use it to calculate the quasi stationary distribution and the eigenvalue. This has the benefit of avoid the machinery that one needs

to deal with to calculate the eigenvalues and the spectrum.

$$\lambda_1 = \frac{v^2}{4\sigma^2} \quad (3.124)$$

$$Q_{st}(x) = \frac{v^2}{4\sigma^4 x} \left(\frac{x}{\epsilon}\right)^{-\frac{v}{2\sigma^2}} \log\left(\frac{x}{\epsilon}\right) \quad (3.125)$$

3.3.4 Extension to arbitrary times

In the standard case and in the extension to absorbing systems, the perturbation occurs either at stationarity or at long times when the solution to the FPE/ME is dominated by the leading eigenvalue and the eigenfunction. But the perturbation can also occur at a general non-stationary state. In the standard case with non-absorbing boundaries, the modified fluctuation dissipation theorem was derived by [167, 187]. We slightly modify the notation used so far to be in line with the previous work on out-of-equilibrium fluctuation-dissipation theorem [167]. In a discrete system with an external field h , the response function is given by

$$R_A(t, t') = -\frac{d}{dt'} \langle A(t) \partial_h \psi(t') |_{h=0} \rangle \quad (3.126)$$

Here, $\{c\}$ are the set of states, h_t is the time dependant perturbation and the probability distribution, with the time dependant perturbation replaced by a constant perturbation h is given by $\rho_t(c, h) = e^{-\psi_t(c, h)}$. Now, ψ_t is an explicit time-dependent potential which at large times, leads to ϕ of the standard case (or see later for appropriate modification for absorbing case) that we were employing previously.

The deviation from the observable A is then given by

$$\delta \langle A_t \rangle_h = \int_0^t dt' h_{t'} R_A(t, t') \quad (3.127)$$

where the subscript of h is used to identify perturbed observable, equivalent to $F(t)$ from previous derivations.

Similar to previous procedures, we condition the observable to survival. Then,

$$\delta \frac{\langle A_t \rangle_h}{\langle \chi_t \rangle_h} = \frac{1}{\langle \chi_t \rangle_0} \delta \langle A_t \rangle_h - \frac{\langle A_t \rangle_0}{\langle \chi_t \rangle_0} \frac{\delta \langle \chi_t \rangle_h}{\langle \chi_t \rangle_0} \quad (3.128)$$

The subscript 0 is used to denote unperturbed dynamics. Writing the conditioned observable with response functions,

$$\delta \frac{\langle A_t \rangle_h}{\langle \chi_t \rangle_h} = \int_0^t dt' h_{t'} \left[\frac{R_A(t, t')}{\langle \chi_t \rangle_0} - \frac{\langle A_t \rangle_0}{\langle \chi_t \rangle_0} \frac{R_\chi(t, t')}{\langle \chi_t \rangle_0} \right] \quad (3.129)$$

Since the distribution decays to zero in the presence of absorbing boundary,

the solution to ME with constant perturbation also needs to be conditioned to survival. Defining a new potential as

$$\phi_t(c) = \psi_t(c) + \log(\langle \chi_t \rangle) \quad (3.130)$$

we obtain the conditioned distribution $\rho/\langle \chi \rangle$. Since $\log(\langle \chi_t \rangle)$ is independent of states,

$$\begin{aligned} \frac{1}{\langle \chi_t \rangle} \langle A_t [\partial_h \phi_{t'} - \log(\langle \chi_t \rangle)] \rangle = \\ \frac{1}{\langle \chi_t \rangle} \langle A_t \partial_h \phi_{t'} \rangle - \frac{\langle A_t \rangle}{\langle \chi_t \rangle} \log(\langle \chi_t \rangle) \end{aligned} \quad (3.131)$$

Similarly, the term involving χ results in

$$\begin{aligned} \frac{\langle A_t \rangle}{\langle \chi_t \rangle^2} \langle \chi_t [\partial_h \phi_{t'} - \log(\langle \chi_t \rangle)] \rangle = \\ \frac{\langle A_t \rangle}{\langle \chi_t \rangle^2} \langle \chi_t \partial_h \phi_{t'} \rangle - \frac{\langle A_t \rangle}{\langle \chi_t \rangle^2} \langle \chi_t \rangle \log(\langle \chi_t \rangle) \end{aligned} \quad (3.132)$$

We have dropped the subscript 0 and the evaluation at $h = 0$ of $\partial_h \phi_{t'}$ for visual simplicity in calculations. The last two terms in (3.131) and (3.132) cancel out. Then, the modified FDT has two contributions to the effective response function.

$$\hat{R}_A(t, t') = -\frac{d}{dt'} \left[\frac{1}{\langle \chi_t \rangle_0} \langle A(t) \partial_h \phi(t') \rangle - \frac{\langle A_t \rangle_0}{(\langle \chi_t \rangle_0)^2} \langle \chi(t) \partial_h \phi(t') \rangle \right] \quad (3.133)$$

At the long time limit, i.e. $t_0 \rightarrow -\infty$, the form of χ_t depends only on the second right eigenvector and eigenvalue giving us result of previous calculations. It is to be noted that this is not entirely straightforward from the initial formula without introducing survival. The quantities in (3.126) end up becoming trivial under long time limit. Furthermore, the considerations of entropy production in [167] do not hold valid when there is absorbing boundary and therefore outgoing rate out of boundary state is zero.

We verify the modification of the FDT for a general non-stationary perturbation. The calculations of the quantities are more intensive, since there is no simplification arising out of asymptotic long time limit. Hence, we consider the earlier Three-State System in which we know the eigensystem completely. Figure 3.2 shows remarkable agreement with the simulations at various perturbation times. Furthermore, the evolution of the response function with changing perturbation times is clearly seen, with the approach to the analytically predicted response from quasi stationary state.

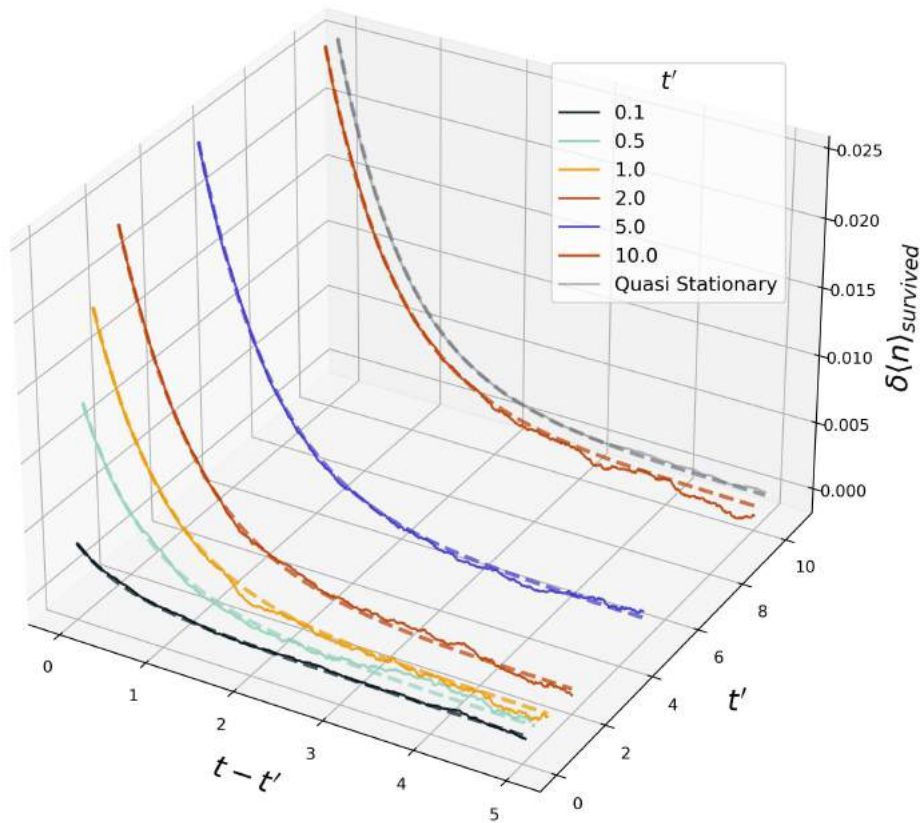


Figure 3.2: Verification of modification of FDT to non stationary perturbation with absorbing boundary in three state system. The perturbation is applied at time t' with the system being prepared at $t_0 = 0$. The legend shows the different perturbation times with the system starting at $x_0 = 2$. The dashed line represent the predictions from (3.133). The gray lines represent the prediction and the simulation from the quasi stationary state

3.3.5 Biological Examples

Having seen many standard examples of stochastic processes and verified out FDT, we proceed to use this in some biologically relevant examples. A crucial point similar to the continuous system is that if the state space is discrete and infinite, the eigenvalue heirarchy is no longer guaranteed. But the dynamics might be such that the heirarchy is still satisfied, which happens in the Birth-Death model of forest ecosystems presented in the Introduction chapter. We then also apply the FDT in a biochemical regime with an example of DNA target search by proteins.

Birth-Death Process

The birth-death process is a common starting point for modelling stochastic population dynamics in ecological communities. A random fluctuation may lead a species to reach zero population, from where it will never recover (without immigration). To investigate how populations approach extinction, we consider a model where the effective (per capita) rates of reproduction and death of an individual are constant. Thus, the rates of the master equation are given by $W_{n+1,n} = b_n = bn$ (birth event), and $W_{n-1,n} = d_n = dn$ (death event). Here the population size of a species is given by the discrete variable $n = 0, 1, 2, \dots$. Under the neutrality assumption [48, 188], the probability distribution of n gives the distribution of the population of all species in the system. When $b < d$ the state $n = 0$ is an absorbing boundary. The eventual probability that all species' populations reach zero is one since there are no possible birth events when a species has gone extinct.

A key point is that the birth-death process is an infinite state system, but still satisfies the requisite eigenvalue spectrum since they are discrete and are given by $\lambda_k = (d - b)k$ for $k \geq 1$. Hence, we proceed to use the derived response theory and FDT since the necessary hierarchy is still satisfied. With $b_{-1} = 0$, the Master equation is given by

$$\dot{P}_i(t) = b_{i-1}P_{i-1}(t) + d_{i+1}P_{i+1}(t) - (b_i + d_i)P_i(t) \quad i \geq 0 \quad (3.134)$$

The second eigenvector and the eigenvalue can be obtained by the generating function [16]

$$G(z, t) = \sum_{n \geq 0} P_n(t)z^n = \left(\frac{1 - \mathcal{A}(z, t)}{1 - (1 - \nu)\mathcal{A}(z, t)} \right)^{n_0} \quad (3.135)$$

with $P_n(t=0) = \delta_{n,n_0}$, $\nu = 1 - b/d$, $\mathcal{A}(z, t) = (1 - z)(1 - (1 - \nu)z)^{-1}e^{-\nu t}$. At large times $\mathcal{A}(z, t)$ is small enough to use the approximation $1/(1 - x)^y \approx 1 + yx$. Since the coefficient of the slowest exponential in the long-time state gives the second eigenvector, we obtain $\varphi_{1n} = \nu(1 - \nu)^{n-1}$. The time-dependent solution to the Master equation is calculated by using the Meixner Polynomials [189].

Figure 3.3a shows the comparison between results from simulation, the new theory given by Eq. (3.58), and the standard-equivalent case given by only the first term of Eq. (3.58). The first term of the generalized FDT is similar to the standard FDT, but with the quasi-stationary distribution in place of the stationary distribution, corresponding to a direct substitution. We consider the average population squared, i.e., $\langle n^2 \rangle$, since this shows a significant deviation from standard theory. It is immediately apparent that the standard-equivalent case significantly underestimates the response of the system while the predictions from the new theory and results from simulations match very well, as expected from the several examples presented before. This also indicates that the direct replacement of the distribution is a wrong approach and could result in an incorrect estimate of the response.

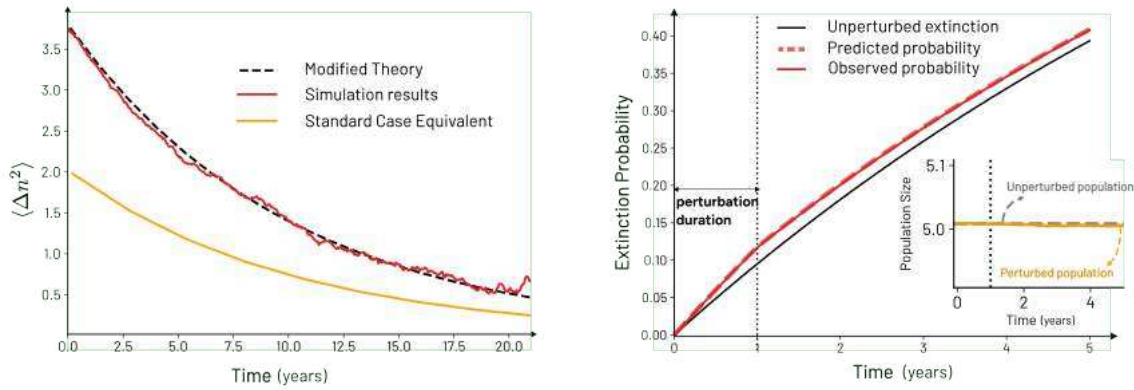


Figure 3.3: **Simulated and predicted responses in the birth-and-death process with absorbing boundaries:** **a)** Comparison between modified response theory, standard-equivalent case, and simulations of the system. The observable considered is the average population size squared ($A_n = n^2$). The plots show the deviation of survived observable from the unperturbed value. The green line indicates the contribution from the first term of the generalized theorem. The black line is the prediction using both terms, and the magenta line is the deviation observed in simulations. The perturbation strength is $\Delta b = b/10$. **b)** Increase in extinction probability of a species due to sustained perturbation for a period of $t = 1$ year in both birth and death rates. Inset shows the average survived population (from simulations) against time in both perturbed and unperturbed cases. The dotted black line in both plots indicates the time till which perturbation occurs. Solid black line shows the extinction probability in an unperturbed scenario. Dashed lines are predictions, and coloured solid lines are observations from simulations with perturbation strengths $\Delta b = b/10$, and $\Delta d = d/10$. Common parameters are $b = 0.4$ and $d = 0.5$.

An important quantity for ecosystems is the survival probability of species. An increase or decrease in this quantity could mean the difference between extinction and persistence. To study this, we consider a sustained period of perturbation in both rates, reasoning that any increase in death rate caused by natural or man-made causes results in more available resources, thereby also increasing the birth rate. After computing the response function for survival probability, it is possible to compute the extinction probability which is given by $1 - \langle \chi \rangle_t$.

Figure 3.3b shows the extinction probability for a perturbation in both the birth rate and the death rate that lasts for a period of $t = 1$ year while comparing it to the extinction probability in the unperturbed case. The inset shows the change in average survived population size during and after the perturbation. It is seen that the average population size is unaffected by this perturbation. While not plotted, the quasi-stationary distributions in both cases remain the same, despite the perturbation, which indicates that the observed relative species abundance distribution can appear to be constant in time. The critical

point of note is that the extinction probability of the species immediately increases, especially during the period of perturbation, and remains larger than the unperturbed case even after the perturbation has ended. The increase in extinction rate caused by the changing population distribution in both cases is exactly compensated by the changing survival probability, which leads to the constant quasi-stationary distributions, but the increase in death rate is not aptly compensated by the birth rate increase and hence, more species could go extinct. This means that even though the observed average population size and the abundance distribution of the system stay constant, the total number of species in the system decreases faster than usual, and this effect persists beyond the perturbed duration.

While the constant population size and the relative species abundance is ultimately an effect of the particular choice of same perturbation strength for the birth and death rate, the observed phenomenon of increased extinction probability demonstrates the importance of investigating ecological systems using more comprehensive statistical tools.

Targeted Search on DNA by Proteins

We move from the ecological time and length scales to the biochemical scale involving proteins and DNA. Proteins search for a specific set of base pairs on a DNA to which they have a strong binding affinity, thereby forming an absorbing site in the dynamics. We consider a discrete state model of the targeted search for the binding site, which has already been described in the literature [190, 191]. The model consists of $L - 1$ non-specific sites and one specific binding site on the DNA (called 'target'). The protein slides along the DNA with a constant diffusion rate u in either direction, until it reaches the target site. At every non-specific site, the protein can get detached from the DNA strand with the rate k_{off} (which determines the average sliding length), and this results in the protein being in free space. Since diffusion in free space is much faster than diffusion in 1D, we consider free space as a single site. From this site, the protein can attach itself to any spot of the DNA strand with the rate k_{on} . Due to faster diffusion in 3D, all sites are reachable with equal probability, and hence, k_{on} is the same for all sites.

Under this framework, we consider rates estimated from observed experimental data, and extract the eigenvalues and eigenvectors of the transition matrix to perform the computations. For all the simulations of the system, the protein starts from free space and moves according to the transitions described above. Eventually, every simulation will end when the protein reaches the target. But, at any given time, a fraction of them will still have the protein not bound to the target site (which we shall term survived realizations, equivalent to survived species in the birth-death process). The long-time probability of finding the protein at a particular site in these survived realizations is equal to the quasi-stationary eigenvector of the transition matrix.

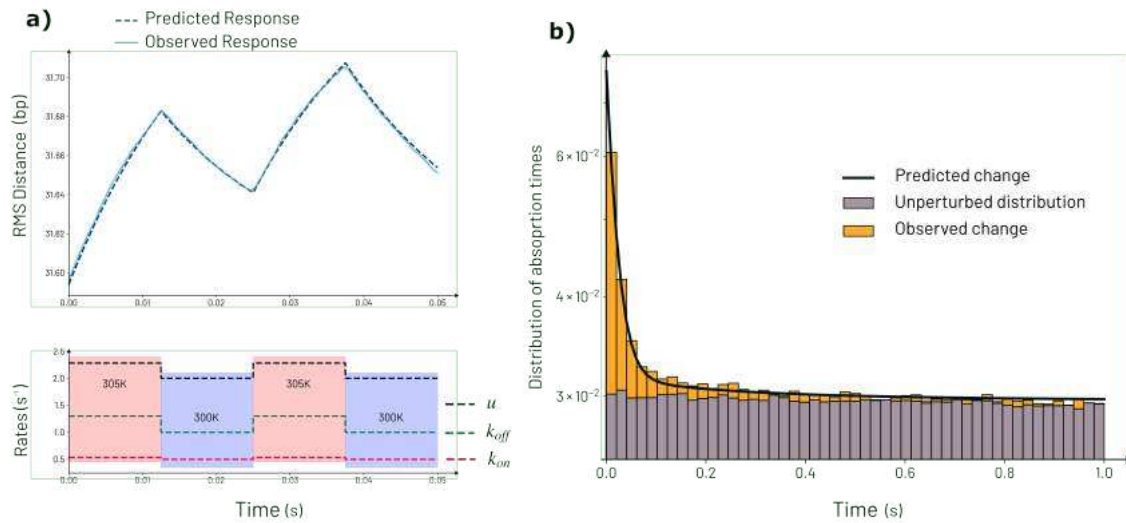


Figure 3.4: **Prediction of responses in targeted search by proteins on DNA:**

a) Top panel: Root mean squared distance of the protein from the target DNA site for periodic changes in temperature. The RMS distance is given in terms of base pairs, where $1\text{bp} = 340\text{pm}$. The blue dashed line is the prediction and the solid line is observations from simulations of the protein distance. Bottom panel: Change in the rates of the system assuming Arrhenius rate law. Blue regions indicate the normal temperature (300K), and red regions indicate the higher temperature (305K). The colored dashed lines indicate the rates as given in the legend. **b)** Prediction of deviation of absorption time distribution with a delta-perturbation of k_{off} in the system. The histogram of absorption time distribution computed through multiple simulations is represented by the bars with the corresponding probability of absorption on the y-axis. Grey bars indicate the unperturbed absorption time distribution, and the orange bars are the deviation upon perturbation. The solid black line is the prediction from the theory. Perturbation strength is $\Delta k_{off} = k_{off}/10$. The unperturbed first passage time distribution is exponential with a large characteristic time, hence appearing flat at plotted scales. The effect of the delta-perturbation is observed only at times much shorter than the characteristic timescale.

Binding and detachment of the protein happen through chemical reactions, whose rates can be approximated by the Arrhenius law, given by $rate = const \times e^{-E_{rate}/RT}$, where $E_{rate} > 0$ is the activation energy of the reaction, R is the gas constant, and T is the temperature of the system. Assuming the Arrhenius law for each of the rates, we consider a periodic temperature change of 5°C (from 300K to 305K). This results in a perturbation of the rates, which changes the distance of the protein from the target. We compute this change through the root mean squared (rms) distance of the protein from the target. Figure 3.4a shows that even though the observed pattern of change in distance is non-trivial, the new response theory is able to predict it quite well. The specific pattern of whether the protein moves away from the target or towards it depends on the activation energies. In a chosen experimental setting, the

activation energies can be first computed and the theory can then be used to predict the change in distance due to temperature change exactly using the generalized theorem.

The time to extinction is an essential random variable in absorbing processes. The average of this distribution, also called the mean first passage time, provides important information about the protein reaching the target [191]. Figure 3.4b shows the change in the absorption time distribution from simulations and from theory when there is a delta-perturbation in the rate of detachment, k_{off} . We see that the probability of absorption at short times immediately increases by a significant proportion. Since a delta-perturbation is considered, at large times, the change in distribution will be minimal, which is seen in the figure where the perturbed and the unperturbed distributions converge at times much larger than the time of perturbation. The flat nature of the unperturbed distribution is due to it being an exponential decay with a characteristic scale much larger than the time which is plotted. The matching between simulations and the theory opens new possibilities in ensemble experiments to control mean first passage time through perturbations.

3.4 Conclusion

Our results apply to a broad class of systems that were previously intractable from the lens of response theory. Conditioning to survival is a common tool in mathematical literature of quasi-stationary processes. The generalized fluctuation-dissipation theorem provides insights into how this conditioning affects the response to perturbations. Specifically, this new insight is needed because by direct replacement of the stationary distribution with the quasi-stationary one significantly underestimates the actual response. Though perturbation of finite linear operators has been studied previously, obtaining the transient dynamics and connections to statistical mechanics and relevant examples are missing to the best of our knowledge. In order to take into account the inherent decay of the system and to predict the response, the generalized theorem is necessary.

Absorbing processes form a large class of systems which are ubiquitous in nature. Their disruption of equilibrium and stationarity in general occurs in a very specific manner which disrupts what we know of the relations between fluctuations and dissipations. Starting from quasi-stationarity is still similar to starting near equilibrium. Though our results can be generalized to be applicable at all times, the computation of the necessary quantities becomes complicated, especially in situations where a non-equilibrium stationary state is present. In this context, changes in fluctuation relations caused to changes in entropy production and subsequent connections to quasi-stationary distributions is a pertinent topic for future research.

In the various models discussed, including the birth-death forest model, an underlying assumption is that of locality of dynamics. However, in natural set-

tings, this assumption often falls short due to spatial influences and interactions from neighbouring areas. Even in fragmented habitats, there's typically some level of species migration, which means local extinction doesn't necessarily equate to global extinction. Therefore, a species' absorbing state is more realistically considered at the global extinction level. To grasp the interplay between extinctions and the spatial structure of populations, an expanded theoretical framework is necessary, which incorporates not just local dynamics but also the broader spatial effects, including extinction and recolonization processes, thereby offering a more accurate understanding of population dynamics and species survival in complex and varied natural environments.

**EXTINCTION OF BIOLOGICAL POPULATIONS IN COMPLEX
LANDSCAPES**

The following chapter is the basis of published work [192] “Emergent encoding of dispersal network topologies in spatial metapopulation models” [G. Nicoletti, P. Padmanabha*, S. Azaele, S. Suweis, A. Rinaldo, and A. Maritan; Proc. Natl. Acad. Sci 120 (46) e2311548120 (2023)]. Parts of the contents presented, including displayed figures, are taken with permission from the published work.*

4.1 Introduction

Classical theoretical ecology models such as the Lotka-Volterra models and the MacArthur Consumer Resource models, including recent stochastic counterparts coming from Neutral theory mainly focus on the population dynamics of a given set of species in a local patch of interest. Effects of the landscape and migration are usually considered through constant immigration rates which get incorporated into the dynamics [193]. But frequently, species reside in complex landscapes and the structure of this landscape impacts the dynamics of focal set of species.

Certain landscape configurations might be more prone to extinction, which is considered an absorbing state when it occurs across all local patches. The response theory for absorbing states presented in the previous chapter is general in prescription, but the chosen biological systems to demonstrate the applicability are yet rooted in the hypothesis of locality of dynamics. Counting for dispersal and migration between different habitats of species involves a set of interacting local patches, each undergoing similar dynamics. Historically, such models are termed metapopulation models, in order to highlight their facet of dealing with population of populations. While classical metapopulation models are successful and widely used, they often stem from phenomenological or empirical observations rather than first principles.. Hence, before proceed-

ing to analyse the effects of stochasticity and demographic fluctuations in the flavour of statistical mechanics, it is necessary to provide a more foundational formalism to derive classical models.

Understanding spatial ecology and unravelling the intricate dynamics of ecological interactions in relation to biodiversity and population dynamics has been a longstanding pursuit in ecological research [194, 195, 196, 197, 198, 199]. Models of metapopulations [200, 201] proved central to the description of extinction and colonization events, especially in connection with population persistence and dynamics [202, 203]. Habitat patches arise from, and are decisively influenced by, the spatiotemporal changes of landscapes, and play a crucial role in the persistence and extinction of metapopulation [204, 202, 205].

The application of network theory to ecological problems, particularly in the field of spatial ecology, has emerged as a valuable approach [196, 206, 207], but it often overlooks exact results derived in the context of river networks [208, 209, 210]. Graph theory, which allows the representation of space as a network comprising of interconnected habitats and fragmented dispersal pathways [211], enables a shift in focus from spatially continuous characteristics to the relationships between patches [212, 213, 214]. Networks, *sensu* Southwood [215], act as templates for ecological strategies. This network-based perspective has yielded valuable insights into how networks of habitat patches can support metapopulations and how connectivity affects a multitude of properties including persistence and invasibility, in both experimental and field studies [205, 216, 217, 218, 219]. Such studies underscore the profound influence of network structure on ecological dynamics [220, 197, 221].

In this context, the pioneering work of Hanski and Ovaskainen (HO) holds particular significance [200, 201, 222, 213]. It introduced a novel measure known as metapopulation capacity, derived from a phenomenological metapopulation model, to assess survivability in fragmented landscapes [222]. This measure can be readily applied to both randomly fragmented landscapes [223] and real-world networks of habitat fragments where the areas and connectivities of the patches are known [224, 213]. Technically, metapopulation capacity is quantified as the leading eigenvalue of a carefully defined landscape matrix [222]. By comparing the metapopulation capacity of a landscape to a threshold value determined by species-specific properties, predictions can be made regarding species persistence in that landscape [222]. This measure offers a convenient ranking system for assessing the ability of different landscapes to support viable metapopulations [222, 225, 213]. Furthermore, similar results have been independently derived outside of ecology and metacommunities, most notably in the context of epidemic spreading [226, 227] where the influence of networks and stochasticity have been extensively investigated [228, 229, 230].

Motivated by the need for a deeper understanding of metapopulation dynamics, our study introduces a fundamental approach that aims at capturing the essential ingredients of spatial ecology in arbitrarily connected patches. Our framework explicitly distinguishes between two groups of individuals within

the metapopulation: the “settled population” comprising individuals that remain in a specific habitat patch, and the “explorers” who venture out to colonize new regions. By incorporating this distinction, we construct a stochastic individual-based model that accounts for the specific landscape characteristics and fundamental processes driving metapopulation dynamics. We propose a general exact solution to our model, which allows us to derive an explicit metapopulation kernel that naturally reflects both the microscopic dynamical features and the underlying dispersal network. We then study how this mechanism interacts with the ecological template on various structures, including real topographic landscapes, whose features are ultimately encoded in the global metapopulation dynamics.

4.2 Historic models of metapopulation

It is necessary to demonstrate briefly classical metapopulation models and show the phenomenological assumptions before proceeding to generalize them.

The Levins model, introduced by Richard Levins in 1969, represents a foundational model in metapopulation theory [231]. It was developed to describe the dynamics of a species dispersed across a landscape in a series of habitat patches. The central idea is that the species does not occupy all available patches at all times due to local extinctions and recolonizations. Instead, the model considers the fraction of patches occupied over time, denoted by p . The model is defined by two primary parameters: the colonization rate c and the extinction rate e . The colonization rate refers to the rate at which unoccupied patches are colonized by the species, while the extinction rate refers to the rate at which the species goes extinct in occupied patches. The dynamics governing the fraction of occupied patches is given by

$$\dot{p} = -ep + c(1 - p)p \quad (4.1)$$

This dynamical equation is exactly that of the mean field contact process. Similar to the critical parameter value $\lambda = 1$ in the contact process, $\delta \equiv e/c$ governs whether the fraction of occupied patches is zero or otherwise. If $\delta > 1$, then, extinction process dominates and hence, the set of patches reaches extinction, Otherwise, a non-zero value can be obtained.

The Levins model, through its mean-field like assumption ends up with all patches equally accessible and each having the same probability of colonization and extinction, essentially treating the metapopulation as a series of identical and independently fluctuating patches. However, real landscapes are more complex, with habitat patches varying in size, quality, and isolation, all of which affect colonization and extinction rates. Recognizing the need for a more realistic approach, Hanski and Ovaskainen expanded upon the original Levins model to incorporate spatial structure into metapopulation dynamics, leading to what is often referred to as the “spatially realistic” Levins model.

This spatially realistic version, instead of analysing the fraction of occupied patches, deals with the probability of occupancy of a single patch, termed stochastic patch occupancy model. Similar processes of extinction occur on each patch, but instead, colonization processes now depend on pairs of patches. In a spatially embedded network of habitats, each pairs of patches i and j are separated by a distance d_{ij} . The phenomenological assumption of Hanski and Ovaskainen was that colonization rates decay exponentially with distance between patches [222]. Hence, including this modification into the Levins model results in a system of dynamical equations for each patch governing its probability of occupancy p_i given by

$$\frac{dp_i}{dt} = -\frac{e}{A_i}p_i + (1 - p_i) \sum_{j \neq i} ce^{-d_{ij}/\alpha} p_j A_j \quad (4.2)$$

where α is the characteristic dispersal length of the focal species and A_i and A_j are patch quality parameters that denote the quality of the patch and its effect towards extinction and colonization.

This model has been notably successful in predicting the occupancy patterns of the Glanville fritillary butterfly (*Melitaea cinxia*) in the Åland islands of Finland. The model's ability to connect landscape structure with species' life history parameters into a cohesive framework has been a significant advancement in metapopulation and conservation biology.

However, the model relies on two crucial assumptions that limit its applicability to more general scenarios without further modifications. The first assumption is that colonization rates decay exponentially with distance, which might not accurately reflect all species' dispersal patterns. The second assumption is that the network of habitats is fully connected and undirected, an idealization that may not hold in more complex or fragmented landscapes or in cases like river networks where flow direction can heavily influence dispersal patterns.

While additional modifications to the model can extend its applicability to these more complex landscape structures, a derivation of the model from first principles would allow it to be more directly applied without necessitating continuous ad-hoc adjustments. A first-principles approach would adapt more naturally to various ecological contexts and landscape configurations, providing a more robust framework for metapopulation studies.

4.3 Microscopic model and derivations

4.3.1 Model

We model the dynamics of a given species in a network of N patches. Figure 4.1 illustrates the core ideas of our microscopic model. We make the explicit distinction between individuals that stay in a given patch and do not move, i.e.,

the “settled population”, and those that instead move between patches, i.e., the “explorers”.

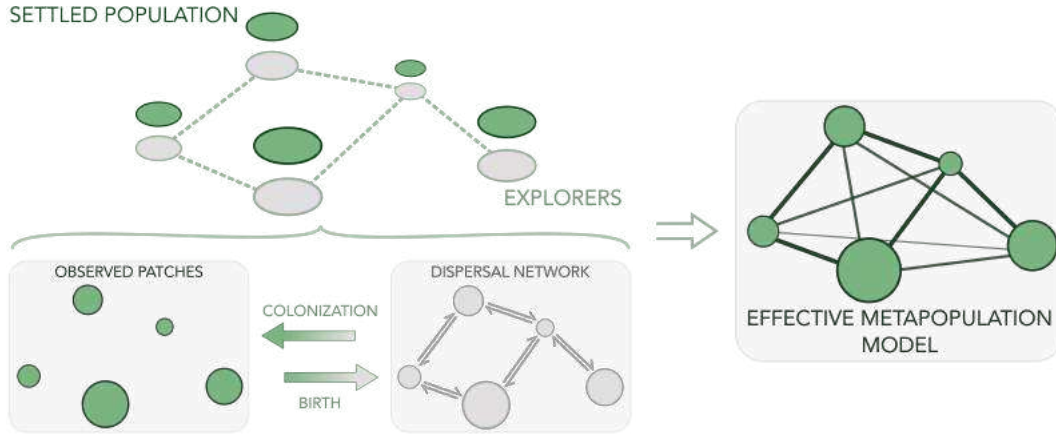


Figure 4.1: Sketch of the microscopic derivation of the metapopulation model. We explicitly consider a dispersal network and describe, in each of its patches, the local population of a given species. These settled individuals may give birth to explorers, whose role is to diffuse along the dispersal network. At any time, an explorer can attempt colonization by settling on a new patch. By assuming that only the settled population can be observed, we derive an effective metapopulation model with an all-to-all dispersal kernel that explicitly includes the effects of the underlying dispersal topology.

Each patch $i = 1, \dots, N$ is inhabited by a local settled population. We denote a single individual in patch i with S_i , and the total number of settled individuals by $[S_i]$. We further assume that each patch can accommodate at most M individuals, so that $\max([S_i]) = M$. Individuals of the settled population die at a rate e_i , denoted by the reaction



where \emptyset_i denotes an individual empty site in patch i . Notice that, at any time, $[S_i] + [\emptyset_i] = M$. In principle, we could also include reproduction - e.g., $S_i + \emptyset_i \rightarrow S_i + S_i$ - and other reactions on the same patch without qualitatively changing our results.

Although settled individuals S_i do not move, they can produce explorers in another patch j at a rate C_{ij} . We denote a single explorer in patch j with X_j . In the present work, we focus on the reaction

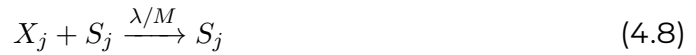


which may describe, e.g., seed production by trees. Once more, modifications to this reaction - such as settled to explorer conversion, $S_i \rightarrow \emptyset_i + X_j$ - can be easily included. Explorers can move between patches, and thus we assume

they do not occupy any of the M spaces. We denote the rate of moving from patch i to patch j with $D_{i \rightarrow j} = D_{ij}$, namely



With a given rate λ , an explorer may attempt to settle on one of the M available patches. Intuitively, this corresponds to diffusion with a stochastic stopping time modeled by a Poisson process [9], which translates into the reactions



where the rate λ/M takes into account that the single individual explorer in patch j , X_j , needs to choose one specific site on the patch. Notice that, if the explorer tries to settle on an already occupied space, it will die - hence, only empty sites on the patch can be colonized. This corresponds to a neutral-like assumption, where all sites on a patch are equal when it comes to explorers' attempts at colonization. Notice that one may add an intrinsic mortality rate for explorers, e.g., a constant death rate d_X . It can be easily shown that this would introduce a new dimensionless parameter in the model d_X/λ , without changing the form of the equations nor qualitatively affecting the results. In particular, we recover the present model in the limit $d_X \ll \lambda$, which amounts to assuming that explorers attempt settling much faster than they die.

Importantly, we take $D_{ij} = 0$ if the two patches are not connected, $D_{ii} = 0$, and $C_{ii} = 0$. Further, we take $C_{ij} = c_i h(D/\lambda) A_{ij}$, where c_i is the colonization rate, the function h encodes the feasibility of such creation, and A_{ij} are the elements of the adjacency matrix \hat{A} describing the dispersal network. With these choices, the microscopic dynamics of the explorers is local - they are created in neighboring patches and, to reach distant patches, they must move along the dispersal network. Without loss of generality, we write the diffusion rate as $D_{ij} = D A_{ij}$, where D is a baseline rate. Note that the dispersal network may be directed and weighted, in principle, and thus \hat{A} may not be symmetric or binary.

4.3.2 Rate equations

We can write the master equation for the probability $p(\vec{[S]}, \vec{[X]}, t)$, where $\vec{[S]} = ([S]_1, \dots, [S]_N)$ and $\vec{[X]} = ([X]_1, \dots, [X]_N)$ are the numbers of settled individuals and explorers across patches, respectively. From the master equation, one can

easily obtain the equations for their means in a given patch,

$$\langle S_i \rangle (t) = \sum_{[S_i]=0}^M [S_i] p(S_i, t) \quad (4.9)$$

$$\langle X_i \rangle (t) = \sum_{[X_i]=0}^{+\infty} [X_i] p(X_i, t), \quad (4.10)$$

which read

$$\begin{aligned} \frac{d\langle S_i \rangle}{dt} &= -e_i \langle S_i \rangle + \lambda/M(M - \langle S_i \rangle) \langle X_i \rangle \\ \frac{d\langle X_i \rangle}{dt} &= - \left[\lambda/MM \langle X_i \rangle - h \left(\frac{D}{\lambda} \right) \sum_{j=1}^N A_{ji} c_j \langle S_j \rangle \right] + D \sum_{j=1}^N (A_{ji} \langle X_j \rangle - A_{ij} \langle X_i \rangle) \end{aligned} \quad (4.11)$$

where we used the fact that $\langle S_i \rangle + \langle \emptyset_i \rangle = M$. (4.11) can be also understood as the first term of the Kramers-Moyal expansion of the master equation.

We define the density of settled population $\rho_i = \langle S_i \rangle / M$ and the number of explorers per empty site $x_i = \langle X_i \rangle / M$. Hence, we rewrite (4.11) as

$$\begin{aligned} \dot{\rho}_i &= -e_i \rho_i + \lambda(1 - \rho_i) x_i \\ \dot{x}_i &= - \left[\lambda x_i - h \left(\frac{D}{\lambda} \right) \sum_{j=1}^N A_{ji} c_j \rho_j \right] + D \sum_{j=1}^N (A_{ji} x_j - A_{ij} x_i) \end{aligned} \quad (4.12)$$

which are the rate equations reported in the Material and Methods of the main text. Let us also note that, even if we introduce a patch-dependent number of sites M_i , the relative densities $\rho_i = \langle S_i \rangle / M_i$ and $x_i = \langle X_i \rangle / M_i$ would follow the same equations.

4.3.3 Quasistationary approximation

We now make the crucial but physically meaningful assumption that we cannot observe the explorers directly and that their dynamics is much faster than that of the settled population. That is, we only have access to the density of the settled population in a given patch, and thus we want an effective equation for ρ_i that takes into account the otherwise hidden dynamics of explorers. In practice, this means that, in order to solve (4.12), we employ the quasistationary approximation

$$\dot{x}_i = 0, \quad \forall i$$

for the explorer dynamics. Note that this approximation does not affect the steady state of the settled populations. Recalling that $f = D/\lambda$, we obtain

$$\lambda \vec{x}(t) = \hat{F}^{-1} \hat{C}^T \vec{\rho}(t) \quad (4.13)$$

where

$$F_{ij} = \delta_{ij} + fL_{ji}. \quad (4.14)$$

and L_{ij} are the elements of the out-degree Laplacian matrix of the network,

$$L_{ij} = \delta_{ij}q_i - A_{ij}, \quad (4.15)$$

with $q_i = \sum_j A_{ij}$ the weighted out-degree of patch i . Overall, by inserting (4.13) in (4.12), we obtain an effective equation for the density of the settled population in patch i ,

$$\dot{\rho}_i = -e_i\rho_i + (1 - \rho_i) \sum_{j=1}^N \sum_{k=1}^N (\hat{F}^{-1})_{ik} C_{jk} \rho_j \quad (4.16)$$

and notice that, although \hat{A} is in general a sparse matrix, \hat{F}^{-1} is always dense - and therefore it introduces effective couplings between all patches, regardless of the underlying connections.

To understand the properties of the all-to-all effective couplings appearing in (4.16), we need to find the inverse \hat{F}^{-1} which is, in general, a challenging task. In this particular setting, it is possible to compute \hat{F}^{-1} directly in the eigenspace of \hat{L} . However, as a general method to take into account possible extensions in which \hat{F} does not contain the identity matrix, we resort to the recursive form of the Woodbury matrix identity [232]. We have

$$\hat{F}^{-1} = (\hat{G} - \hat{E})^{-1} = \hat{G}^{-1} + \hat{G}^{-1}\hat{E}(\hat{G} - \hat{E})^{-1} = \sum_{n=0}^{\infty} (\hat{G}^{-1}\hat{E})^n \hat{G}^{-1}, \quad (4.17)$$

where, in our case, $\hat{G} = \mathbb{I}$ is the identity matrix, and $\hat{E} = -f\hat{L}^T$. Notice that, in this case, the Woodbury identity is equivalent to the Neumann series $(I - A)^{-1} = \sum_{k=0}^{\infty} A^k$. However, more complex microscopic dynamics may lead to a matrix \hat{G} that is different from the identity, and the Woodbury expansion would still be useful in such scenarios. In general, it is fundamental to highlight that the infinite sum appearing in (4.17) must be interpreted in terms of its analytic continuation, and can only be written provided that the inverse of \hat{F} exists. We check a posteriori that this is indeed the case. We have that

$$\hat{F}^{-1} = \sum_{n=0}^{\infty} (-1)^n f^n (\hat{L}^T)^n. \quad (4.18)$$

(4.18) can be drastically simplified in the eigenspace of the transpose Laplacian. We denote with ω_i is the i -th eigenvalue of \hat{L}^T with eigenvector $\vec{v}^{(i)}$, and with $(\hat{V})_{ij} = v_i^{(j)}$ the matrix of the eigenvectors. Recalling the analytic continuation of the generalized hypergeometric function ${}_1F_0$,

$$\sum_{n=0}^{\infty} (-1)^n (f\omega_k)^n = {}_1F_0(1; ; -f\omega_k) = \frac{1}{1 + f\omega_k},$$

we obtain

$$(F^{-1})_{ij} = \sum_{k=1}^N \frac{V_{ik}(\hat{V}^{-1})_{kj}}{1 + f\omega_k} \quad (4.19)$$

which is an explicit expression for the matrix inverse of \hat{F} . It can be trivially checked that $\hat{F}\hat{F}^{-1} = \mathbb{I}$ for all values of f and all network topologies.

4.3.4 Explicit dispersal kernel

We introduce the dispersal kernel, defined as

$$K_{ji} = \sum_{k=1}^N (\hat{F}^{-1})_{ik} \frac{C_{jk}}{c_j}$$

which, using the results of the previous sections, we can write as

$$K_{ji} = h(f) \sum_{l=1}^N A_{jl} \sum_{k=1}^N \frac{V_{ik}(V^{-1})_{kl}}{1 + f\omega_k} \quad (4.20)$$

so that the effective metapopulation model reads

$$\dot{\rho}_i = -e_i \rho_i + (1 - \rho_i) \sum_{j=1}^N K_{ji} c_j \rho_j. \quad (4.21)$$

Notice that, in a q -regular network where all nodes have the same degree q , we can immediately write

$$F_{ij} = (1 + fq)\delta_{ij} - fA_{ji},$$

which leads to

$$(\hat{F}^{-1})_{ij} = \sum_{n=0}^{\infty} \frac{f^n}{(1 + fq)^{n+1}} (\hat{A}^n)_{ji}. \quad (4.22)$$

Crucially, the recursive nature of the Woodbury matrix identity now acquires a clear physical interpretation. The sum in (4.22) is, in fact, a sum over all possible paths of length n between j and i , whose number is determined by the elements of the n -th power of the adjacency matrix $(\hat{A}^n)_{ji}$. Each path needs to be weighted appropriately so that shorter paths are more likely and longer paths are not - depending on the value of f , which represents how far an explorer can diffuse before stopping. Remarkably, we can assign a finite result to this sum - here, we can write it as

$$(\hat{F}^{-1})_{ij} = \sum_{k=1}^N \frac{U_{ik}U_{kj}^{-1}}{1 + f(q - \gamma_k)},$$

where γ_i is the i -th eigenvalue of the adjacency matrix, and $U_{ij} = u_i^{(j)}$ is the matrix of its eigenvectors.

We also note that, in general, in the $f \rightarrow \infty$ the kernel becomes

$$K_{ji} \xrightarrow{f \rightarrow \infty} \xi \sum_{k=1}^N \frac{A_{jk}(\hat{V}^{-1})_{1k}}{\sqrt{N}} \quad \forall i \quad (4.23)$$

where we assume that ω_1 is the zero eigenvalue of the Laplacian. This implies that the effective coupling from patch j to patch i does not depend on i , so explorers can reach all patches uniformly.

The results of Hanski and Ovaskainen [200, 201, 222, 213] can be directly applied to (4.21). In particular, we may assume $c_i = c \mathcal{A}_i$ and $e_i = e/\mathcal{A}_i$, where \mathcal{A}_i is the area of patch i . The survival of a species is determined by the maximum eigenvalue of the landscape matrix $M_{ij} = K_{ij} \mathcal{A}_i \mathcal{A}_j$, i.e., the metapopulation capacity λ_M - if $\lambda_M > e/c$ the species survives, otherwise it goes extinct. In our case, λ_M will depend on the form of the function $h(f)$.

Although we cannot find a general analytical expression for λ_M , we can compute it in certain limits in undirected dispersal networks. Not surprisingly, $f \rightarrow 0$ gives $\lambda_M \rightarrow 0$, implying that in the absence of exploration, survival is not possible. On the other hand, in the opposite limit of large exploration efficiency $f \rightarrow \infty$, the metapopulation capacity is proportional to the average out-degree of the network. This clearly shows that the topological features of the dispersal network affect a species' persistence. In particular, we expect more densely connected networks to have larger metapopulation capacity, whereas species in highly fragmented landscapes are more prone to extinction. This result had been pinpointed earlier for patchy landscapes [225, 203, 224] and for dendritic metapopulations [233, 234] using the original kernel, and it is reinforced by the present results employing a more general framework.

4.4 Results

4.4.1 Effects of network topology

In Figure 4.2 we study how the topological features of the dispersal network affect both species survival and dynamics. We first focus on the simple case of a ring network, which represents a one-dimensional model with periodic boundary conditions. We find that the kernel elements K_{ij} decay exponentially with the network distance d_{ij} , in striking similarity with the HO effective kernel where this decay was phenomenologically assumed (Figure 4.2a). Notably, the characteristic decay length increases with f , leading to a stronger effective coupling between patches at large distances. This suggests a direct relation between the exploration efficiency f and the average dispersal distance, α , appearing in the HO model.

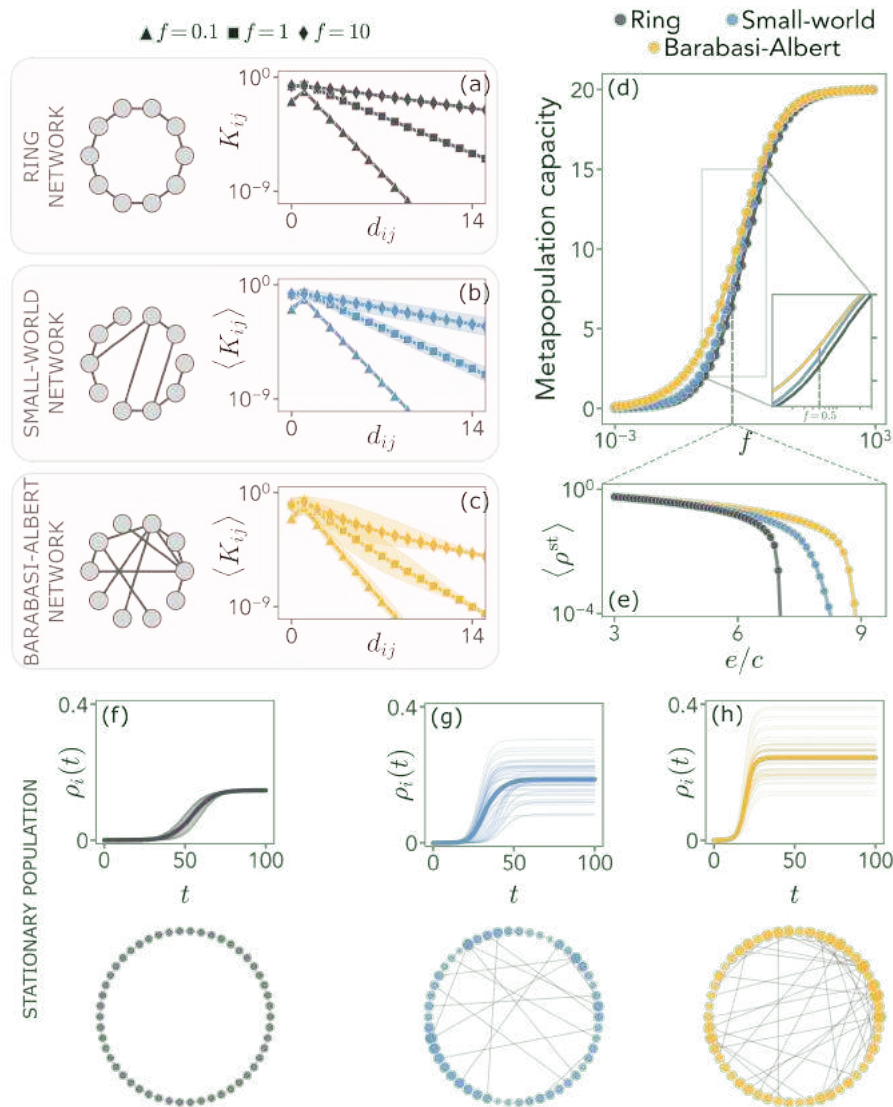


Figure 4.2: Effects of network topology on the effective dispersal kernel. (a) Behavior of the kernel elements K_{ij} as a function of the network distance d_{ij} in ring networks (sketched on the left). The kernel decays exponentially with d_{ij} regardless of the patches' identities, and larger values of f imply a larger characteristic length of such decay. (b-c) Behavior in small-world and Barabasi-Albert networks. At the same distance d_{ij} there are, in general, multiple values of K_{ij} , which depend on all possible paths between patch i and j . Scatter points represent their average $\langle K_{ij} \rangle$, and the shaded area is the area between their maximum and minimum value. (d-e) The metapopulation capacity as a function of f (at fixed $\xi = 10$) and the average stationary population $\langle \rho^{st} \rangle$ as a function of e/c (at $f = 0.5$) show that, in general, survival is favored by more heterogeneous topologies. (f-h) Dynamical evolution of the population density in different patches ρ_i (shaded lines) and its average (solid line) at $e/c = 6$. The stationary population shows localization in heterogeneous topologies, e.g., with a larger population in the hubs of Barabasi-Albert networks.

Crucially, we are now able to study how changes in the underlying dispersal network topology are reflected in the metapopulation model. In particular, small-world networks [235] introduce long-range connections between patches that may be otherwise very far apart. In Figure 4.2b we show that such connections have a deep impact on the kernel elements K_{ij} , which are not solely a function of the network distance d_{ij} , i.e., of the minimum number of edges that connect the two patches. Rather, at fixed d_{ij} we have a distribution of values of K_{ij} . This effect becomes especially relevant at higher f , and it is a direct consequence of the fact that K_{ij} encodes contributions from all possible paths between patch j and patch i and thus it will depend on the entire network structure rather than on distance alone. Although on average the kernel $\langle K_{ij} \rangle$ still displays an exponential behaviour with the network distance, heterogeneity in the network structure induces heterogeneity in the elements of the kernel matrix at fixed d_{ij} . In other words, for a given pair of patches i and j , there are two contributions to the kernel K_{ji} : an approximately exponential decay like in the original HO model, and an entropic contribution associated with the multiplicity of paths connecting i and j . Such a contribution emerges naturally and was not present in previous approaches.

In the case of Barabasi-Albert dispersal networks [236], few patches behave as hubs, connecting to a large number of other nodes and resulting in a scale-free degree distribution. This highly heterogeneous structure translates into very diverse kernel elements at equal distances, as we show in Figure 4.2c. This is not surprising, since being closer or farther from a hub introduces significant differences in the number of steps an explorer needs to take before reaching farther parts of the network.

Furthermore, topological features also affect the survival of a species. In particular, the metapopulation capacity increases with the heterogeneity of the network (Figure 4.2d). This effect is particularly significant at intermediate values of exploration efficiency f , where the fine structure of the dispersal network is most relevant. Conversely, in the limit $f \rightarrow \infty$ explorers can reach all patches before attempting colonization (see Supporting Information). The relevance of dispersal network structure at intermediate values of f consequently affects the average stationary population as well (Figure 4.2e). Such differences across diverse dispersal topologies result not only in distinct extinction thresholds but also in different approaches to extinction. For instance, in small-world networks, a species' decay to extinction is slower than in a ring, which could have a significant impact when demographic stochasticity is considered.

Finally, we observe marked differences in both the total population and the population in each patch. In Figure 4.2f-h, we show that settlement is more favored in nodes with a higher degree, and hubs in particular. Overall, heterogeneity and long-range connections drive faster colonization dynamics and strongly boost the total population. These results imply that the same species may colonize and survive in, e.g., a small-world dispersal network, but go extinct in a ring topology at the same value of extinction threshold, e/c . Such benefi-

cial effects on survivability are not unexpected. However, our results arise in a global metapopulation model derived from purely local microscopic dynamics, demonstrating its fundamental improvements over previous approaches.

4.4.2 Effects of modularity and fragmentation

A crucial aspect of dispersal networks that has important ecological implications is the presence of multiple weakly interconnected communities, with each community consisting of strongly connected patches. This modular structure (Figure 4.3a) reflects that of ecological corridors, with few corridors between ecosystems for species to move across. Understanding dynamics in such structures is a key ingredient in habitat conservation efforts [237].

In Figure 4.3b we show that a modular dispersal network is associated with a block-like metapopulation kernel, where patches belonging to the same community are more strongly coupled. Notably, the metapopulation capacity increases with the probability of connection between different communities (Figure 4.3c). Thus more connections between ecosystems allow for easier dispersal, thereby increasing survivability. It is a natural consequence of the entropic effect alluded to above, which is associated with the multiplicity of corridors connecting ecosystems. Hence, sparsity is detrimental to a species, whereas more dense networks are less prone to extinction.

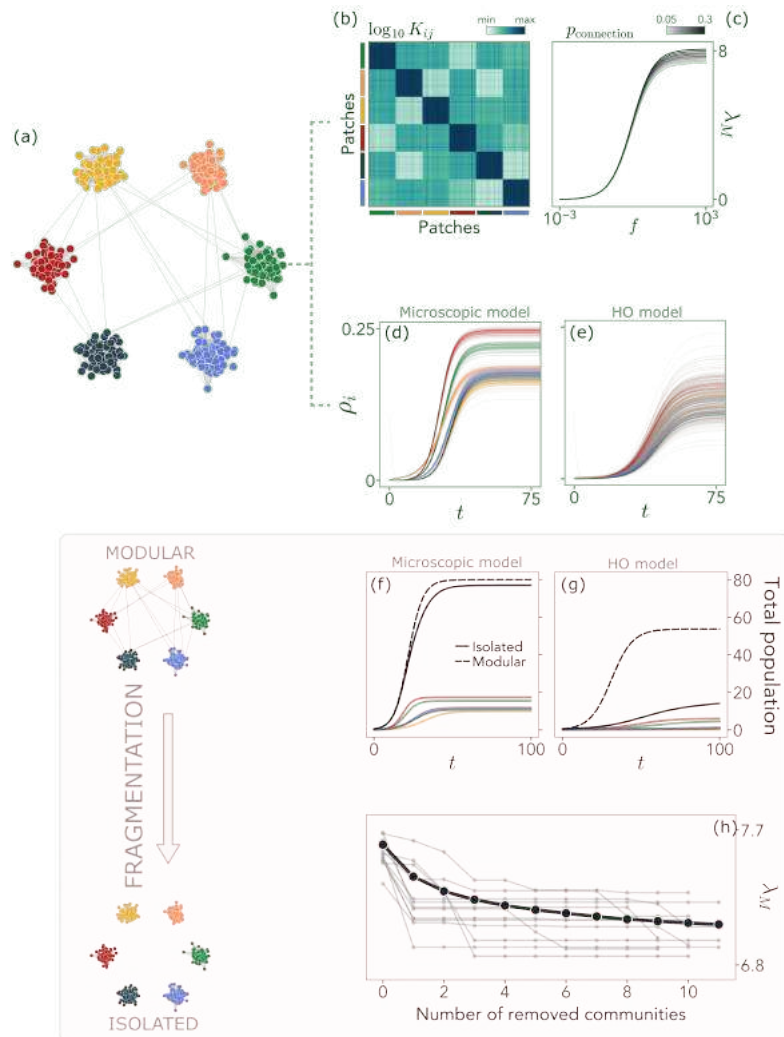


Figure 4.3: Effects of modularity and fragmentation on the metapopulation model. (a) A modular network comprised of six realizations of Erdős–Rényi networks [238, 239] with the same wiring probability $p_{\text{intra}} = 0.05$ and interconnection probability $p_{\text{connection}} = 0.2$. (b) The matrix kernel displays a block structure, with larger elements between patches belonging to the same community. (c) The metapopulation capacity increases with the connection probability between communities. (d-e) Evolution of the settled population ρ_i in each patch, and comparison with the HO model. Each color represents patches in different communities. (f-g) Comparison of the total population in the modular network (dashed black line) and the isolated network (solid black line), where all links across communities have been removed, in our and in the HO model. (h) Effect of fragmentation on the metapopulation capacity on a modular network with 11 communities. As we randomly isolate communities from the network, the metapopulation capacity decreases, showing that a fragmented landscape hinders survival. The gray lines represent a single realization of the stochastic disconnection process.

The modular structure of the network is also reflected in the dynamics. This

point represents a crucial difference between our microscopic model and the HO model. Figures 4.3d-e show that the dynamics in the microscopic model immediately reflects the different communities, with patches of a given community being colonized together. On the contrary, this is completely absent in the dynamical evolution predicted by the HO model, since only the patch distances are considered. As a consequence, pair of patches at the same distance are equivalent in the HO model regardless of the communities they belong to, whereas such topological information is naturally encoded in our approach.

This fundamental difference is especially relevant to understand the resilience of the metapopulation model in events of landscape fragmentation [240]. In particular, the presence of ecological corridors favors a larger total population, both in HO and our microscopic model (Figure 4.3f-g). However, since the HO effective kernel does not distinguish between communities, the total population in the absence of inter-community connections drastically decreases. On the contrary, in our microscopic model, the settled population in each community does not solely depend on the presence of corridors among them.

Finally, we can study in detail the effect of landscape fragmentation by randomly disconnecting communities from the rest of the network. Figure 4.3h shows the decreasing metapopulation capacity of the whole network with increasing fragmentation. Hence, isolation is detrimental to survivability, and the metapopulation capacity eventually saturates to that of the weakest isolated community. Remarkably, this shows that although the overall change to the total population may not appear significant (Figure 4.3f), fragmentation - and sparsity in general - drastically reduces a species' persistence.

4.4.3 Effects of landscape topography

Topography plays a vital role in shaping the ecological features of real landscapes [241], from hindering the movement of species in mountain regions to impacting the behavior of fishes inhabiting lakes located far apart in terms of water flow. The presence or absence of such topographic features could significantly alter the effective distance between two areas. We now exploit our microscopic approach to study how elevation gradients affect metapopulation models.

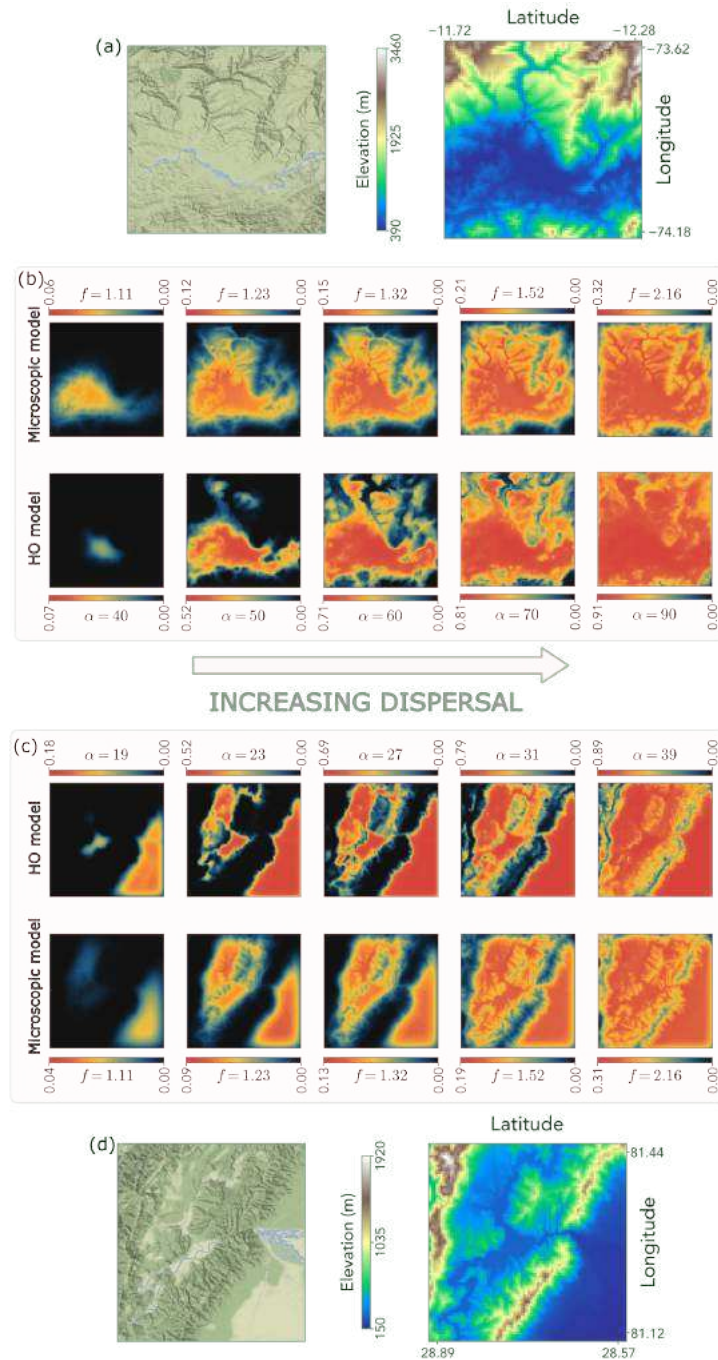


Figure 4.4: Stationary populations in Digital Elevation Models (DEMs). (a) Topography and DEM of a region of the Ene River in Peru, South America and (b) Comparison between the stationary population at different values of f and α (d) Similar to (a), but for Kauriala River, Nepal and the subsequent comparisons in (c)

HydroSHEDS Digital Elevation Models (DEM) [242] provide elevation data at 15 arc-second resolution obtained from NASA Shuttle Radar Topography Mission. We select two mountainous areas of interest (Figure 4.4a-b): a part of

Ene River in Peru, in the Andes region, and the Kauriala River in Nepal, in the Himalayas. These areas show geographic features that could potentially have ecological effects - the Ene region displays a fractal-like flow channel structure, and the Kauriala region includes a bottleneck-like passage between two zones of high elevation. In each region, we construct a grid of points at the latitudes and longitudes where elevation data exists. From this grid, we construct the exponential HO kernel using an elevation-dependent distance matrix with a characteristic migration distance α . Our model, however, allows for biased exploration. Thus, in our case, we consider exploration along the elevation gradient, with a downhill diffusion rate much larger than the uphill one.

Figures 4.4c and 4.4d show the stationary population density at each grid point for increasing dispersal parameter - α and f - for the chosen regions. At low dispersal parameters, the resulting metapopulation capacity is low, and in both models, the only surviving population is in low-lying areas. With increasing dispersal, it becomes easier and easier to move against the elevation difference. Hence, perhaps unsurprisingly, species with different dispersal parameters experience the topography differently.

While both models predict similar qualitative behaviors, there are stark differences in the stationary populations. In the HO model, species immediately occupy low-lying areas at significantly high population densities with respect to higher-elevation zones. Conversely, in the microscopic model, the densities increase smoothly along the elevation gradient.

This difference is a direct consequence of the fact that, in the HO kernel, the dispersal between two points at different elevations is the same regardless of whether the species is trying to colonize uphill or downhill. This naturally leads to a preference for connected regions at similar elevation levels, but does not take into account the fine topographic structure that arises from changes in the elevation gradients. Hence, only the overall topography is qualitatively reflected in the stationary population densities, which is strongly biased towards colonizing uniformly regions at the same elevation. This is in clear contrast with our model, where downhill exploration is intrinsically favored and thus allows for elevation gradients to be encoded into the dynamics through the entropic contribution due to the multiplicity of paths between two points. As a result, species are able to settle along the fractal-like flow channel structure in the Ene region and are forced to move across the bottleneck of the Kauriala region. The reflection of the topographic structure is not only limited to the DEM, as it does follow the dendritic river network constructed from elevation data. Therefore, topography influences and is clearly reflected in the species dynamics.

In principle, this allows for a deeper understanding of how changes to the landscape topography directly affect metapopulation models, e.g., changes in river flow due to natural or anthropogenic causes, landslides changing the elevation of a region, urbanization creating more flat areas, etc. When topography is involved, the basic assumption of unbiased colonization would become invalid, further highlighting the need for a consistent microscopic description.

4.5 Conclusion

Through derivation of a general metapopulation model by incorporating the fundamental characteristics of the dispersal networks and the detailed dynamics of settlers and explorers, we have found that the metapopulation capacity, which determines whether a species survives or goes extinct, is manifestly dependent on the substrate for ecological interactions. This approach encompasses asymmetric interactions, allowing for the study of real landscapes and biased colonization.

The presented work generalizes the classical model through providing microscopic reactions. Since a finite size of the patch exists, at low patch capacities, fluctuations in the population become important. This is underscored especially in the context of the absorbing boundary. In the deterministic equations, if λ_M is greater than δ , then, persistence always holds. But, in reality, there is always a chance of demographic fluctuations to drive populations to extinction. Our ongoing work on utilizing the Kramers-Moyal and van Kampen expansions indicates that the type of arising stochasticity is quite interesting, indicating connections to the previously analysed forest model of Eq (1.28), but with absorbing boundary. Furthermore, under conditions of deterministic persistence, the slow explorer regime indicates a sort of non-equilibrium quasi-stationary state for the absorbing boundary, with flux between the explorers and settled populations. These bring back to fore our analyses into violation of FDT in absorbing boundary systems.

Another direction of future work is to continue to utilize the generalized model in the deterministic setting to answer classical theoretical ecology questions, of which a key one is that of coexistence. Here, we have considered a single focal species. But the microscopic reactions can easily be generalized to multiple species competing for space and subsequent effects of topology on coexistence can be analysed. Furthermore, our model presents a tractable approach for the study of the interplay between metapopulations and the underlying physical constraints, trade-offs and universality of river and optimal channel networks [243, 244].

Notably, the presented deterministic setting provides a good example of ignoring stochastic effects at large population numbers, a situation frequently encountered in microbial communities in the laboratory. These communities comprise of species with populations in the order of hundreds of thousands, which effectively dampen the demographic systems inherent in the system to negligible levels. Nevertheless, these communities reside in an external environment which can always experience fluctuations. The effect of these fluctuations is then manifest in the dynamics through stochastic parameters, which brings it back into the foray of tools from stochastic processes.

FORCED FLUCTUATIONS OF MICROBIAL COMMUNITIES**5.1 Introduction**

The persistence of populations across extensive landscapes is dependent on the structure of these landscapes and their interaction with species dynamics. Such populations are vulnerable to stochastic effects and demographic fluctuations, particularly as they approach extinction thresholds. But at the opposite scale, microbes exist at such large population numbers even on a small scale that demographic fluctuations don't really play a role in determining whether they survive or not. In this instance, the species' properties appear to be more important, allowing us to consider the deterministic limit of stochastic differential equations.

Mathematical formulations of a community of microbial species immediately run into a problem when analysed from the level of resource usage. Commonly referred to as competitive exclusion principle / Gause's law [47], it states that the number of species cannot exceed the number of resources in a system. This is clearly in disagreement with observations in the natural world. The most famous of this is the "paradox of the plankton" where the estimated number of species is approximated at 10^6 [245], which presents an improbable number for the types of resources.

However, in the natural world, there are many environmental factors that are not described by simple mathematical models. Even in laboratory conditions, where fine control of environment is possible, frequently, on a single carbon source, more than one species coexist [246]. The most common explanation of this is the ability of microbes to use the by products of metabolism of another species, called cross-feeding [247]. While on surface this appears to violate the Gause's law, when accounted for these additional resources, some evidence suggests that competitive-exclusion principle still holds [248].

Resolving the paradoxical observations that challenge Gause's law requires an exploration of potential mechanisms that could facilitate the coexistence of

more species than the number of distinct resources. One such mechanism, widely observed in the natural world, is the impact of seasonality, which introduces potentially aperiodic fluctuations in resource availability. In macroecological studies, such seasonality and resource fluctuations are often found to foster coexistence [249], particularly in predator-prey models, suggesting a broader application of these principles to smaller scales, like microbial communities.

When applied to microbial systems, these periodic fluctuations introduce a continual source of variability, consistently driving the system out of equilibrium. This persistent disequilibrium could, in theory, allow for the violation of the competitive exclusion principle by creating niches or opportunities for additional species to persist. These fluctuations might not act in isolation but could interact synergistically with other biological or environmental factors, further promoting diversity and coexistence [250]. To fully understand these complex interactions and their implications, it is essential to develop a robust understanding of how systems compare across different intensities and patterns of fluctuation.

In this Chapter, we revisit the constraints disallowing coexistence of more species than resources and show how serial transfers, a common laboratory technique, allows violation of this principle. Then, through certain heuristic arguments and experimental data, the interdependent relation between different parameters of transfer mechanism is shown, allowing for a consistent comparison across different transfer frequencies. This leads to interesting and potentially important effects, especially when this forced fluctuation is coupled with a systematic stochasticity that can inherently occur due to human or machine inaccuracy. The initial results here serve as potential seeds for future research on control of microbial systems to optimize specific functions, both on theoretical and experimental settings.

5.2 Competitive exclusion principle

The dynamics of species in ecological systems are often studied using their population time series data. From these data, effective interactions between species can be inferred, typically manifesting as so within the context of Generalized Lotka-Volterra (gLV) equations [251]. However, it's crucial to understand that these interactions are effective rather than direct representations of interspecies dynamics. The gLV equations offer a simplified view, capturing the essence of species interactions through coefficients that represent competition, predation, or mutualism.

Yet, in many cases, the interactions between species are not direct but are mediated through shared resources, leading to competition or facilitation indirectly. This more nuanced view of interspecies dynamics can be captured by the MacArthur consumer-resource (CR) model. The CR model explicitly ac-

counts for the shared pool of resources that species compete for, providing a more detailed and realistic description of how species interact within an ecosystem [252].

Under certain simplifying assumptions, the CR model can resemble the gLV equations, particularly when the resource competition is linear and species have similar consumption patterns. However, in most realistic scenarios, especially under controlled laboratory conditions, the CR model diverges significantly from the gLV model. This distinction is especially important in experimental settings, where resource availability and consumption patterns are carefully controlled and monitored [253].

Consider a flask with n_s species and n_r resources which is connected to a source of resources and an outlet for drainage. Such a system is termed chemostat, which conserves the total volume of the flask, and eventually reaches equilibrium. Each species uses all resources to grow, albeit with different growth rates. For a general resource usage function, we can write the equations of growth and usage as,

$$\begin{aligned}\dot{n}_i &= \left(\sum_{\mu} g_{i,\mu}(r_{\mu}) - \delta_f \right) n_i \\ \dot{r}_{\mu} &= \delta_f (s_{\mu} - r_{\mu}) - \sum_i \frac{g_{i,\mu}(r_{\mu})}{y_{i,\mu}} n_i\end{aligned}\quad (5.1)$$

where δ_f is the rate of inflow and outflow with $y_{i,\mu}$ being the yield per unit use of resource μ for species i and s_{μ} being the supply of concentration of resource μ . At stationarity, the effective flux of resources is balanced by the usage, and the population outflow is balanced by growth. This leads to

$$\sum_{\mu}^{n_r} g_{i,\mu}(r_{\mu}^*) = \delta_f \quad (5.2)$$

$$\sum_i^{n_s} \frac{g_{i,\mu}(r_{\mu}^*)}{y_{i,\mu}} n_i^* = \delta_f (s_{\mu} - r_{\mu}^*) \quad (5.3)$$

Notice that Eq (5.2) has to be satisfied for n_s different species, but there are only n_r growth functions. This means that the stationary growth values of at least two species have to be the same for all the resources. This problem then simplifies to show that two species cannot coexist on one resource.

When Eqs (5.3) and (5.2) are written for two species and one resource, we obtain

$$g_1(r^*) = g_2(r^*) = g(r^*) = \delta_f \quad (5.4)$$

$$g(r^*) \left(\frac{n_1^*}{y_1} + \frac{n_2^*}{y_2} \right) = \delta_f (s - r^*) \quad (5.5)$$

Eq (5.5) shows that there exists a coexistence solution, based on the ratio of the yields. But any small change in r^* means that $g_1(r^*) \neq g_2(r^*)$ anymore, thereby implying that one of the species has a beneficial growth compared to the other for this small perturbation. Hence, the predicted coexistence solution is unstable and can never be reached unless the populations started exactly from that value.

But this is clearly not what is observed in the laboratory when species are grown on a single carbon source, such as glucose. This is because during the metabolism cycle, other byproducts such as acetate are produced which can then be used both by the species that produced it and potentially other species as well. This cross-feeding mechanism then raises the limit of CEP. Without resorting to cross-feeding, coexistence could still be possible by a fine-tuned set of growth rates, or by time-varying resource usage strategies.

5.3 Serial transfer induced coexistence

When $\delta_f = 0$ in the CR equation, there exists a central manifold in the dynamics of the species. In the phase space of species populations, there are infinitely many coexistence states in this case, with each coexistence state depending on the initial conditions. Experimentally, this corresponds to a batch-culture experiment where microbes are grown in a flask with a concentration of resources that are determined at the beginning of the experiment [254, 255]. Eventually, when all the resources are used up, the system reaches the central manifold where the species populations do not change and both of them coexist. This state is neither stable nor unstable, i.e., any small perturbation of species population will result in no deviation from the perturbed value, as long as the resource remains zero. Any non zero δ_f immediately disrupts this state making it unstable, with the new steady state having only one surviving species.

A frequently used laboratory technique to enable long experiments is that of serial transfers (also called serial dilutions). At the end of each batch-culture cycle, a small fraction of the volume in the flask is inoculated in another flask with a certain amount of resources, where the new flask now corresponds to a fresh batch-culture cycle. This technique is both cheap and easy to implement. By repeating this cycle multiple times, the regime of experimental timescales can be extended to much beyond a single batch-culture experiment without needing technically sensitive setups such as a chemostat. Such setups have been used to run long evolution experiments, the most notable of which has

spanned thirty five years and is still ongoing [256].

From the perspective of the dynamics of the system, serial transfer corresponds to a forced perturbation once the system reaches the central manifold. This system is going to then reach a new point on the central manifold due to different initial conditions, especially in the resource concentration. Eventually, this cycle will reach some form of steady state where the perturbation from the central manifold will reach the same point at the end of each cycle. This steady state is not in equilibrium, since there is a periodic and predictable fluctuations. This predictable fluctuation can be represented in the CR equations. In a series of batch-culture experiments, if we denote the set of times when the transfers occur by $(\tau_1, \tau_2 \cdots \tau_N)$, then, the dynamical equations are

$$\begin{aligned}\dot{n}_i &= n_i \sum_{\mu} g_{i,\mu}(r_{\mu}) - \sum_{k=1}^N \delta(t - \tau_k) \Delta_{n_i} n_i \\ \dot{r}_{\mu} &= \sum_{k=1}^N \delta(t - \tau_k) \Delta_{r_{\mu}} - \sum_i \frac{g_{i,\mu}(r_{\mu})}{y_{i,\mu}} n_i\end{aligned}\quad (5.6)$$

where $\delta(x - x_0)$ is the Dirac delta function, and Δ_{n_i} and $\Delta_{r_{\mu}}$ are the spiking death rates and resource influx rates happening at times of transfer. Note that the functional forms of supply of resource and death of species is different from that of the chemostat. In a chemostat, the continuous dilutions provide a simpler way to write the terms arising from the flow. However, dilutions occur discretely in time and there is not influx of resources or death of species due to outflow in the times between dilutions. Hence, representation of the dilution events has to be done through Dirac delta functions that peak at times of dilutions.

The delta functions in the equations present difficulties in attempts to obtain a solution. Alternatively, each batch-culture can be analysed individually by using a fraction of the steady state population at the end of one batch-culture as the initial conditions for the next, thereby mirroring the experimental technique.

To do this, we need to assume a form of the growth function $g_{i,\mu}(r_{\mu})$. A common assumption for this function is that of Monod form, with the idea that growth rate saturates at a certain concentration level of the resource, beyond which an increase in resource concentration has no noticeable effect on the growth of microbes. Such a function then takes the form

$$g_{i,\mu}(r_{\mu}) = \alpha_{i,\mu} \frac{r_{\mu}}{K_{i,\mu} + r_{\mu}} \quad (5.7)$$

where $\alpha_{i,\mu}$ is the maximal growth rate and $K_{i,\mu}$ is the half-saturation constant. Figure 5.1 shows an example growth curve for different concentrations of a carbon resource, with highlighted α and K .

For two species and one resource with Monod growth dynamics, the equa-

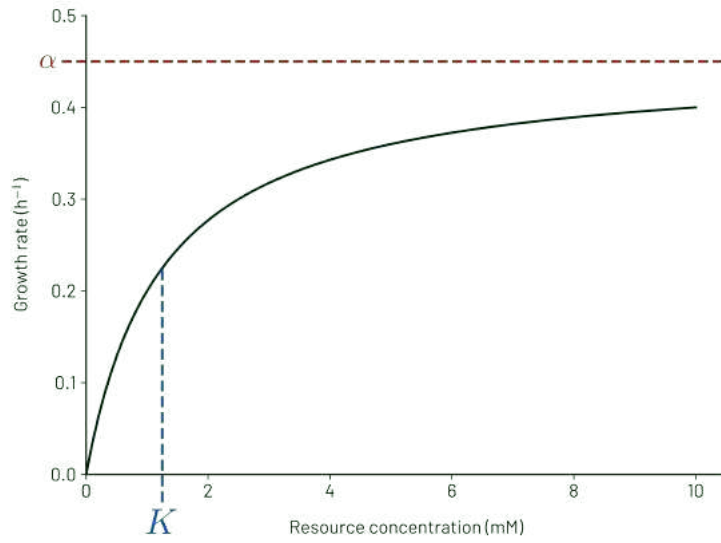


Figure 5.1: Example of Monod growth function with α representing the maximal growth rate and K showing the half-saturation constant, where the growth rate is half the maximal rate

tions in a batch culture are

$$\begin{aligned} \dot{n}_1 &= n_1 \alpha_1 \frac{r}{K_1 + r} \\ \dot{n}_2 &= n_2 \alpha_2 \frac{r}{K_2 + r} \\ \dot{r} &= -n_1 \frac{\alpha_1}{y_1} \frac{r}{K_1 + r} - n_2 \frac{\alpha_2}{y_2} \frac{r}{K_2 + r} \end{aligned} \quad (5.8)$$

where the Greek index has been suppressed since there is only one resource. Since we are considering the equations in a single batch and not across multiple dilutions, there are no terms representing the influx of resources or outflux of species. If at the beginning of the culture, if $r(0)$ resource is supplied, the concentration monotonically decreases. Under the assumption that the resource has been almost completely used up, i.e., $r(t) \approx 0$, then, the beginning of the new batch starts again with the resource concentration $r(0)$ and the initial conditions of the populations as fractions of previous populations, i.e., $n_{1/2}^{i+1}(0) = n_{1/2}^i(\infty)/D$, where the superscript refers to the batch-culture number / transfer.

Checking for coexistence of two species can also be done by checking their mutual invasion probabilities, initially done in [257]. If both species can invade each other, then, the only feasible solution is the coexistence of two species. Assuming that only species 1 is present, the serial transfer dynamics give the steady state solution of the populations based on the dilution factor D , since

the quantity $n_1 + y_1 r$ is always conserved.

Hence, for a single species and one resource,

$$\begin{aligned} n_1^i(t) + y_1 r^i(t) &= \text{const} \\ \implies n_1^*/D + y_1 r_0 &= n^* \\ \implies n^* &= \frac{D}{D-1} y_1 r_0 \end{aligned} \quad (5.9)$$

where n^* is the steady state transfer population of species 1.

Once species 1 has reached its steady state value, if a small population of species 2 is introduced at the beginning of the transfer, then, during one batch-culture, the resource usage will be dominated by species 1. Hence, Eq (5.8) can be approximated by ignoring the depletion of resource due to species 2. Hence, the conserved quantity now is given by $n_1(t) + n_2(t) + y_1 r(t)$. In such a case, the invasion probability of species 2 is given by the ratio of the final population to the initial population, which if greater than unity, implies growth and hence, invasion. This quantity is given by [257, 258]

$$w_{2,1} = \frac{1}{D} \left[\left(1 + \frac{r_0}{K_2} \right)^{K_1 - K_2} D^{K_2 + \frac{r_0 D}{D-1}} \right]^{\frac{\alpha_2/\alpha_1}{K_2 + \frac{r_0 D}{D-1}}} \quad (5.10)$$

and a similar expression given by $w_{1,2}$ for invasion of species 1 in a dominant population of species 2. When both $w_{1,2}$ and $w_{2,1}$ are greater than unity, coexistence is ensured. For a range of parameters [258], these conditions are satisfied, especially when there is a trade-off between the maximal growth rate, α and the half-saturation constant, K , i.e., a high maximal growth rate implies a high half-saturation constant [259]. Intuitively, the coexistence can be understood in terms of temporal niches. When the new batch-culture is begun, one of the species grows faster than the other. But eventually, the slow grower with a higher maximal growth rate takes over towards the end of the transfer cycle. Due to repeating this procedure, we create temporal niches in the resource consumption where different species are favoured at different times.

In practice, this scheme presents problems, primarily being, one cannot wait infinite time before performing another transfer. Frequently, the growth rate parameters are such that timescales of resource usage are fairly fast, especially at lower initial resource concentrations. In such cases, the question is, where does this time enter in Eq (5.10).

5.3.1 Scaling of parameters

If we assume that dilution is happening at an interval of $\Delta\tau$ which is constant, then, we can derive a heuristic relation between the times between transfers, the dilution factor and the initial resource concentration after transfer.

First, let us consider the scenario in which there are no species. Then, transfers should not change the concentration, especially when compared to the chemostat. Let us assume that the concentration of resource in the new batch culture is r_0 . Then, a fraction $1/D$ is carried over from the previous batch and a fraction $(1 - 1/D)$ comes from the new batch. Consequently, the evolution of resource concentrations can be written in the serial transfer system and the chemostat as

$$\dot{r}_{ST} = \left(r_0 \left(1 - \frac{1}{D} \right) + \frac{r^*}{D} \right) \sum_k \delta(t - \tau_k) \quad (5.11)$$

$$\dot{r}_{CH} = \delta_f (s - r_{CH}) \quad (5.12)$$

where r_{ST} and r_{CH} are the serial transfer and chemostat resources, δ_f is the chemostat flow rate, r^* is the concentration of resource just before dilution, and s is the chemostat supply concentration. Note that since there are no species using the resources, the concentration in both systems have to remain constant. By comparing the concentrations, we obtain the relation that the resource concentration in the new flask in terms of the supply concentration of the chemostat:

$$r^{i+1}(0) = s \left(1 - \frac{1}{D} \right) + \frac{r^i(\Delta\tau)}{D} \quad (5.13)$$

where i refers to the serial transfer cycle number.

Similarly, if we assume that a species exists in the transfer, then, the dynamics of the logarithm of the population is given by

$$\frac{d \log(n_{ST})}{dt} = g(r) - \Delta_n \sum_k \delta(t - \tau_k) \quad (5.14)$$

$$\frac{d \log(n_{CH})}{dt} = g(r) - \delta_f \quad (5.15)$$

We can assume that in the chemostat, resource dynamics are at a timescale such that $g(r)$ is effectively constant, i.e., the resource concentration quickly changes to the instantaneous steady state value based on the usage by the species. This argument is somewhat similar to analysing the species growth and death keeping the resource concentration fixed. Then, in a given time interval $[0, T]$, the total change in log-abundance of the species is given by

$$\log \left(\frac{n_{CH}(T)}{n_{CH}(0)} \right) = (g(r^*) - \delta_f) T \quad (5.16)$$

where r^* is the quasi-stationary value of the resource. A similar procedure cannot be done in the serial transfer equation since the resources also change with every dilution, and hence, cannot be considered to be at stationarity. Instead, if we consider the growth in one single batch-culture between $[0, \Delta\tau]$, then, the

total growth can be given by

$$\log \left(\frac{n_{ST}(\Delta\tau)}{n_{ST}(0)} \right) = g(r^*)\Delta\tau \quad (5.17)$$

Here, $g(r^*)$ is an approximation, since by the end of the batch culture, all resources are used up. But if the initial resource concentration is well beyond the half-saturation constant, then, most of the growth occurs with a constant rate, given by the maximum growth rate. At the end of the batch-culture, when the species are transferred to a new flask, then, the subsequent population is given by $n_{ST}(\Delta\tau)/D$. By equating the chemostat concentration at $T = \Delta\tau$ to the initial condition of the new batch-culture, we obtain that

$$D = e^{\Delta\tau\delta_f} \quad (5.18)$$

which connects the dilution rate in the chemostat to the dilution factor in serial transfers, depending on the time between dilutions. It indicates that the longer the dilution times are, the larger the dilution factors must be, in order to conserve the total growth when compared to a chemostat.

This sort of scaling is important for comparison, especially when we observe that competitive exclusion principle can be violated. Since the CEP holds strictly true in the chemostat system, it is necessary to have a single system of reference to compare across dilution times, which means that all three factors of serial transfer are interlinked. Previous studies have found that varying dilution factors in a community of multiple species can lead to different effects, based on the dilution factor, including changing of dominant species and multiple stable states [260]. Crucially, the dilution times was kept constant, which meant that the chemostats being referred to were different for each of the serial transfer systems, potentially contributing to the different results.

This is especially highlighted in Fig 5.2 where the dilution factors and the dilution times are varied independently in a simulated two species, single resource consumer resource system and the equivalent chemostat corresponding to that dilution rate and dilution factor is displayed. Each species grows according to the Monod growth curve, with a tradeoff between the maximal growth rate and the half-saturation constant, i.e, a higher α of a species corresponds to a higher K . Two key results observed here are that serial dilution systems show coexistence of two species consistently at different sets of dilution factors and times, but also, the corresponding chemostat changes the dominant species. This is a simple two species system with only one carbon source whose results will further complicate on addition of more species.

When the effective dilution rate in the chemostat and the supply concentration for different sets of dilution times and dilution factors are compared in Fig 5.3a and Fig 5.3b, it becomes apparent that the referenced chemostats have different parameters, and hence, is not a surprise that there are different species compositions for different parameters. Specifically, in the three di-

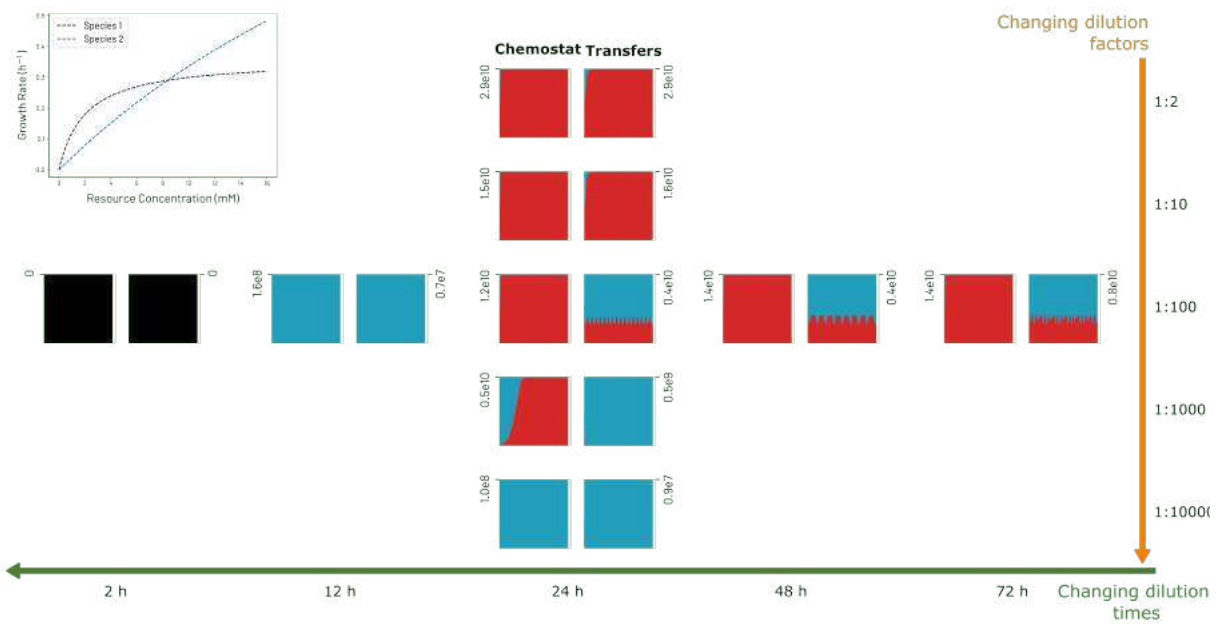


Figure 5.2: Consequences of serial transfer with different dilution factors and dilution times without scaling them accordingly. Top left inset shows the Monod growth curves for two species on one resource. Plots along the orange line indicates changing dilution factors while those along the green line indicates changing dilution times. Each serial transfer system is accompanied with its equivalent chemostat that would correspond to the value of the particular parameters of transfer. Each chemostat and serial transfer time series is plotted with the proportion of species 1 (red) and 2 (blue) with the total population marked at the top.

mensional phase space of the serial transfer parameters, referencing a single chemostat draws a parametric curve, that changes with the dilution rate as seen in Fig 5.3c. Ignoring this parametric curve and manipulating the parameters individually draws perpendicular lines in this phase space.

When these scaling factors are incorporated, we can look at the emergence of coexistence solely due to the mechanism of serial transfer, and not changing compositions due to changing chemostats. In Fig 5.4, we see that at certain intermediate values of dilution times, there is a broad region of coexistence. The region of coexistence shrinks with increasing resource supply. At a certain concentration of resource supply, this becomes a region of zero measure, i.e., a single point on the y-axis which corresponds to the case in the chemostat when the growth rates of the two species intersect which is in line with the idea that on the y-axis, the serial transfer system is effectively a chemostat and hence, cannot allow coexistence apart from this point of zero measure.

In an experimental system, we cannot control against crossfeeding, a mechanism wherein a species secretes a secondary carbon source due to the metabolism

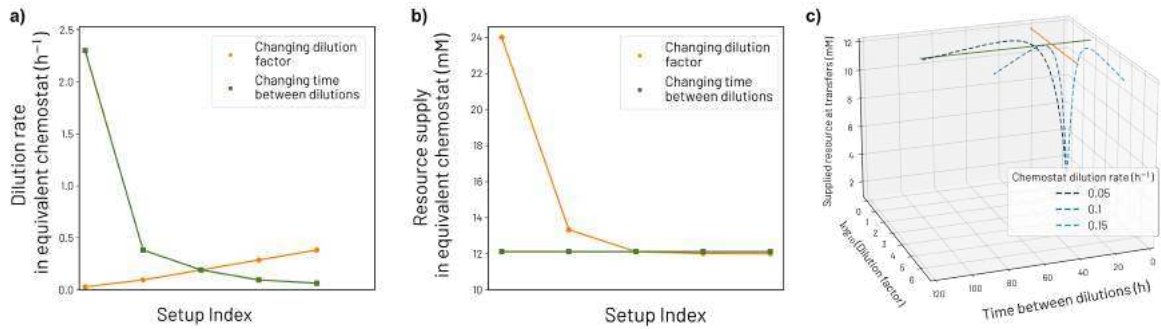


Figure 5.3: a) Equivalent chemostat dilution rate and b) resource supply concentration from each of the serial transfer system in Fig 5.2. Orange lines indicate transfer systems where dilution time was fixed and green line indicates fixed dilution factor. Setup index refers to the transfer system number in Fig 5.2. c) Phase plot of all three serial transfer parameters with parametric curves indicating referencing the same chemostat, with different chemostat dilution rates. Orange and green lines provide comparison to constant dilution times and constant dilution factors case presented in a) and b).

of a primary resource. Such crossfeeding mechanisms break the CEP if only the primary sources are considered. Nevertheless, on designing an in-house automated setup that can perform serial transfers at any chosen arbitrary dilution times and factors, we observed that population curves of different dilution times collapse onto a single curve. Figure 5.5 shows population time series data for two species of bacteria, *Agrobacterium tumefaciens* and *Comamonas testosteroni* grown in a medium comprising of Fumaric Acid at a concentration of 8 mM. The cultures were subject to dilution times ranging from 4 hours to 24 hours which was done by the specially designed automated transfer setup. To compute the populations, for each dilution time setup, at intervals of 24 hours, 20 μ L of the sample was diluted and plated onto plates containing specific antibiotics for each species. The number of colonies were measured after a period of 48 hours in an incubator at 37 °C, giving an indicator of total population through colony forming units per mL (CFU/mL). Even though the dilution times are significantly different, the population time series show remarkable similarities for both species, indicating that the scaling arguments holds true and is necessary to compare across different transfer parameters.

While Fig 5.5 only deals with two species, when communities of larger number of species are considered, more interesting effects start to emerge. A long standing debate in microbial ecology has been whether community assembly is predictive, i.e., whether information from smaller communities can be used to predict compositions of larger communities. Instances have been found where this is both true and false [246, 261]. The cheapest way to do these experiments is to use a batch-culture set-up, which automatically brings with it the possible additional effects of serial transfer mechanism. In Fig 5.6 we show that when

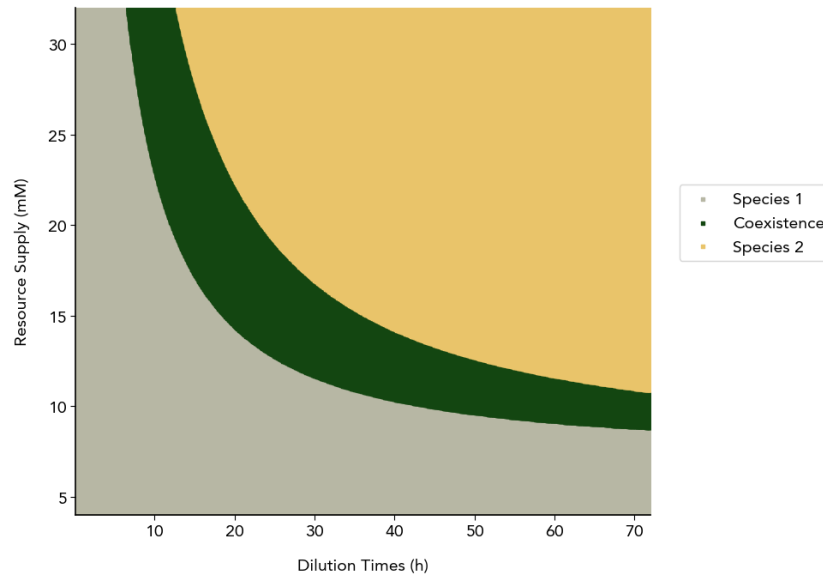


Figure 5.4: Theoretical prediction of coexistence of two species on one resource with correct scaling of serial transfer parameters. Prediction was made using invasion criteria analysis given by Eq (5.10). Both the species have the same Monod growth curves as in Fig 5.2.

three species are considered on a single carbon source, using pairwise predictive rules fails to account for emergent coexistence between two species when compared to a simulated system. The presence of one of the species has a strong competitive effect on another species which allows the third one to find a temporal niche thanks to constant serial transfers. This is effectively an emergent property that cannot be predicted solely from pairwise invasion criteria. Additionally, incorporating stochasticity in serial transfer mechanism seems to indicate that extinction of species is delayed significantly, especially close to the coexistence boundary, potentially due to the stochasticity enabling some temporal niches of coexistence, allowing for effectively longer survival times.

5.4 Conclusion

Effect of environmental variability in ecological setting has a long theoretical history coming from macro-ecology. But in such examples, manipulations of considered systems are neither feasible nor recommended due to their impact on local climate and possible long term environmental repercussions. Indeed, perturbation of large scale macro-ecological systems has to be done in very controlled manner such that there is no spillover effects, thereby severely limiting our ability to corroborate theoretical studies. However, microbial systems readily offer the solution to this conundrum. Not only are they amenable to a variety of manipulations, but, a particular kind of forced fluctuation is a commonplace experimental technique used to prolong the time-scales of the

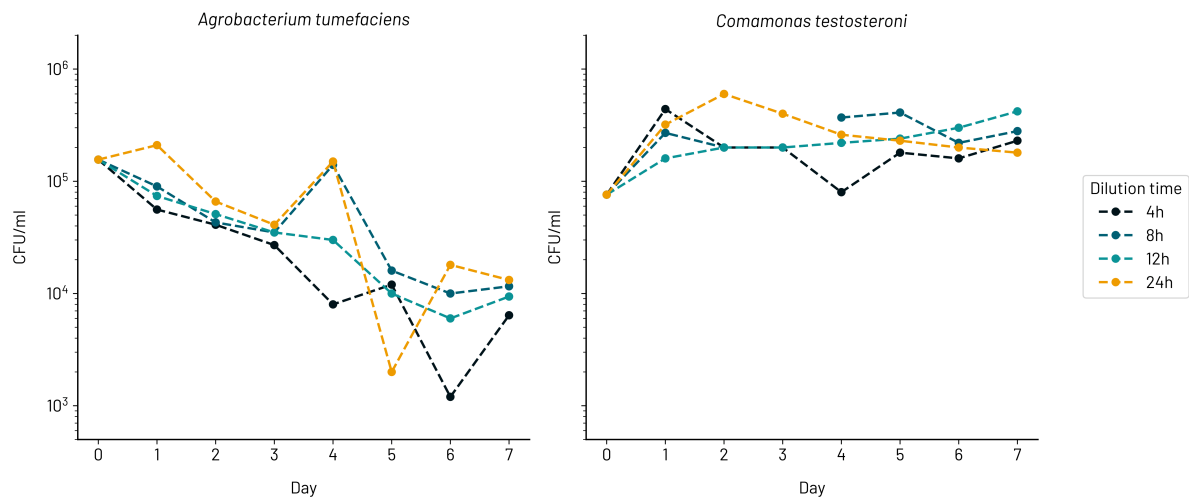


Figure 5.5: Experimental verification of scaling of parameters in a system of two species grown on one carbon source (Fumaric Acid) at different dilution times. Different colours represent different dilution times. Each plotted point refers to a data measurement at 24h intervals of colony forming units (CFU) per mL of culture.

study. Before proceeding to test various theories of environmental switching, understanding the role of this forced fluctuation and its implications is an important endeavour.

In this context, analysing one of the basic predictions of theoretical ecology is paramount. This is true especially in light of the multitude of studies on community assembly and coexistence outcomes being done currently. These studies not only deepen our understanding of biological systems at micro scale but also present potential applications in areas of bioreactors. But such applications necessitate a functioning community of microbes. Additionally, cheap and ready-to-scale technologies quite likely mean that batch-culture methods will be used for any potential applications. Ultimately, this leads to a requirement to understand the effect of serial transfer on community existence and functions. Studies into this have started to pick up pace in the last decade [262, 263, 264, 265]. In the presented analysis, we show that the parameters used in current literature are not independent, and not counting for this dependence could conflate results from different mechanisms. Furthermore, with an initial experimental validation of the scaling hypothesis and computational insights into fluctuation driven emergent effects in community assembly, there appears to be a lot of potential for future work in this area.

The serial transfer mechanism, at its heart, is a deterministic and periodic fluctuation. But tools from statistical physics can easily be incorporated, with real world implications. The mechanism of serial transfer, whether performed manually or automated has an intrinsic and systematic error associated with

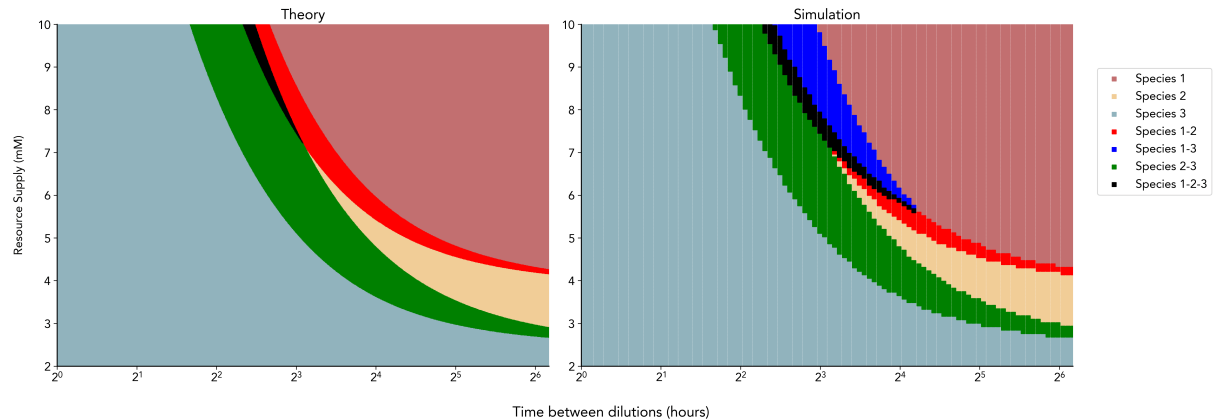


Figure 5.6: Emergent community assembly in three species system with one resource. Theoretical prediction on the left is made from pairwise invasion criteria analysis while phase plot on the right is from simulation of the system. Blue region indicates coexistence of species 1 and 3 which is absent in the pairwise analysis.

it. Such errors result in a noisy dilution factor, which in a continuous flow system results in a chemostat with a noisy dilution rate. This noisy dilution factor appears to significantly delay extinction in certain regimes. Chemostats with noisy dilution rates correspond to an environmental stochasticity that is usually seen in ecological SDEs [266, 267, 268]. Consequently, tools from statistical physics become applicable to deal with this inherent noise in the system, and potentially offer ways to control system composition or functional outcome by controlling the source of the stochasticity.

Ultimately, even though we are looking at scales where the demographic fluctuations arising from population numbers is significantly suppressed due to large populations, variability in the environment brings the issue back into the spotlight of statistical physics. This presents an application where though the inherent noise is not thermal, the source of the stochasticity is known, and hence, can be controlled. Forced fluctuations arising from serial transfers offers us the same possibilities of studying out-of-equilibrium behaviour as processes with thermal noise in a non-equilibrium regime, albeit in a different kind of system altogether with its own set of interesting questions and paradoxes to answer.

CONCLUSION AND DISCUSSION

In this thesis, I have presented a culmination of my research into fluctuations at different scales and its implications using tools from statistical physics and demonstrating applications in theoretical and experimental biology.

At the starting point of this exploration is the concept of entropy production, a fundamental marker of non-equilibrium conditions. By developing a graphical method to compute exact moments of entropy production for discrete-state Markovian systems, this work gives a window of exploration of the potential effects of non-Gaussian behaviour of environmental entropy production. This method's application to the run-and-tumble model demonstrates curious scaling laws present in the system. This non-equilibrium system, driven primarily by the heat bath which switches the average direction of motion, still results in a non-equilibrium steady state. Such a steady state captures fluctuations in various currents whose average is non zero. However, an extension to equilibrium systems can also occur through a non-equilibrium regime where there exists no steady state, or equivalently, the steady state is trivial and has no fluctuations.

Such steady states, occurring in the presence of absorbing states, present a conundrum for powerful statistical mechanics theorem connecting equilibrium fluctuations and out-of-equilibrium dissipations. Through the use of conditioning of survived trajectories, we obtained a generalization of the classical fluctuation-dissipation theorem that applies to a large class of previously little-explored systems. Demonstration of this generalization in various standard statistical mechanics examples and biochemically relevant examples shows both its validity and applicability, including extending the standard FDTs to trajectory-dependent quantities which was previously not feasible.

Moving one step above, the work on metapopulations considers the question of absorbing boundary at a larger spatial scale. Extinction of multiple local populations residing on a network of habitats has important ecological implications. Classical models to analyse such questions about persistence include ob-

servational and phenomenological assumptions. Generalizing this to obtain a metapopulation theory valid for heterogeneous landscape structures through the use of common stochastic processes tools extends our ability to investigate questions about species' persistence in more complex network structures and include effects of demographic stochasticity and population fluctuations from a first principles approach.

In a shift to a smaller scale of microbial populations where demographic fluctuations are weak due to the large population size involved, we investigated the idea of environmental fluctuations, through the mechanism of serial transfers, which have an interplay with the dynamics. Such environmental fluctuations brings about a constant driving that keeps the system out of equilibrium, thereby bringing about new behaviours in terms of coexistence of multiple species. Such forced fluctuations also bring about emergent effects in the assembly of system constituents, i.e., in the community composition. Going beyond theoretical analyses, we also experimentally investigated scaling relations between parameters necessary in such fluctuating systems to observe consistent comparison across systems.

Throughout the thesis, a common thread is the interplay between deterministic models and the stochastic nature of biological systems. Each chapter builds upon the last, through a narrative that highlights the importance of considering both macroscopic patterns and microscopic details, equilibrium behaviors, and far-from-equilibrium dynamics. In line with the philosophy presented in the Introduction, most of the chapters focus on the concept of generalising a given problem or method to be applicable to a larger class of systems. Though motivations and applications occur in certain examples, the results eventually demonstrate applicability to a wide variety of systems, being in line with both a holistic perspective and a theoretical physics demand.

Each result by itself provides multiple threads to unravel for future studies. In the case of entropy fluctuations, the provided method is not just general across systems for application to compute entropy production moments, but similar methods of jump correlations can be used to calculate the moments of any current in the system that depends on changing of states. Both cumulants of entropy production and arbitrary currents feature significantly on Thermodynamic Uncertainty Relations, giving a window into possibility of extending these very general relations to include higher cumulants beyond the mean and the variance. The ability to compute exactly the third cumulant and the convergence to a continuous state system provides a possibility of classifying the effect of non-Gaussian current behaviour in terms of the non-equilibriumness of the system.

In the case of response theory in absorbing systems, the validity of generalized fluctuation-dissipation theorem lends itself to applicability in various examples that show interesting behaviour, such as systems with stochastic amplification. The method of conditioning to survived trajectories raises important and fundamental statistical physics questions on what is the relation between

the conditioning process and actual observation in an experimental setting, bringing us to compare the provided conditioning against Doob's h -transform which is commonly used in literature [269]. Implications of the additional term of generalized FDT and its connection to Kullback-Leibler divergence of the quasi-stationary distribution against the Doob's conditioned stationary distribution remains to be investigated to understand a better picture of the effects of absorbing boundary on the dynamics.

Moving to a bottom up approach to metapopulation models provides not only the framework to incorporate diverse life-cycles and behaviours in complex landscapes, but also gives the opportunity to analyse the effects of landscape close to extinction where demographic stochasticity is crucial [270]. Extending the proposed framework from single to multiple species potentially has coexistence effects that depend on the translational invariance of the underlying space. Heterogeneous network habitats introduce trade-offs in species dispersal which impact its survivability potentially leading to landscape-based optimality and adaptation. Another potential thread is that of classical metapopulation models to riverine populations which live on a network with dendritic connectivity following flow distance rather than geodesic distance.

Serial transfers which induce forced fluctuations though periodic are not constant in real experimental settings. The second order stochasticity further intertwines with already present environmental fluctuations, potentially leading to different coexistence outcomes. Community function potentially adapts to changing environmental conditions, with evidences being seen in adaptations of growth rate to transfer frequency [271]. There exists a large gap in how to optimize community function using serial transfers. Furthermore, similar ideas can be extended to chemostats with noisy dilution rates which drives the system out of equilibrium through stochasticity acting in a multiplicative manner.

While each chapter delves into distinct scales - from the microscale of individual particles in non-equilibrium steady states (NESS) to the macroscale of metapopulations and microbial communities - they are unified by the underlying theme of fluctuations, whether arising intrinsically or driven by the environment. The use of common analytical tools across these examples not only merely address specific questions at each scale but also builds connections between them.

The analyses of higher-order cumulants of currents in a NESS can be used to distinguish the nature of disequilibrium brought about by absorbing boundaries. Such insights can then be extended to understand the response of systems close to extinction, utilizing the generalized fluctuation-dissipation theorem (FDT). This approach is not restricted to microscale phenomena; it is equally applicable to metapopulations, offering a valuable perspective on the persistence and extinction dynamics of interacting local populations. Moreover, the development of first principles metapopulation models, integrating detailed landscape information, can be leveraged to enhance our understanding of mi-

crobial ecology. By applying these models to microbial communities, one can begin to account for effect of spatial heterogeneity of natural structures on species coexistence and community function. Such interconnections are only possible due to the interwoven thread of common tools and the generality of obtained results, owing testament to the strength of statistical mechanics to bridge various spatiotemporal scales and diverse fields.

The introduction to this thesis strongly focussed on holism and the philosophy of anti-reductionist approaches. Arguments were made through the historic lens of statistical physics, which although went against reductionism, was still rooted in traditional physics domain. A natural extension of this philosophy comes through in complex systems which strongly promoted interdisciplinary areas of research. The presented topics cover both fundamental statistical physics questions with connections to traditional physics and also include biological applications, both in a theoretical and an experimental setting, bringing to it the quantification and rigour of theoretical analyses. Hopefully, through these chapters, this thesis has successfully highlighted the possibilities and the necessities of a new and fast growing lens of research – one that seeks not to dissect the natural world into its finest details but to understand and explain the wondrous variety of behaviours observed across different scales of life.

7.1 Appendix A

Third order jump correlations

In order to compute the third cumulant, we require all the third order correlations for the number of jumps between states. In this section, following the graphical method, we show some of the terms that arise in this computation. From Fig. 2.3, we choose three orderings of different kinds, a) $k > k' > k''$ where all three k -s are different, b) $k > k' = k''$ where only two of the k -s are different, and c) $k = k' = k''$ where all three k -s are equal.

For $k > k' > k''$, the contribution to third order correlation is

$$\begin{aligned}
 \langle n_{m\ell} n_{m'\ell'} n_{m''\ell''} \rangle_{\Gamma_{\text{MC}}} &= \sum_{k=0}^{M-1} \sum_{k'=0}^k \sum_{k''=0}^{k'} A_{m\ell} \\
 &\times \mathcal{P}(\ell, k\Delta t | m', (k'+1)\Delta t) A_{m'\ell'} \\
 &\times \mathcal{P}(\ell', k'\Delta t | m'', (k''+1)\Delta t) \\
 &\times A_{m''\ell''} P(\ell'', k''\Delta t).
 \end{aligned} \tag{7.1}$$

Similarly for $k > k' = k''$,

$$\begin{aligned}
 \langle n_{m\ell} n_{m'\ell'} n_{m''\ell''} \rangle_{\Gamma_{\text{MC}}} &= \sum_{k=0}^{M-1} \sum_{k'=0}^k A_{m\ell} \\
 &\times \mathcal{P}(\ell, k\Delta t | m', (k'+1)\Delta t) \delta_{m', m''} \\
 &\times \delta_{\ell', \ell''} A_{m'\ell'} P(\ell', k'\Delta t),
 \end{aligned} \tag{7.2}$$

and for $k = k' = k''$,

$$\begin{aligned} \langle n_{m\ell} n_{m'\ell'} n_{m''\ell''} \rangle_{\Gamma_{\text{MC}}} &= \sum_{k=0}^{M-1} \delta_{m,m'} \delta_{\ell,\ell'} \delta_{m',m''} \delta_{\ell',\ell''} \\ &\quad \times A_{m\ell} P(\ell, k\Delta t) \\ &= \langle n_{m,\ell} \rangle_{\Gamma_{\text{MC}}} \delta_{m,m'} \delta_{\ell,\ell'} \delta_{m',m''} \delta_{\ell',\ell''}. \end{aligned} \quad (7.3)$$

The contributions from $k < k' = k''$, and $k > k' = k''$ can be written in terms of the second order jump correlations and the first moment of jumps, i.e.,

$$\begin{aligned} \langle n_{m\ell} n_{m'\ell'} n_{m''\ell''} \rangle_{\Gamma_{\text{MC}}} &= \langle n_{m\ell} n_{m'\ell'} \rangle_{\Gamma_{\text{MC}}} \delta_{m',m''} \delta_{\ell',\ell''} \\ &\quad - \langle n_{m,\ell} \rangle_{\Gamma_{\text{MC}}} \delta_{m',m''} \delta_{\ell',\ell''} \\ &\quad \times \delta_{m',m''} \delta_{\ell',\ell''} \end{aligned} \quad (7.4)$$

Conversely, starting from a stationary state, P^{st} , and taking the limit $\Delta t \rightarrow 0$ to recover the master equation formalism, the term arising from Eq. (7.1) gives the following integral:

$$\begin{aligned} \langle n_{m\ell} n_{m'\ell'} n_{m''\ell''} \rangle_{\Gamma} &= W_{m\ell} W_{m'\ell'} W_{m''\ell''} P^{\text{st}}(\ell'') \\ &\quad \times \int_0^T dt \int_0^t dt' \mathcal{P}(\ell, t | m', t') \\ &\quad \times \int_0^{t'} dt'' \mathcal{P}(\ell', t' | m'', t'') \end{aligned} \quad (7.5)$$

Using the eigenvector expansion for the transition probability $\mathcal{P}(i, t | i_0, t_0)$ (see Eq. (2.21)), the integrals on the right-hand side of Eq. (7.5) give \mathcal{T}_{j_1, j_2} , i.e, Eq. (2.24).

7.2 Appendix B

Perron-Frobenius proof of eigenvalue hierarchy

Consider an infinitesimal increment in time ϵ . Then, the Master equation can be discretized to the Markov chain

$$P(t + \epsilon) = P(t) + \epsilon H P(t) \quad (7.6)$$

Consequently, define $T \equiv (\mathbb{I} + \epsilon H)$ where \mathbb{I} is the identity matrix. We are considering an irreducible system. Hence, T is a non negative, irreducible matrix of size $N \times N$ where N is the number of states. The eigenvalues of T are simply $\alpha_i = 1 - \epsilon \lambda_i$. We consider the submatrix of T corresponding to the interior. Let T^* be a matrix of size $(N-1) \times (N-1)$ accounting for the interior states. Since we are in an irreducible system, there exists a path from one state to another, and hence, there always exists a $k_{xy} > 0$ for which the $(W_{xy})^{k_{xy}}$ is non zero. There are $(N-1)^2$ such positive numbers. Choosing the largest of these numbers ensures that T^* is primitive, i.e., $(T^*)^{k_{largest}} > 0$, if ϵ is sufficiently small (see below).

The characteristic function of the eigenvalues of T^* is the characteristic function of T without the $(\alpha - 1)$ factor coming from the first eigenvalue. Hence, finding the eigenvalues of T^* is equivalent to finding the eigenvalues of T . Note that $T_{xy}^* \geq 0$ when $x \neq y$ and $T_{xx}^* = 1 - \epsilon \sum_z W_{zx}$ which is bounded allowing us to choose sufficiently small ϵ such that $T_{xy}^* \geq 0 \forall x, y$. Thus, we can apply the Perron-Frobenius theorem [272] on the matrix T^* . Then, we have a leading real eigenvalue $\alpha_1 > 0$. For any other eigenvalue α_2 , then, $\alpha_1 > |\alpha_2|$. Since $T = \mathbb{I} + \epsilon H$, and from the eigenvalue definition in (3.34), the eigenvalues are related as $\alpha = 1 - \epsilon \lambda$. Then, with $\text{Re}(z)$ and $\text{Im}(z)$ representing the real and imaginary parts of z ,

$$\begin{aligned} \alpha_1 &> |\alpha_2| \\ \implies (1 - \epsilon \lambda_1)^2 &> |1 - \epsilon \text{Re}(\lambda_2) - i \epsilon \text{Im}(\lambda_2)|^2 \\ \implies \epsilon^2 \lambda_1^2 - 2\epsilon \lambda_1 &> \epsilon^2 (\text{Re}(\lambda_2)^2 + \text{Im}(\lambda_2)^2) - 2\epsilon \text{Re}(\lambda_2) \end{aligned} \quad (7.7)$$

In the limit $\epsilon \rightarrow 0$, which is the correct limit to get the Master equation back, we have $\text{Re}(\lambda_2) > \lambda_1$.

The Perron-Frobenius Theorem also guarantees that the left and the right eigenvector of T^* corresponding to the eigenvalue α_1 (equivalently, λ_1) are non-degenerate and have components strictly positive. If φ_1 and ψ^1 are the right and left eigenvectors of H corresponding to $-\lambda_1$, then, $\varphi_{1x}, \psi_x^1 > 0 \forall x \neq 0$. Hence, we can choose the normalization such that $\sum_{x \neq 0} \varphi_{1x} = 1$. Since $0 = \sum_x \psi_x^0 \varphi_{1x} = \sum_x \varphi_{1x} \implies \varphi_{10} = -1$. Then, if at least one of the W_{0y} is positive,

$$\lambda_1 = -\lambda_1 \varphi_{10} = \sum_y H_{0y} \varphi_{1y} = \sum_{y \neq 0} W_{0y} \varphi_{1y} > 0 \quad (7.8)$$

BIBLIOGRAPHY

- [1] Raj Kumar Pathria. *Statistical mechanics*. Elsevier, 2016.
- [2] Albert Einstein. *Investigations on the Theory of the Brownian Movement*. Courier Corporation, 1956.
- [3] MA Islam. Einstein–smoluchowski diffusion equation: a discussion. *Physica Scripta*, 70(2-3):120, 2004.
- [4] Umberto Marini Bettolo Marconi, Andrea Puglisi, Lamberto Rondoni, and Angelo Vulpiani. Fluctuation–dissipation: response theory in statistical physics. *Physics reports*, 461(4-6):111–195, 2008.
- [5] Hong Qian and Hao Ge. *Stochastic Chemical Reaction Systems in Biology*. Springer, 2021.
- [6] Federico S Gnesotto, Federica Mura, Jannes Gladrow, and Chase P Broedersz. Broken detailed balance and non-equilibrium dynamics in living systems: a review. *Reports on Progress in Physics*, 81(6):066601, 2018.
- [7] Sybren Ruurds De Groot and Peter Mazur. *Non-equilibrium thermodynamics*. Courier Corporation, 2013.
- [8] Crispin W Gardiner et al. *Handbook of stochastic methods*, volume 3. springer Berlin, 1985.
- [9] Nicolaas Godfried Van Kampen. *Stochastic processes in physics and chemistry*, volume 1. Elsevier, 1992.
- [10] Hannes Risken. Fokker-planck equation. In *The Fokker-Planck Equation*.
- [11] Anatoly B Kolomeisky. Physics of protein–dna interactions: mechanisms of facilitated target search. *Physical Chemistry Chemical Physics*, 13(6):2088–2095, 2011.
- [12] Harley H McAdams and Adam Arkin. Stochastic mechanisms in gene expression. *Proceedings of the National Academy of Sciences*, 94(3):814–819, 1997.

- [13] Vahid Shahrezaei and Peter S Swain. The stochastic nature of biochemical networks. *Current opinion in biotechnology*, 19(4):369–374, 2008.
- [14] Paul C Bressloff. *Stochastic processes in cell biology*, volume 41. Springer, 2014.
- [15] Silvia Zaoli and Jacopo Grilli. A macroecological description of alternative stable states reproduces intra-and inter-host variability of gut microbiome. *Science Advances*, 7(43):eabj2882, 2021.
- [16] Sandro Azaele, Samir Suweis, Jacopo Grilli, Igor Volkov, Jayanth R Banavar, and Amos Maritan. Statistical mechanics of ecological systems: Neutral theory and beyond. *Reviews of Modern Physics*, 88(3):035003, 2016.
- [17] Marc Barthelemy. The statistical physics of cities. *Nature Reviews Physics*, 1(6):406–415, 2019.
- [18] Wolfgang Paul and Jörg Baschnagel. Stochastic processes. *From Physics to finance*, 1999.
- [19] Paul Langevin. On the theory of brownian motion. *CR Acad Sci (Paris)*, 146:530, 1908.
- [20] Nicolaas G Van Kampen. Itô versus stratonovich. *Journal of Statistical Physics*, 24:175–187, 1981.
- [21] Kiyosi Ito, Kiyosi Itô, Kiyosi Itô, Japon Mathématicien, Kiyosi Itô, and Japan Mathematician. *On stochastic differential equations*, volume 4. American Mathematical Society New York, 1951.
- [22] Ruslan Leont’evich Stratonovich. Conditional markov processes. In *Non-linear transformations of stochastic processes*, pages 427–453. Elsevier, 1965.
- [23] Harry Nyquist. Thermal agitation of electric charge in conductors. *Physical review*, 32(1):110, 1928.
- [24] Lino Reggiani and Eleonora Alfinito. Fluctuation dissipation theorem and electrical noise revisited. *Fluctuation and Noise Letters*, 18(01):1930001, 2019.
- [25] J Weber. Fluctuation dissipation theorem. *Physical Review*, 101(6):1620, 1956.
- [26] Lars Onsager. Reciprocal relations in irreversible processes. i. *Physical review*, 37(4):405, 1931.
- [27] Lars Onsager. Reciprocal relations in irreversible processes. ii. *Physical review*, 38(12):2265, 1931.

- [28] Ryogo Kubo. Statistical-mechanical theory of irreversible processes. i. general theory and simple applications to magnetic and conduction problems. *Journal of the Physical Society of Japan*, 12(6):570–586, 1957.
- [29] Rep Kubo. The fluctuation-dissipation theorem. *Reports on progress in physics*, 29(1):255, 1966.
- [30] Christian Maes. Local detailed balance. *SciPost Physics Lecture Notes*, page 032, 2021.
- [31] John C Baez and Blake S Pollard. Relative entropy in biological systems. *Entropy*, 18(2):46, 2016.
- [32] Udo Seifert. Stochastic thermodynamics, fluctuation theorems and molecular machines. *Reports on progress in physics*, 75(12):126001, 2012.
- [33] Junang Li, Jordan M Horowitz, Todd R Gingrich, and Nikta Fakhri. Quantifying dissipation using fluctuating currents. *Nature communications*, 10(1):1–9, 2019.
- [34] Jorge Kurchan. Fluctuation theorem for stochastic dynamics. *Journal of Physics A: Mathematical and General*, 31(16):3719, 1998.
- [35] Joel L Lebowitz and Herbert Spohn. A gallavotti–cohen-type symmetry in the large deviation functional for stochastic dynamics. *Journal of Statistical Physics*, 95(1):333–365, 1999.
- [36] Andreas Dechant. Multidimensional thermodynamic uncertainty relations. *Journal of Physics A: Mathematical and Theoretical*, 52(3):035001, 2018.
- [37] Gavin E Crooks. Entropy production fluctuation theorem and the nonequilibrium work relation for free energy differences. *Physical Review E*, 60(3):2721, 1999.
- [38] Christopher Jarzynski. Nonequilibrium equality for free energy differences. *Physical Review Letters*, 78(14):2690, 1997.
- [39] Andrea Crisanti and Felix Ritort. Violation of the fluctuation–dissipation theorem in glassy systems: basic notions and the numerical evidence. *Journal of Physics A: Mathematical and General*, 36(21):R181, 2003.
- [40] James P Sethna. *Statistical mechanics: entropy, order parameters, and complexity*, volume 14. Oxford University Press, USA, 2021.
- [41] Daniel T Gillespie. Exact stochastic simulation of coupled chemical reactions. *The journal of physical chemistry*, 81(25):2340–2361, 1977.

- [42] Anastasios Noulas, Salvatore Scellato, Renaud Lambiotte, Massimiliano Pontil, and Cecilia Mascolo. A tale of many cities: universal patterns in human urban mobility. *PloS one*, 7(5):e37027, 2012.
- [43] Sandro Azaele, Amos Maritan, Stephen J Cornell, Samir Suweis, Jayanth R Banavar, Doreen Gabriel, and William E Kunin. Towards a unified descriptive theory for spatial ecology: predicting biodiversity patterns across spatial scales. *Methods in Ecology and Evolution*, 6(3):324–332, 2015.
- [44] Andrew J Black and Alan J McKane. Stochastic formulation of ecological models and their applications. *Trends in ecology & evolution*, 27(6):337–345, 2012.
- [45] Peter Chesson. Macarthur's consumer-resource model. *Theoretical Population Biology*, 37(1):26–38, 1990.
- [46] Kevin D Lafferty, Giulio DeLeo, Cheryl J Briggs, Andrew P Dobson, Thilo Gross, and Armand M Kuris. A general consumer-resource population model. *Science*, 349(6250):854–857, 2015.
- [47] Garrett Hardin. The competitive exclusion principle: an idea that took a century to be born has implications in ecology, economics, and genetics. *science*, 131(3409):1292–1297, 1960.
- [48] Stephen P Hubbell. The unified neutral theory of biodiversity and biogeography (mpb-32). In *The Unified Neutral Theory of Biodiversity and Biogeography (MPB-32)*. Princeton University Press, 2011.
- [49] Sandro Azaele, Simone Pigolotti, Jayanth R Banavar, and Amos Maritan. Dynamical evolution of ecosystems. *Nature*, 444(7121):926–928, 2006.
- [50] John C Cox, Jonathan E Ingersoll Jr, and Stephen A Ross. A theory of the term structure of interest rates. In *Theory of valuation*, pages 129–164. World Scientific, 2005.
- [51] Fischer Black and Myron Scholes. The pricing of options and corporate liabilities. *Journal of political economy*, 81(3):637–654, 1973.
- [52] Ashish B George and James O'Dwyer. Universal abundance fluctuations across microbial communities, tropical forests, and urban populations. *Proceedings of the National Academy of Sciences*, 120(44):e2215832120, 2023.
- [53] Aant Elzinga. Huygens' theory of research and descartes' theory of knowledge ii. *Zeitschrift für allgemeine Wissenschaftstheorie*, 3(1):9–27, 1972.
- [54] Hein van den Berg and Boris Demarest. Axiomatic natural philosophy and the emergence of biology as a science. *Journal of the History of Biology*, 53(3):379–422, 2020.

- [55] William C Wimsatt. *Re-engineering philosophy for limited beings: Piecewise approximations to reality*. Harvard University Press, 2007.
- [56] Philip W Anderson. More is different: Broken symmetry and the nature of the hierarchical structure of science. *Science*, 177(4047):393–396, 1972.
- [57] John Burdon Sanderson Haldane. *Possible worlds*. Routledge, 1927.
- [58] Roman Frigg and Charlotte Werndl. Philosophy of Statistical Mechanics. In Edward N. Zalta and Uri Nodelman, editors, *The Stanford Encyclopedia of Philosophy*. Metaphysics Research Lab, Stanford University, Spring 2024 edition, 2024.
- [59] Thomas S Kuhn. *The structure of scientific revolutions*. University of Chicago press, 2012.
- [60] Richard Levins. The strategy of model building in population biology. *American scientist*, 54(4):421–431, 1966.
- [61] Simon Levin. Complex adaptive systems: exploring the known, the unknown and the unknowable. *Bulletin of the American mathematical Society*, 40(1):3–19, 2003.
- [62] Norbert Wiener. *The human use of human beings: Cybernetics and society*. Number 320. Da capo press, 1988.
- [63] Prajwal Padmanabha, Daniel Maria Busiello, Amos Maritan, and Deepak Gupta. Fluctuations of entropy production of a run-and-tumble particle. *Physical Review E*, 107(1):014129, 2023.
- [64] Ilya Prigogine and Gregoire Nicolis. Biological order, structure and instabilities1. *Quarterly reviews of biophysics*, 4(2-3):107–148, 1971.
- [65] Erwin Schrödinger. *What is Life? The Physical Aspect of the Living Cell*. Cambridge University Press, 1944.
- [66] Xiaona Fang, Karsten Kruse, Ting Lu, and Jin Wang. Nonequilibrium physics in biology. *Reviews of Modern Physics*, 91(4):045004, 2019.
- [67] Felix Ritort. Nonequilibrium fluctuations in small systems: From physics to biology. *Advances in chemical physics*, 137:31, 2008.
- [68] Carlos Bustamante, Jan Liphardt, and Felix Ritort. The nonequilibrium thermodynamics of small systems. *arXiv preprint cond-mat/0511629*, 2005.
- [69] Étienne Fodor, Cesare Nardini, Michael E Cates, Julien Tailleur, Paolo Visco, and Frédéric Van Wijland. How far from equilibrium is active matter? *Physical review letters*, 117(3):038103, 2016.

- [70] Giovanni Diana and Massimiliano Esposito. Mutual entropy production in bipartite systems. *Journal of Statistical Mechanics: Theory and Experiment*, 2014(4):P04010, 2014.
- [71] Daniel M Busiello, Jorge Hidalgo, and Amos Maritan. Entropy production in systems with random transition rates close to equilibrium. *Physical Review E*, 96(6):062110, 2017.
- [72] Daniel M Busiello, Jorge Hidalgo, and Amos Maritan. Entropy production for coarse-grained dynamics. *New Journal of Physics*, 21(7):073004, 2019.
- [73] Daniel M Busiello and Amos Maritan. Entropy production in master equations and fokker–planck equations: facing the coarse-graining and recovering the information loss. *Journal of Statistical Mechanics: Theory and Experiment*, 2019(10):104013, 2019.
- [74] Udo Seifert. Entropy production along a stochastic trajectory and an integral fluctuation theorem. *Physical review letters*, 95(4):040602, 2005.
- [75] Ken Sekimoto. *Stochastic energetics*, volume 799. Springer, 2010.
- [76] R Van Zon and EGD Cohen. Stationary and transient work-fluctuation theorems for a dragged brownian particle. *Physical Review E*, 67(4):046102, 2003.
- [77] Frédéric Douarche, Sylvain Joubaud, Nicolas B Garnier, Artyom Petrosyan, and Sergio Ciliberto. Work fluctuation theorems for harmonic oscillators. *Physical review letters*, 97(14):140603, 2006.
- [78] Sanjib Sabhapandit. Heat and work fluctuations for a harmonic oscillator. *Physical Review E*, 85(2):021108, 2012.
- [79] GM Wang, Edith M Sevick, Emil Mittag, Debra J Searles, and Denis J Evans. Experimental demonstration of violations of the second law of thermodynamics for small systems and short time scales. *Physical Review Letters*, 89(5):050601, 2002.
- [80] Sergio Ciliberto, Alberto Imparato, Antoine Naert, and Marius Tanase. Heat flux and entropy produced by thermal fluctuations. *Physical review letters*, 110(18):180601, 2013.
- [81] Deepak Gupta and Sanjib Sabhapandit. Partial entropy production in heat transport. *Journal of Statistical Mechanics: Theory and Experiment*, 2018(6):063203, 2018.
- [82] A Puglisi, S Pigolotti, Lamberto Rondoni, and A Vulpiani. Entropy production and coarse graining in markov processes. *Journal of Statistical Mechanics: Theory and Experiment*, 2010(05):P05015, 2010.

- [83] R. van Zon and E. G. D. Cohen. Extension of the fluctuation theorem. *Phys. Rev. Lett.*, 91:110601, Sep 2003.
- [84] Paolo Visco. Work fluctuations for a brownian particle between two thermostats. *Journal of Statistical Mechanics: Theory and Experiment*, 2006(06):P06006, 2006.
- [85] Anupam Kundu, Sanjib Sabhapandit, and Abhishek Dhar. Large deviations of heat flow in harmonic chains. *Journal of Statistical Mechanics: Theory and Experiment*, 2011(03):P03007, 2011.
- [86] Ignacio A Martínez, Édgar Roldán, Luis Dinis, Dmitri Petrov, Juan MR Parrondo, and Raúl A Rica. Brownian carnot engine. *Nature physics*, 12(1):67–70, 2016.
- [87] Christian Van den Broeck, Niraj Kumar, and Katja Lindenberg. Efficiency of isothermal molecular machines at maximum power. *Physical review letters*, 108(21):210602, 2012.
- [88] Gatién Verley, Massimiliano Esposito, Tim Willaert, and Christian Van den Broeck. The unlikely carnot efficiency. *Nature communications*, 5(1):1–5, 2014.
- [89] Deepak Gupta and Sanjib Sabhapandit. Stochastic efficiency of an isothermal work-to-work converter engine. *Physical Review E*, 96(4):042130, 2017.
- [90] Deepak Gupta. Exact distribution for work and stochastic efficiency of an isothermal machine. *Journal of Statistical Mechanics: Theory and Experiment*, 2018(7):073201, 2018.
- [91] Giovanni Gallavotti and Ezechiel Godert David Cohen. Dynamical ensembles in stationary states. *Journal of Statistical Physics*, 80:931–970, 1995.
- [92] Michele Campisi, Peter Talkner, and Peter Hänggi. Fluctuation theorem for arbitrary open quantum systems. *Physical review letters*, 102(21):210401, 2009.
- [93] Gavin E Crooks. Nonequilibrium measurements of free energy differences for microscopically reversible markovian systems. *Journal of Statistical Physics*, 90(5):1481–1487, 1998.
- [94] Marco Baiesi and Christian Maes. An update on the nonequilibrium linear response. *New Journal of Physics*, 15(1):013004, 2013.
- [95] Marco Baiesi, Christian Maes, and Bram Wynants. Fluctuations and response of nonequilibrium states. *Physical review letters*, 103(1):010602, 2009.

- [96] Andre C Barato and Udo Seifert. Thermodynamic uncertainty relation for biomolecular processes. *Physical review letters*, 114(15):158101, 2015.
- [97] Todd R Gingrich, Jordan M Horowitz, Nikolay Perunov, and Jeremy L England. Dissipation bounds all steady-state current fluctuations. *Physical review letters*, 116(12):120601, 2016.
- [98] Jordan M Horowitz and Todd R Gingrich. Thermodynamic uncertainty relations constrain non-equilibrium fluctuations. *Nature Physics*, 16(1):15–20, 2020.
- [99] Sreekanth K Manikandan, Subhrokoli Ghosh, Avijit Kundu, Biswajit Das, Vipin Agrawal, Dhruvadya Mitra, Ayan Banerjee, and Supriya Krishnamurthy. Quantitative analysis of non-equilibrium systems from short-time experimental data. *Communications Physics*, 4(1):1–10, 2021.
- [100] Biswajit Das, Sreekanth K Manikandan, and Ayan Banerjee. Inferring entropy production in anharmonic brownian gyrators. *arXiv preprint arXiv:2204.09283*, 2022.
- [101] Tan Van Vu, Yoshihiko Hasegawa, et al. Entropy production estimation with optimal current. *Physical Review E*, 101(4):042138, 2020.
- [102] Dominic J Skinner and Jörn Dunkel. Estimating entropy production from waiting time distributions. *Physical review letters*, 127(19):198101, 2021.
- [103] Shun Otsubo, Sosuke Ito, Andreas Dechant, and Takahiro Sagawa. Estimating entropy production by machine learning of short-time fluctuating currents. *Physical Review E*, 101(6):062106, 2020.
- [104] Édgar Roldán and Juan MR Parrondo. Estimating dissipation from single stationary trajectories. *Physical review letters*, 105(15):150607, 2010.
- [105] Shun Otsubo, Sreekanth K Manikandan, Takahiro Sagawa, and Supriya Krishnamurthy. Estimating time-dependent entropy production from non-equilibrium trajectories. *Communications Physics*, 5(1):1–10, 2022.
- [106] Boris Lander, Jakob Mehl, Valentin Blickle, Clemens Bechinger, and Udo Seifert. Noninvasive measurement of dissipation in colloidal systems. *Physical Review E*, 86(3):030401, 2012.
- [107] Arnab Saha, Sourabh Lahiri, and AM Jayannavar. Entropy production theorems and some consequences. *Physical Review E*, 80(1):011117, 2009.
- [108] Deepak Gupta and Sanjib Sabhapandit. Fluctuation theorem for entropy production of a partial system in the weak-coupling limit. *EPL (Europhysics Letters)*, 115(6):60003, 2016.

- [109] Deepak Gupta and Sanjib Sabhapandit. Entropy production for partially observed harmonic systems. *Journal of Statistical Mechanics: Theory and Experiment*, 2020(1):013204, 2020.
- [110] Thomas Martynec, Sabine HL Klapp, and Sarah AM Loos. Entropy production at criticality in a nonequilibrium potts model. *New Journal of Physics*, 22(9):093069, 2020.
- [111] C Tietz, S Schuler, T Speck, U Seifert, and J Wrachtrup. Measurement of stochastic entropy production. *Physical review letters*, 97(5):050602, 2006.
- [112] Thomas Speck, Valentin Blickle, Clemens Bechinger, and Udo Seifert. Distribution of entropy production for a colloidal particle in a nonequilibrium steady state. *EPL (Europhysics Letters)*, 79(3):30002, 2007.
- [113] JV Koski, T Sagawa, OP Saira, Y Yoon, A Kutvonen, P Solinas, M Möttönen, T Ala-Nissila, and JP Pekola. Distribution of entropy production in a single-electron box. *Nature Physics*, 9(10):644–648, 2013.
- [114] Sergio Ciliberto. Experiments in stochastic thermodynamics: Short history and perspectives. *Physical Review X*, 7(2):021051, 2017.
- [115] Daniel S Seara, Vikrant Yadav, Ian Linsmeier, A Pasha Tabatabai, Patrick W Oakes, SM Tabei, Shiladitya Banerjee, and Michael P Murrell. Entropy production rate is maximized in non-contractile actomyosin. *Nature communications*, 9(1):1–10, 2018.
- [116] Sriram Ramaswamy. The mechanics and statistics of active matter. *Annu. Rev. Condens. Matter Phys.*, 1(1):323–345, 2010.
- [117] Ignacio A Martinez, Édgar Roldán, Luis Dinis, and Raúl A Rica. Colloidal heat engines: a review. *Soft matter*, 13(1):22–36, 2017.
- [118] Daniel M Busiello, Shiling Liang, Francesco Piazza, and Paolo De Los Rios. Dissipation-driven selection of states in non-equilibrium chemical networks. *Communications Chemistry*, 4(1):1–7, 2021.
- [119] Avinash Vicholous Dass, Thomas Georgelin, Frances Westall, Frédéric Foucher, Paolo De Los Rios, Daniel M Busiello, Shiling Liang, and Francesco Piazza. Equilibrium and non-equilibrium furanose selection in the ribose isomerisation network. *Nature Communications*, 12(1):1–10, 2021.
- [120] Sreekanth K Manikandan, Deepak Gupta, and Supriya Krishnamurthy. Inferring entropy production from short experiments. *Physical review letters*, 124(12):120603, 2020.

- [121] Thomas Speck and Udo Seifert. Integral fluctuation theorem for the housekeeping heat. *Journal of Physics A: Mathematical and General*, 38(34):L581, 2005.
- [122] Andreas Dechant and Shin-ichi Sasa. Entropic bounds on currents in langevin systems. *Physical Review E*, 97(6):062101, 2018.
- [123] Patrick Pietzonka, Andre C Barato, and Udo Seifert. Universal bounds on current fluctuations. *Physical Review E*, 93(5):052145, 2016.
- [124] M Cristina Marchetti, Jean-François Joanny, Sriram Ramaswamy, Tanniemola B Liverpool, Jacques Prost, Madan Rao, and R Aditi Simha. Hydrodynamics of soft active matter. *Reviews of modern physics*, 85(3):1143, 2013.
- [125] Sriram Ramaswamy. Active matter. *Journal of Statistical Mechanics: Theory and Experiment*, 2017(5):054002, 2017.
- [126] Jacques Prost, Frank Jülicher, and Jean-François Joanny. Active gel physics. *Nature physics*, 11(2):111–117, 2015.
- [127] Joakim Stenhammar, Raphael Wittkowski, Davide Marenduzzo, and Michael E Cates. Light-induced self-assembly of active rectification devices. *Science advances*, 2(4):e1501850, 2016.
- [128] Yunfei Du, Huijun Jiang, and Zhonghuai Hou. Self-assembly of active core corona particles into highly ordered and self-healing structures. *The Journal of Chemical Physics*, 151(15):154904, 2019.
- [129] Joakim Stenhammar, Raphael Wittkowski, Davide Marenduzzo, and Michael E Cates. Activity-induced phase separation and self-assembly in mixtures of active and passive particles. *Physical review letters*, 114(1):018301, 2015.
- [130] Mingfeng Pu, Huijun Jiang, and Zhonghuai Hou. Reentrant phase separation behavior of active particles with anisotropic janus interaction. *Soft matter*, 13(22):4112–4121, 2017.
- [131] Yaouen Fily and M Cristina Marchetti. Athermal phase separation of self-propelled particles with no alignment. *Physical review letters*, 108(23):235702, 2012.
- [132] Dibyendu Mandal, Katherine Klymko, and Michael R DeWeese. Entropy production and fluctuation theorems for active matter. *Physical review letters*, 119(25):258001, 2017.
- [133] Lorenzo Caprini, Umberto Marini Bettolo Marconi, Andrea Puglisi, and Angelo Vulpiani. The entropy production of ornstein–uhlenbeck active particles: a path integral method for correlations. *Journal of Statistical Mechanics: Theory and Experiment*, 2019(5):053203, 2019.

- [134] David Martin, Jérémy O'Byrne, Michael E Cates, Étienne Fodor, Cesare Nardini, Julien Tailleur, and Frédéric van Wijland. Statistical mechanics of active ornstein-uhlenbeck particles. *Physical Review E*, 103(3):032607, 2021.
- [135] Thomas Speck. Stochastic thermodynamics for active matter. *EPL (Europhysics Letters)*, 114(3):30006, 2016.
- [136] Grzegorz Szamel. Stochastic thermodynamics for self-propelled particles. *Physical Review E*, 100(5):050603, 2019.
- [137] Subhasish Chaki and Rajarshi Chakrabarti. Effects of active fluctuations on energetics of a colloidal particle: Superdiffusion, dissipation and entropy production. *Physica A: Statistical Mechanics and its Applications*, 530:121574, 2019.
- [138] Cesare Nardini, Étienne Fodor, Elsen Tjhung, Frédéric Van Wijland, Julien Tailleur, and Michael E Cates. Entropy production in field theories without time-reversal symmetry: quantifying the non-equilibrium character of active matter. *Physical Review X*, 7(2):021007, 2017.
- [139] Suraj Shankar and M Cristina Marchetti. Hidden entropy production and work fluctuations in an ideal active gas. *Physical Review E*, 98(2):020604, 2018.
- [140] Zhiyu Cao, Jie Su, Huijun Jiang, and Zhonghuai Hou. Effective entropy production and thermodynamic uncertainty relation of active brownian particles. *arXiv preprint arXiv:1907.11459*, 2019.
- [141] Dominic J Skinner and Jörn Dunkel. Improved bounds on entropy production in living systems. *Proceedings of the National Academy of Sciences*, 118(18), 2021.
- [142] Deepak Gupta and David A Sivak. Heat fluctuations in a harmonic chain of active particles. *Physical Review E*, 104(2):024605, 2021.
- [143] Gianmaria Falasco, Richard Pfaller, Andreas P Bregulla, Frank Cichos, and Klaus Kroy. Exact symmetries in the velocity fluctuations of a hot brownian swimmer. *Physical Review E*, 94(3):030602, 2016.
- [144] Howard C Berg. *E. coli in Motion*. Springer, 2004.
- [145] Jens Elgeti and Gerhard Gompper. Run-and-tumble dynamics of self-propelled particles in confinement. *EPL (Europhysics Letters)*, 109(5):58003, 2015.
- [146] Thibaut Demaerel and Christian Maes. Active processes in one dimension. *Physical Review E*, 97(3):032604, 2018.

- [147] Kanaya Malakar, V Jemseena, Anupam Kundu, K Vijay Kumar, Sanjib Sabhapandit, Satya N Majumdar, S Redner, and Abhishek Dhar. Steady state, relaxation and first-passage properties of a run-and-tumble particle in one-dimension. *Journal of Statistical Mechanics: Theory and Experiment*, 2018(4):043215, 2018.
- [148] Philip Rosenau. Random walker and the telegrapher's equation: A paradigm of a generalized hydrodynamics. *Physical Review E*, 48(2):R655, 1993.
- [149] George H Weiss. Some applications of persistent random walks and the telegrapher's equation. *Physica A: Statistical Mechanics and its Applications*, 311(3-4):381–410, 2002.
- [150] Martin R Evans and Satya N Majumdar. Run and tumble particle under resetting: a renewal approach. *Journal of Physics A: Mathematical and Theoretical*, 51(47):475003, 2018.
- [151] Abhishek Dhar, Anupam Kundu, Satya N Majumdar, Sanjib Sabhapandit, and Grégory Schehr. Run-and-tumble particle in one-dimensional confining potentials: steady-state, relaxation, and first-passage properties. *Physical Review E*, 99(3):032132, 2019.
- [152] Luca Angelani. Run-and-tumble particles, telegrapher's equation and absorption problems with partially reflecting boundaries. *Journal of Physics A: Mathematical and Theoretical*, 48(49):495003, 2015.
- [153] Nitzan Razin. Entropy production of an active particle in a box. *Physical Review E*, 102(3):030103, 2020.
- [154] Massimiliano Esposito, Katja Lindenberg, and Christian Van den Broeck. Entropy production as correlation between system and reservoir. *New Journal of Physics*, 12(1):013013, 2010.
- [155] Heinz Georg Schuster. *Nonequilibrium statistical physics of small systems: Fluctuation relations and beyond*. John Wiley & Sons, 2013.
- [156] Daniel M Busiello, Deepak Gupta, and Amos Maritan. Entropy production in systems with unidirectional transitions. *Physical Review Research*, 2(2):023011, 2020.
- [157] Daniel M Busiello and Carlos Fiore. Hyperaccurate bounds in discrete-state markovian systems. *arXiv preprint arXiv:2205.00294*, 2022.
- [158] Prajwal Padmanabha, Sandro Azaele, and Amos Maritan. Generalisation of fluctuation-dissipation theorem to systems with absorbing states. *New Journal of Physics*, 25(11):113001, 2023.
- [159] Jean Zinn-Justin. *Quantum field theory and critical phenomena*, volume 171. Oxford university press, 1996.

- [160] D Villamaina, A Baldassarri, A Puglisi, and A Vulpiani. The fluctuation-dissipation relation: how does one compare correlation functions and responses? *Journal of Statistical Mechanics: Theory and Experiment*, 2009(07):P07024, 2009.
- [161] Andrea Crisanti, Andrea Puglisi, and Dario Villamaina. Nonequilibrium and information: The role of cross correlations. *Physical Review E*, 85(6):061127, 2012.
- [162] Leticia F Cugliandolo, Jorge Kurchan, and Giorgio Parisi. Off equilibrium dynamics and aging in unfrustrated systems. *Journal de Physique I*, 4(11):1641–1656, 1994.
- [163] Gregor Diezemann. Fluctuation-dissipation relations for markov processes. *Physical Review E*, 72(1):011104, 2005.
- [164] Udo Seifert and Thomas Speck. Fluctuation-dissipation theorem in nonequilibrium steady states. *EPL (Europhysics Letters)*, 89(1):10007, 2010.
- [165] Raphael Chetrite, Gregory Falkovich, and Krzysztof Gawedzki. Fluctuation relations in simple examples of non-equilibrium steady states. *Journal of Statistical Mechanics: Theory and Experiment*, 2008(08):P08005, 2008.
- [166] Gatien Verley, K Mallick, and D Lacoste. Modified fluctuation-dissipation theorem for non-equilibrium steady states and applications to molecular motors. *EPL (Europhysics Letters)*, 93(1):10002, 2011.
- [167] Gatien Verley, Raphaël Chétrite, and David Lacoste. Modified fluctuation-dissipation theorem for general non-stationary states and application to the glauber–ising chain. *Journal of Statistical Mechanics: Theory and Experiment*, 2011(10):P10025, 2011.
- [168] Maurice Stevenson Bartlett. Stochastic population models; in ecology and epidemiology. Technical report, 1960.
- [169] Phil K Pollett. Quasi-stationary distributions: a bibliography. Available at <http://www.maths.uq.edu.au/>, 2008.
- [170] Sylvie Méléard and Denis Villemonais. Quasi-stationary distributions and population processes. *Probability Surveys*, 9:340–410, 2012.
- [171] John N Darroch and Eugene Seneta. On quasi-stationary distributions in absorbing discrete-time finite markov chains. *Journal of Applied Probability*, 2(1):88–100, 1965.
- [172] John N Darroch and Eugene Seneta. On quasi-stationary distributions in absorbing continuous-time finite markov chains. *Journal of Applied Probability*, 4(1):192–196, 1967.

- [173] Marcelo Martins de Oliveira and Ronald Dickman. How to simulate the quasistationary state. *Physical Review E*, 71(1):016129, 2005.
- [174] APF Atman and Ronald Dickman. Quasistationary distributions for the domany-kinzel stochastic cellular automaton. *Physical Review E*, 66(4):046135, 2002.
- [175] Erik A Van Doorn. Quasi-stationary distributions and convergence to quasi-stationarity of birth-death processes. *Advances in Applied Probability*, 23(4):683–700, 1991.
- [176] Servet Martinez and Jaime San Martin. Quasi-stationary distributions for a brownian motion with drift and associated limit laws. *Journal of applied probability*, 31(4):911–920, 1994.
- [177] Ronald Dickman and Marcelo Martins de Oliveira. Quasi-stationary simulation of the contact process. *Physica A: Statistical Mechanics and its Applications*, 357(1):134–141, 2005.
- [178] Shun Ogawa and Yoshiyuki Y Yamaguchi. Linear response theory in the vlasov equation for homogeneous and for inhomogeneous quasistationary states. *Physical Review E*, 85(6):061115, 2012.
- [179] Aurelio Patelli, Shamik Gupta, Cesare Nardini, and Stefano Ruffo. Linear response theory for long-range interacting systems in quasistationary states. *Physical Review E*, 85(2):021133, 2012.
- [180] Rick Durrett. *Probability: theory and examples*, volume 49. Cambridge university press, 2019.
- [181] Sidney Redner. *A guide to first-passage processes*. Cambridge university press, 2001.
- [182] Venkataraman Balakrishnan. *Elements of nonequilibrium statistical mechanics*, volume 3. Springer, 2008.
- [183] K Voigtlaender and H Risken. Eigenvalues of the fokker—planck and bgk operators for a double-well potential. *Chemical physics letters*, 105(5):506–510, 1984.
- [184] M Brics, J Kaupuzs, and R Mahnke. How to solve fokker-planck equation treating mixed eigenvalue spectrum? *arXiv preprint arXiv:1303.5211*, 2013.
- [185] MT Araujo and Elso Drigo Filho. A general solution of the fokker-planck equation. *Journal of Statistical Physics*, 146:610–619, 2012.
- [186] Sheldon M Ross. *Introduction to probability models*. Academic press, 2014.

- [187] Federico Corberi, Eugenio Lippiello, and Marco Zannetti. Fluctuation dissipation relations far from equilibrium. *Journal of Statistical Mechanics: Theory and Experiment*, 2007(07):P07002, 2007.
- [188] Igor Volkov, Jayanth R Banavar, Stephen P Hubbell, and Amos Maritan. Neutral theory and relative species abundance in ecology. *Nature*, 424(6952):1035–1037, 2003.
- [189] Samuel Karlin and James McGregor. Linear growth, birth and death processes. *Journal of Mathematics and Mechanics*, 7(4):643–662, 1958.
- [190] Alexey A Shvets, Maria P Kochugaeva, and Anatoly B Kolomeisky. Mechanisms of protein search for targets on dna: theoretical insights. *Molecules*, 23(9):2106, 2018.
- [191] Junji Iwahara and Anatoly B Kolomeisky. Discrete-state stochastic kinetic models for target dna search by proteins: Theory and experimental applications. *Biophysical chemistry*, 269:106521, 2021.
- [192] Giorgio Nicoletti, Prajwal Padmanabha, Sandro Azaele, Samir Suweis, Andrea Rinaldo, and Amos Maritan. Emergent encoding of dispersal network topologies in spatial metapopulation models. *Proceedings of the National Academy of Sciences*, 120(46):e2311548120, 2023.
- [193] Felix Roy, Matthieu Barbier, Giulio Biroli, and Guy Bunin. Complex interactions can create persistent fluctuations in high-diversity ecosystems. *PLoS computational biology*, 16(5):e1007827, 2020.
- [194] R. Durrett and S.A. Levin. Stochastic spatial models: A user's guide to ecological applications. *Philosophical Transactions of the Royal Society of London. Series B: Biological Sciences*, 343(1305):329–350, 1994.
- [195] D. Tilman. Niche tradeoffs, neutrality, and community structure: A stochastic theory of resource competition, invasion, and community assembly. *Proceedings of the National Academy of Sciences*, 101(30):10854–10861, 2004.
- [196] P.A. Marquet, R.A. Quiñones, S. Abades, F. Labra, M. Tognelli, M. Arim, and M. Rivadeneira. Scaling and power-laws in ecological systems. *The Journal of Experimental Biology*, 208:1749–1769, 2005.
- [197] Pablo A Marquet, Andrew P Allen, James H Brown, Jennifer A Dunne, Brian J Enquist, James F Gilgooly, Patricia A Gowaty, Jessica L Green, John Harte, Steve P Hubbell, et al. On theory in ecology. *BioScience*, 64(8):701–710, 2014.
- [198] Stefano Allesina and Jonathan M Levine. A competitive network theory of species diversity. *Proceedings of the National Academy of Sciences*, 108(14):5638–5642, 2011.

- [199] Stefano Allesina and Si Tang. Stability criteria for complex ecosystems. *Nature*, 483(7388):205–208, 2012.
- [200] I. Hanski. Metapopulation dynamics. *Nature*, 396:41–49, 1998.
- [201] I. Hanski. *Metapopulation Ecology*. Oxford Univ. Press, Oxford, 1999.
- [202] Juan E Keymer, Pablo A Marquet, Jorge X Velasco-Hernández, and Simon A Levin. Extinction thresholds and metapopulation persistence in dynamic landscapes. *The American Naturalist*, 156(5):478–494, 2000.
- [203] O. Ovaskainen, K. Sato, J. Bascompte, and I. Hanski. Metapopulation models for extinction threshold in spatially correlated landscapes. *Journal of Theoretical Biology*, 215:95–108, 2002.
- [204] A. Rinaldo, M. Gatto, and I. Rodriguez-Iturbe. *River networks as ecological corridors. Species, populations, pathogens*. Cambridge University Press, New York, 2020.
- [205] Bronwyn Rayfield, Celina B Baines, Luis J Gilarranz, and Andrew Gonzalez. Spread of networked populations is determined by the interplay between dispersal behavior and habitat configuration. *Proceedings of the National Academy of Sciences*, 120(11):e2201553120, 2023.
- [206] José M Montoya, Stuart L Pimm, and Ricard V Solé. Ecological networks and their fragility. *Nature*, 442(7100):259–264, 2006.
- [207] Marie-Josée Fortin, Mark RT Dale, and Chris Brimacombe. Network ecology in dynamic landscapes. *Proceedings of the Royal Society B*, 288(1949):20201889, 2021.
- [208] A. Maritan, A. Rinaldo, I. Rodriguez-Iturbe, R. Rigon, and A. Giacometti. Scaling in river networks. *Physical Review E*, 53:1501–1513, 1996.
- [209] J.R. Banavar, A. Maritan, and A. Rinaldo. Size and form in efficient transportation networks. *Nature*, 399:130–132, 1999.
- [210] A. Maritan, R. Rigon, J.R. Banavar, and A. Rinaldo. Network allometry. *Geophysical Research Letters*, 29:1–4, 2002.
- [211] Jordi Bascompte and Ricard V Solé. Habitat fragmentation and extinction thresholds in spatially explicit models. *Journal of Animal Ecology*, pages 465–473, 1996.
- [212] RV Sole and J Bascompte. *Self-Organization in complex ecosystems*. Princeton University Press, New York, 2006.
- [213] Otso Ovaskainen and Ilkka Hanski. Metapopulation dynamics in highly fragmented landscapes. In *Ecology, genetics and evolution of metapopulations*, pages 73–103. Elsevier, 2004.

- [214] Dean Urban and Timothy Keitt. Landscape connectivity: a graph-theoretic perspective. *Ecology*, 82(5):1205–1218, 2001.
- [215] Thomas RE Southwood. Habitat, the templet for ecological strategies? *Journal of Animal Ecology*, 46(2):337–365, 1977.
- [216] Marcel Holyoak. Habitat patch arrangement and metapopulation persistence of predators and prey. *The American Naturalist*, 156(4):378–389, 2000.
- [217] Mirjana Bevanda, Emanuel A Fronhofer, Marco Heurich, Jörg Müller, and Björn Reineking. Landscape configuration is a major determinant of home range size variation. *Ecosphere*, 6(10):1–12, 2015.
- [218] Philip Staddon, Zoë Lindo, Peter D Crittenden, Francis Gilbert, and Andrew Gonzalez. Connectivity, non-random extinction and ecosystem function in experimental metacommunities. *Ecology letters*, 13(5):543–552, 2010.
- [219] Paulina A Arancibia and Peter J Morin. Network topology and patch connectivity affect dynamics in experimental and model metapopulations. *Journal of Animal Ecology*, 91(2):496–505, 2022.
- [220] Robert M May. *Stability and complexity in model ecosystems*, volume 1. Princeton University Press, 2019.
- [221] Luis J Gilarranz and Jordi Bascompte. Spatial network structure and metapopulation persistence. *Journal of Theoretical Biology*, 297:11–16, 2012.
- [222] I. Hanski and O. Ovaskainen. The metapopulation capacity of a fragmented landscape. *Nature*, 404:755–758, 2000.
- [223] Jacopo Grilli, György Barabás, and Stefano Allesina. Metapopulation persistence in random fragmented landscapes. *PLoS Computational Biology*, 11(5):e1004251, 2015.
- [224] O. Ovaskainen and I. Hanski. Transient dynamics in metapopulation response to perturbation. *Theoretical Population Biology*, 61:285–295, 2002.
- [225] O. Ovaskainen and I. Hanski. Spatially structured metapopulation models: Global and local assessment of metapopulation capacity. *Theoretical Population Biology*, 60:281–302, 2001.
- [226] Yang Wang, Deepayan Chakrabarti, Chenxi Wang, and Christos Faloutsos. Epidemic spreading in real networks: An eigenvalue viewpoint. In *22nd International Symposium on Reliable Distributed Systems, 2003. Proceedings.*, pages 25–34. IEEE, 2003.

- [227] Piet Van Mieghem, Jasmina Omic, and Robert Kooij. Virus spread in networks. *IEEE/ACM Transactions On Networking*, 17(1):1–14, 2008.
- [228] Ayalvadi Ganesh, Laurent Massoulié, and Don Towsley. The effect of network topology on the spread of epidemics. In *Proceedings IEEE 24th Annual Joint Conference of the IEEE Computer and Communications Societies.*, volume 2, pages 1455–1466. IEEE, 2005.
- [229] A Jamakovic, RE Kooij, P Van Mieghem, and Edwin Robert van Dam. Robustness of networks against viruses: the role of the spectral radius. In *2006 Symposium on Communications and Vehicular Technology*, pages 35–38. IEEE, 2006.
- [230] Romualdo Pastor-Satorras, Claudio Castellano, Piet Van Mieghem, and Alessandro Vespignani. Epidemic processes in complex networks. *Reviews of Modern Physics*, 87(3):925, 2015.
- [231] Richard Levins. Some demographic and genetic consequences of environmental heterogeneity for biological control. *Bulletin of the ESA*, 15(3):237–240, 1969.
- [232] Max A Woodbury. *Inverting modified matrices*. Department of Statistics, Princeton University, 1950.
- [233] E. Bertuzzo, I. Rodriguez-Iturbe, and A. Rinaldo. Metapopulation capacity of evolving fluvial landscapes. *Water Resources Research*, 51:2696–2706, 2015.
- [234] J. Giezendanner, P. Benettin, N. Durighetto, G. Botter, and A. Rinaldo. A note on the role of seasonal expansions and contractions of the flowing fluvial network on metapopulation persistence. *Water Resources Research*, 57:e2021WR029813, 2021.
- [235] Duncan J Watts and Steven H Strogatz. Collective dynamics of ‘small-world’ networks. *Nature*, 393(6684):440–442, 1998.
- [236] Albert-László Barabási and Réka Albert. Emergence of scaling in random networks. *Science*, 286(5439):509–512, 1999.
- [237] Cheryl-Lesley B Chetkiewicz, Colleen Cassady St. Clair, and Mark S Boyce. Corridors for conservation: integrating pattern and process. *Annu. Rev. Ecol. Evol. Syst.*, 37:317–342, 2006.
- [238] Paul Erdos and Alfréd Rényi. On random graphs i. *Publicationes Mathematicae*, 6(290-297):18, 1959.
- [239] Mark Newman. *Networks*. Oxford University Press, 2018.

- [240] Patrick L Thompson, Bronwyn Rayfield, and Andrew Gonzalez. Loss of habitat and connectivity erodes species diversity, ecosystem functioning, and stability in metacommunity networks. *Ecography*, 40(1):98–108, 2017.
- [241] Catherine Badgley, Tara M Smiley, Rebecca Terry, Edward B Davis, Larisa RG DeSantis, David L Fox, Samantha SB Hopkins, Tereza Jezkova, Marjorie D Matocq, Nick Matzke, et al. Biodiversity and topographic complexity: modern and geohistorical perspectives. *Trends in Ecology & Evolution*, 32(3):211–226, 2017.
- [242] Bernhard Lehner, Kristine Verdin, and Andy Jarvis. New global hydrography derived from spaceborne elevation data. *Eos, Transactions American Geophysical Union*, 89(10):93–94, 2008.
- [243] Riccardo Rigon, Andrea Rinaldo, Ignacio Rodriguez-Iturbe, Rafael L Bras, and Ede Ijjasz-Vasquez. Optimal channel networks: a framework for the study of river basin morphology. *Water Resources Research*, 29(6):1635–1646, 1993.
- [244] Amos Maritan, Francesca Colaiori, Alessandro Flammini, Marek Cieplak, and Jayanth R Banavar. Universality classes of optimal channel networks. *Science*, 272(5264):984–986, 1996.
- [245] G Evelyn Hutchinson. The paradox of the plankton. *The American Naturalist*, 95(882):137–145, 1961.
- [246] Chang-Yu Chang, Djordje Bajić, Jean CC Vila, Sylvie Estrela, and Alvaro Sanchez. Emergent coexistence in multispecies microbial communities. *Science*, 381(6655):343–348, 2023.
- [247] Joost HJ van Opheusden, Lia Hemerik, Mieke van Opheusden, and Wopke van der Werf. Competition for resources: complicated dynamics in the simple tilman model. *SpringerPlus*, 4:1–31, 2015.
- [248] Martina Dal Bello, Hyunseok Lee, Akshit Goyal, and Jeff Gore. Resource–diversity relationships in bacterial communities reflect the network structure of microbial metabolism. *Nature Ecology & Evolution*, 5(10):1424–1434, 2021.
- [249] Peter L Chesson. Environmental variation and the coexistence of species. *Community ecology*, 240:54, 1986.
- [250] Peter B Adler and John M Drake. Environmental variation, stochastic extinction, and competitive coexistence. *The American Naturalist*, 172(5):E186–E195, 2008.
- [251] Theo Gibbs, Jacopo Grilli, Tim Rogers, and Stefano Allesina. Effect of population abundances on the stability of large random ecosystems. *Physical Review E*, 98(2):022410, 2018.

- [252] Oliver J Meacock and Sara Mitri. Environment-organism feedbacks drive changes in ecological interactions. *bioRxiv*, pages 2023–10, 2023.
- [253] Aurore Picot, Shota Shibasaki, Oliver J Meacock, and Sara Mitri. Microbial interactions in theory and practice: when are measurements compatible with models? *Current Opinion in Microbiology*, 75:102354, 2023.
- [254] Paul E Turner, Valeria Souza, and Richard E Lenski. Tests of ecological mechanisms promoting the stable coexistence of two bacterial genotypes. *Ecology*, 77(7):2119–2129, 1996.
- [255] Andrew D Letten and William B Ludington. Pulsed, continuous or somewhere in between? resource dynamics matter in the optimisation of microbial communities. *The ISME Journal*, 17(4):641–644, 2023.
- [256] Richard E Lenski, Michael R Rose, Suzanne C Simpson, and Scott C Tadler. Long-term experimental evolution in escherichia coli. i. adaptation and divergence during 2,000 generations. *The American Naturalist*, 138(6):1315–1341, 1991.
- [257] Frank M Stewart and Bruce R Levin. Partitioning of resources and the outcome of interspecific competition: a model and some general considerations. *The American Naturalist*, 107(954):171–198, 1973.
- [258] Yulia Fridman, Zihan Wang, Sergei Maslov, and Akshit Goyal. Fine-scale diversity of microbial communities due to satellite niches in boom and bust environments. *PLoS computational biology*, 18(12):e1010244, 2022.
- [259] Justus Wilhelm Fink, Noelle A Held, and Michael Manhart. Microbial population dynamics decouple growth response from environmental nutrient concentration. *Proceedings of the National Academy of Sciences*, 120(2):e2207295120, 2023.
- [260] Clare I Abreu, Jonathan Friedman, Vilhelm L Andersen Woltz, and Jeff Gore. Mortality causes universal changes in microbial community composition. *Nature communications*, 10(1):2120, 2019.
- [261] Jonathan Friedman, Logan M Higgins, and Jeff Gore. Community structure follows simple assembly rules in microbial microcosms. *Nature ecology & evolution*, 1(5):0109, 2017.
- [262] Oscar Delaney, Andrew D Letten, and Jan Engelstädter. Frequent, infinitesimal bottlenecks maximize the rate of microbial adaptation. *Genetics*, 225(4):iyad185, 2023.
- [263] Po-Yi Ho, Benjamin H Good, and Kerwyn Casey Huang. Competition for fluctuating resources reproduces statistics of species abundance over time across wide-ranging microbiotas. *Elife*, 11:e75168, 2022.

- [264] Amir Erez, Jaime G Lopez, Benjamin G Weiner, Yigal Meir, and Ned S Wingreen. Nutrient levels and trade-offs control diversity in a serial dilution ecosystem. *Elife*, 9:e57790, 2020.
- [265] Blox Bloxham, Hyunseok Lee, and Jeff Gore. Diauxic lags explain unexpected coexistence in multi-resource environments. *Molecular Systems Biology*, 18(5):e10630, 2022.
- [266] Petros Lenas and Stavros Pavlou. Coexistence of three competing microbial populations in a chemostat with periodically varying dilution rate. *Mathematical Biosciences*, 129(2):111–142, 1995.
- [267] Naomi Ziv, Nathan J Brandt, and David Gresham. The use of chemostats in microbial systems biology. *JoVE (Journal of Visualized Experiments)*, (80):e50168, 2013.
- [268] Ruud A Weusthuis, Jack T Pronk, PJ Van Den Broek, and JP Van Dijken. Chemostat cultivation as a tool for studies on sugar transport in yeasts. *Microbiological reviews*, 58(4):616–630, 1994.
- [269] Satya N Majumdar and Henri Orland. Effective langevin equations for constrained stochastic processes. *Journal of Statistical Mechanics: Theory and Experiment*, 2015(6):P06039, 2015.
- [270] George WA Constable, Alan J McKane, and Tim Rogers. Stochastic dynamics on slow manifolds. *Journal of Physics A: Mathematical and Theoretical*, 46(29):295002, 2013.
- [271] Bram van Dijk, Jeroen Meijer, Thomas D Cuypers, and Paulien Hogeweg. Trusting the hand that feeds: microbes evolve to anticipate a serial transfer protocol as individuals or collectives. *BMC evolutionary biology*, 19:1–18, 2019.
- [272] Eugene Seneta. *Non-negative matrices and Markov chains*. Springer Science & Business Media, 2006.